POLITECNICO DI TORINO

MASTER's Degree in Biomedical Engineering

MASTER's Degree Thesis

Cycle characteristics in roller skiing measured by IMU sensors

Supervisors
Prof. Laura GASTALDI
Prof. Vesa LINNAMO
Ing. Valeria ROSSO

Candidate
Alessandro MAULA

JULY 2020

Abstract

In cross-country (XC) skiing, double poling (DP) is a widely used skiing technique in which skiers push synchronously two poles to generate propulsion. Cycle parameters as cycle time, push and recovery time, cycle speed, and cycle length play an important role in performance assessment. The use of inertial measurement units (IMUs) to assess cycle parameters have the advantages to require a simple setup and to allow measuring skiing kinematics continuously outside. The thesis aimed to identify cycle events (pole hits and lifts) and to calculate cycle parameters by linear acceleration and angular velocity signals collected using IMUs fixed on the skiers, and to assess errors (accuracy and precision) of the results in comparison with a gold standard system.

Two expert skiers performed DP on a treadmill at three speeds and two inclinations. The participants skied using poles with force sensors embedded, which was the gold standard to detect pole cycle events, and they wore 6 IMUs placed on the right arm and forearm (one proximally and one distally), upper back (C7) and right ski. The protocol was repeated with IMUs aligned and rotated with respect to body segments. Three different IMUs signals-based cycle events identification methods were developed: (1) acceleration norm method, (2) angular velocity norm method, and (3) fusion method, based on the fusion of method (1) and (2). In addition, the relationship between the linear acceleration and angular velocity mean, integral, pole lift peak and skiing speed and terrain inclination were assessed. Finally, the ski inclination was calculated with the IMU placed on the ski using two methods: angular velocity integration and accelerometer as inclinometer. The ski velocity and displacement were calculated by integrating linear acceleration along the ski longitudinal axis.

The 4 sensors on the upper limb showed small median error (MD) and interquartile range errors (IQR) in identifying pole hits (MD<44 ms and IQR<30 ms) and in calculating cycle time (MD<2 ms and IQR<14 ms) with all the three cycle events identification methods. The wrist sensor provided the best performance in calculating cycle time (MD<2 ms and IQR<4 ms) and it was the one to be suitable also to calculate push time and rest time (MD<38 ms and IQR<16 ms). The use of the signals norm in the pole events

identification ensured independence from the sensors' orientation. The linear acceleration mean appeared to be particularly sensitive to skiing speed variations, whereas angular velocity integral seemed more influenced by treadmill inclination. Regarding the ski inclination calculation, the inclinometer-based method showed greater agreement with treadmill inclination compared to the angular velocity method, which is subjected to drift. The ski velocity and displacement calculated with the ski sensor agree with the reference depending on the trial; therefore, this methodology must be improved.

In conclusion, this thesis achieved the proposed goal identifying three methods to assess accurately and precisely the DP cycle temporal parameters with one IMU on the wrist and proposed a simple method to investigate the ski inclination in XC skiing DP.

Acknowledgements

Firstly, I would like to thank Professor Laura Gastaldi and Professor Vesa Linnamo for giving me the opportunity to carry out this thesis and for their expert guidance. In addition, I want to express my gratitude to Ing. Valeria Rosso for having wisely advised me in every single phase of this project.

I wish to also acknowledge all the members of Vuokatti Sports Technology Unit (University of Jyväskylä) for helping me for the thesis whenever I needed it and above all for involving me in authentic Finnish experiences making my stay abroad more valuable.

I want to also thank my friend Anssi to have been my skiing fellow with whom I enjoyed countless trips around Vuokatti’s slopes.

A special thank to Irene for visiting me during the Finnish winter despite she did not love the cold, and for have always encouraged my ideas and welcomed my decisions.

Finally, my greatest gratitude goes to my family who once again supported me in every possible way.

Contents

1 Introduction

The cross-country skiing (XC skiing) is an outdoor endurance sport [1] and is an Olympic game since 1924 [2]. XC skiing is a sport in which upper and lower limbs contribute to the propulsion and often also the trunk is used to enhance the propulsion. To generate propulsion by the upper limbs, a pair of poles are used.

In XC skiing there are two main styles, the classical one and the skating one, and each of them involves many sub techniques [1]. Different techniques are chosen by the skiers to optimize performance and depending on the terrain conditions [3]. The classical style main techniques are diagonal stride, double poling, kick double poling and herringbone, while the skating style main techniques are V1-skate, V2-skate, 2-skate, combiskate and diagonal skate [3].

A brief description of each technique for each style is provided below according to Nilsson et al. [3].

Classical style

- Diagonal stride: the arms are moved in a diagonal relationship and when an arm push for the propulsion the contralateral leg kick also for the propulsion.
- Double poling: the arms are moved in parallel to push while a trunk flexion is performed.
- Kick double poling: the arms are used in parallel with a leg to give propulsion.
- Herringbone: the skis are rotated with respect to the skiing direction and legs and arms are moved in a diagonal relationship.

Skating style

- V1-sakte: distinguished by one push with both the arms on every second leg push and an asymmetrical load on one side.
- V2-skate: characterised by one double push every leg push.
- 2-skate: similar to Vi-skate, but less prominent asymmetrical action between the two side of the body.
- Combiskate: only push with legs without poling action.
- Diagonal skate: skating form of the classical diagonal stride.

Among the techniques described above, the double poling is of particular interest for this thesis project. The double poling (DP) is a main XC-skiing technique [4] in which the propulsive forces are symmetrically and synchronously generated during the ground contact of the poles [5]. Therefore, DP technique is a series of pushing cycles in which it is possible to recognize a poling or pushing phase, in which the poles are in contact to the ground, and a recovery phase, in which the poles are not in contact to the ground and are moved forward to start a new pushing phase.

The role of the DP technique in classical XC skiing has increased since the introduction of sprint racing events, which require to reach high DP speeds, particularly in the final fraction of the race [4]. Some studies have also demonstrated that DP is more economical than other techniques, especially in the flat part of the tracks [6].

1.1 Cycle parameters

The cycle parameters in XC skiing are spatio-temporal parameters, which describe the skiing movement just as the spatio-temporal gait parameters in gait analysis [7]. They are commonly calculated to assess performance [4],[8] and to understand the optimal strategy to control skiing speed in different terrains [8],[9]. Regarding the DP, the cycle parameters are defined by the poles events on the ground (poles contacts and detachments from the ground) and by the skis speed. In particular, the poles events allow to define the following temporal parameters: cycle time, push time, rest time and the percentage of push and rest cycle with respect to the entire cycle duration (push phase and rest phase). The knowledge of the skis speed and the poles events allows defining also the following spatial parameters: cycle speed and cycle length (Figure 1) [4],[9],[10]. A DP cycle parameters definition based on the poles events and the ski velocity is provided below [4],[9],[10]:

- Cycle time: duration of the poling cycle, calculated as the time between two consecutive pole contact with the ground (pole hits).
- Poling frequency: the inverse of the cycle time.
- Push time: poling phase duration, calculated as the time between a pole hit and the consecutive pole detachment from the ground (pole lift) of the same pushing cycle. It can also be calculated as the percentage of the pushing cycle.

- Rest time: recovery phase duration, calculated as the time between a pole lift and the consecutive pole hit of the following pushing cycle. It can also be calculated as the percentage of the pushing cycle.
- Cycle speed: the average speed of the skis in a cycle.
- Cycle length: the space covered by the skis in a cycle. It is the product of the cycle time and the cycle speed.

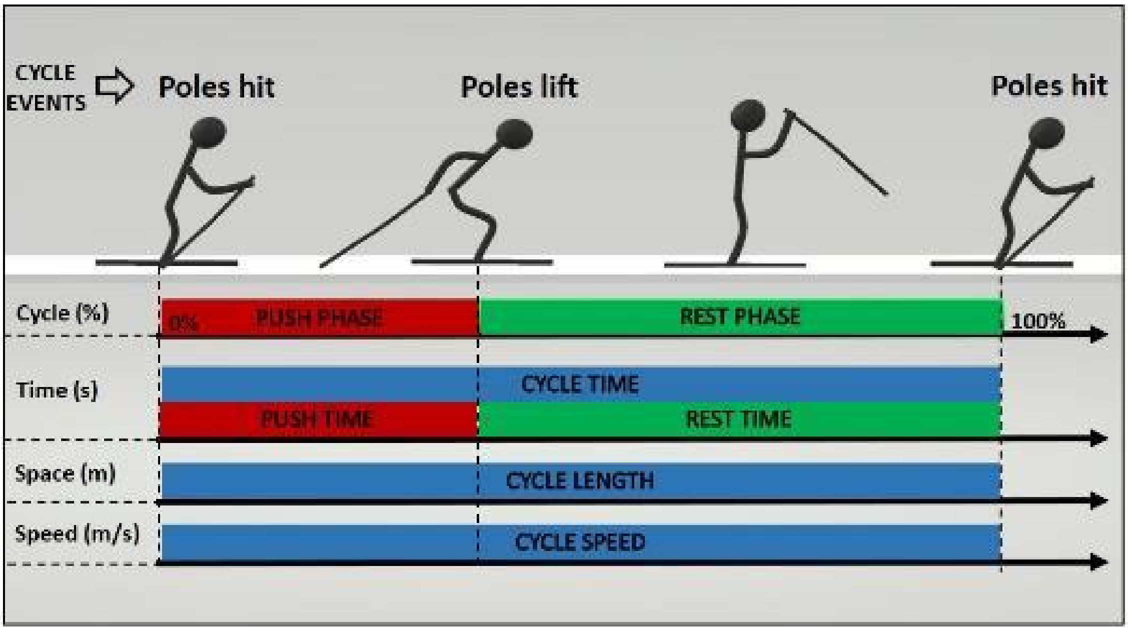

Figure 1 - Double poling cycle events and cycle parameters.

1.2 IMUs in Cross-country skiing

The described cycle characteristics have been usually studied indoor using marker-based stereophotogrammetric systems or video recordings or using pole force sensors and force plates [7],[8]. They are less studied outside, but when investigated they are usually calculated for limited volumes because of the complexity in positioning the acquisition systems along the entire track. The use of inertial measurement units (IMUs) to measure cycle characteristics would be advantageous because it would allow to measure the kinematics continuously outside, during training and competitions with less efforts than the systems mentioned above [8] because they can record without any capture volume restriction [11] and they ensure easy setup. Therefore, the use of IMUs to study the XC-skiing kinematics has increased [12]. To understand the state of the art of IMUs employment in XC-skiing, a bibliographic research has been performed.

The majority of the studies which involve IMUs are interested in the sub-techniques classification and, regarding the cycle parameters, they mainly identify the cycle duration and the number of cycles for each technique [13],[14],[15],[16],[17],[7]. In addition, these recent articles also proposed an IMUs-based cycle parameters analysis [16],[17],[18],[7]. Marsland et al. [19],[14],[8],[20] developed a system with only one sensor (containing an IMU and a GPS) placed on the upper back to classify the XC-skiing sub-techniques. Myklebust et al. (2011) [15] proposed a method to identify the contacts and detachments of the poles from the ground, based on the linear acceleration measured along the pole longitudinal axis. Sakurai et al. studied how to classify the sub-techniques in classic rollers skiing [13] and in skating roller skiing [17] with a system of IMUs placed on the wrists and on the roller skis.

Among the articles that performed a cycle parameters analysis, Fasel et al. 2015 [7] validated an IMUs-based system to identify the ski and pole cycle events and the ski velocity and displacement in diagonal stride XC-skiing technique. For the pole events identification, they used the norm of the acceleration calculated from an IMU placed on the pole. Nikkola et al. (2018) [18] calculated the cycle duration and the push and recovery phases and the ski velocity in XC roller skiing DP technique implementing an IMU-based system (an IMU on the roller ski) enhanced with video recordings and poles force sensors. In this study [18], the pole events were identified with the pole force sensors while the ski velocity was calculated integrating the ski sensor linear acceleration along the ski longitudinal axis and the drift from the integration was reduced sampling the ski velocity at 40, 60 and 80 meters from the start (on a 100 m track) with a camera-based system. In a recent article, Bruzzo et al. 2020 [16] described a system to calculate the pole lean angle and they also proposed a method based on an IMU embedded in the pole grip, to identify the pole hits and the pole lifts in XC-skiing double poling technique. However, in that study [16], the main purpose was the calculation of the lean angle and the pole events identification was compared with a video-based system with a poor temporal resolution, the number of cycles inspected

was small and only a skiing condition (skiing speed, terrain inclination) was inspected. Besides, the authors [16] proposes a very interesting method to identify the pole detachment from the ground that however, is based on the knowledge of the position of the sensor on the pole relatively to the pole tip and it would be more complicated to be implemented if a sensor would be placed on the upper limb instead of on the pole.
The articles found in the literature that implemented an IMUs-based system in XC-skiing are reported and summarized in the table below (Table 1.1).

	Aims of the study	N° of IMUs	IMUs position	Signals analysed	Parameters calculated
Bruzzo 2020 [16]	To resolve the dynamic lean angle of a ski pole during XC-skiing double poling.	1	Embedded in the pole grip.	3D angular velocity, acceleration norm.	Pole lean angle, pole hits, pole lifts.
Baumgart 2019 [21]	To develop a framework for the investigation of speed, power, and kinematic patterns across varying terrain in cross-country (XC) sit-skiing.	1	Right wrist.	Angular velocity about the medio-lateral axis and the linear acceleration along the vertical axis.	Pole hits, cycle time and cycle frequency.
Nikkola 2018 [18]	To demonstrate that inertial measurements, combined with force measurements, are a feasible approach in estimating speed. To compare maximum performance and different equipment in cross-country skiing.	1	Right roller ski.	Velocity obtained by the integration of the acceleration along the antero-posterior axis.	Cycle time, poling phase, recovery phase, cycle speed.
Marsland 2018 [19]	To compare macro kinematics variable of the same athletes during sprint (1.1km) and distance (10.5 km) competitions (classical technique)	1	Middle of the back 5 cm below the neck.	Angular velocity about medio lateral and antero-posterior axes.	Cycle rates, cycle lengths, cycle count (for each technique).
Seeberg 2017 [1]	To study the feasibility of a multi-sensor system (Hr, GNSS, IMUs) for outdoor XC skiing and validate a classification algorithm to distinguish sub-techniques of classical XC skiing.	6	Upper back, lower back, arms, ankles.	Angular velocity about mediolateral axis.	Phase differences between arms and torso and between legs and torso. Cycle frequency and cycle length.
Marsland 2017 [20]	Using an IMU to identify sub-techniques of cross-country skiing and to measure macro-kinematics over the entire length of a distance competition	1	middle of the back 5 cm below the neck.	Angular velocity about medio lateral and antero-posterior axes.	Cycle rates, cycle lengths, cycle count (for each technique)

Sakurai 2016 [17]	The development of an automated sub techniques identification system and the examination of the relationships among the skiing velocities (skating technique).	4	Wrists, roller skis.	Angular velocity about mediolateral axis, vertical acceleration, and acceleration norm from IMUs on the wrists.	Cycle number for each technique. Poles hits cycle time, cycle length. Pole lifts, pushing and recovery phase (he just says it is possible, he does not report them)
Marsland 2015 [8]	To identify automatically the XC-skiing sub-techniques, the cycle length, the cycle frequency, using a single inertial sensor on the upper back.	1	middle of the back 5 cm below the neck.	Angular velocity about medio lateral and antero-posterior axes.	Cycle rates, cycle lengths, cycle count (for each technique)
Fasel 2015 [7]	To design an easy-to-wear system and a method to detect key temporal events and compute cycle speed and length for the diagonal stride in XC skiing.	2	Left pole, left ski.	Acceleration norm for the pole and velocity (integrating acc.) along the anterior posterior axis for the ski.	Pole hits, pole lifts, thrust start, thrust end, gliding start. Cycle duration, cycle speed, cycle length, ski thrust duration, pole push duration, ski gliding duration, ski recovery duration.
Sakurai 2014 [13]	The development of an automated sub techniques identification system and the examination of the relationships among the skiing velocities (classical technique).	4	Wrists, roller skis.	Angular velocity about mediolateral axis, vertical acceleration, and acceleration norm from IMUs on the wrists.	Number of the cycles for each technique.
Marsland 2012 [14]	Feasibility study of a method based on one single inertial sensor to identify specific patterns for each XC-skiing technique.	1	middle of the back 5 cm below the neck.	Angular velocity about medio lateral and antero-posterior axes.	Cycle rates, cycle lengths, cycle count (for each technique)
Myklebust 2011 [15]	To use accelerometers to extract cycle parameters, symmetry between left and right side and to develop a classification of different techniques	5	Lower back, each pole, each heel.	Acceleration, velocity, and position along the vertical axis (pole axis), and acceleration norm from the back sensor.	Pole and ski hits and leaves. From these calculates→ Cycle time, poling/pushing times, recovery times, symmetry between left and right side, technique transition time

Table 1.1 – Studies that make use of IMUs in XC-skiing

2 Purpose of the thesis

Considering the existing background obtained from the bibliographic research on the use of the IMUs in XC skiing, the general purpose of the current thesis was to calculate the cycle parameters in XC skiing DP technique with a set of IMUs sensors fixed on the skiers. In particular, the following goals were defined:

1. To investigate the performance of a number of IMUs-based methods for the identification of cycle events in different skiing speed and terrain inclination conditions. In addition, to assess the influence of the sensor position on the skier’s upper limb and the influence of the sensor orientation.
2. To evaluate the ability of a number of methods to calculate the ski inclination and the ski velocity while performing DP on a treadmill by using the signals directly acquired from the ski sensor.
3. To study the relationship between the IMUs signals and the ski velocity and the terrain inclination.

3 Experimental protocol

All the tests were conducted in Vuokatti in a laboratory belonging to the sports technology unit of the University of Jyvaskyla. During the measurements, the participants were asked to ski on a treadmill using roller skis at three different speed and two different inclinations. The participants skied using the double poling technique and they made use of poles with force sensors embedded. All the trials were recorded by two cameras, one placed laterally, and one placed posteriorly the treadmill. In addition, inertial sensors were fixed on the upper limbs, trunk, and roller ski of the subjects.

3.1 Participants

Two cross-country skiing athletes, a male and a female, performed double poling on a treadmill (Figure 2). The two subjects were expert skiers (30 and 15 years of experience respectively) and they were familiar with the skiing technique and with skiing inside on a treadmill with roller skis. The skiers’ gender, age, weight, and height are reported in the Table 3.1. The participants volunteered in the study and the measurements were performed in accordance with the Declaration of Helsinki.

Participants	Age	Weight (kg)	Height (cm)
Male	40	81	183
Female	30	58	163

Table 3.1 - Subjects information

Figure 2 - A subject performing the double poling technique on the treadmill.

3.2 Measurement systems

In this study, two systems were used to collect the data: the Coachtech system and the inertial measurement system. Coachtech is a system based on wireless nodes and access points for collecting several types of analogical signals (force, angle, EMG) and video recordings. Video and analogical signals are automatically cut and synchronized, and the system is also able to calculate some sport-specific parameters that are made available for coaches and athletes online [22].

The IMUs system is composed of a certain number of IMUs (TSDN121, ATR Promotions) and of a software (SensorController, ATR Promotions) which allows to control the sensors settings and the acquisition modality with a calculator. The IMUs are connected to the calculator wirelessly and they can record the data directly in the PC' s memory or in their own memory or both [23]. In this experiment the number of IMUs used was 6.

3.2.1 Gold standard

The Coachtech system was used as the gold standard system and for the purpose of this experiment it was connected to two cameras, two pole force sensors and a treadmill. The pole force sensors (VTT MIKES, Technical Research Centre of Finland Ltd., Kajaani, Finland) are based on piezoelectric measurement technology (Kistler ForceLink) embedded in the poles grip. The cameras (LiLin UFG1122e) were located laterally and posteriorly, and they recorded the trials to allow a qualitative analysis of the movements performed by the subjects. The data acquired from the treadmill (Rodby RL3500E) concerns the treadmill speed. The sampling frequency of the force signals and of the treadmill's speed was set to 500 Hz, while the cameras recorded at 100 fps with a resolution of 1280x720 pixels.

3.2.2 IMUs system

A total of 6 IMUs, TSDN121, ATR Promotions (Figure 3, Table 3.2) were used for the measurement. Each IMU sensor can collect 3D linear acceleration, 3D angular velocity, and it also contains a 3D magnetometer.

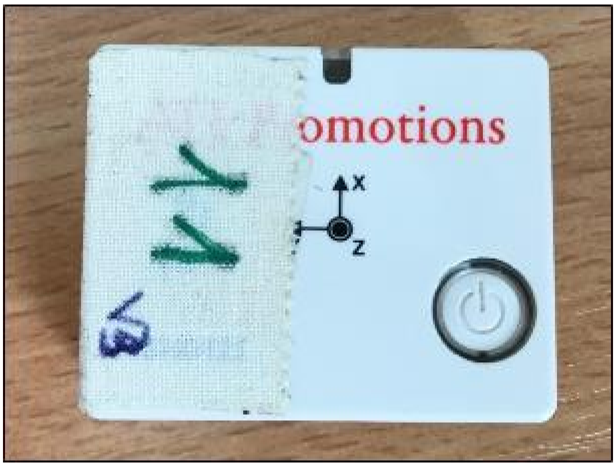

Figure 3 - Inertial measurement unit.

DIMENSIONS	37MM X 46MM X 12MM
WEIGHT	22g
CPU	RX621
OPERATING TIME	About 6 hours
TRANSMISSION PROTOCOL	Bluetooth Ver2.0 + EDR Class2
MEMORY	512Mb (about 5.8 hours with 100Hz sampling frequency)
WIRELINE CONNECTION	USB serial communication
GYROSCOPE AND ACCELEROMETER SENSOR	InvenSense MPU-6050 Sampling: up to 1000Hz (1 to 255 ms period) Acceleration range: ±2G/ ±4G/ ±8G/ ±16 Angular velocity range: ±250dps/ ±500dps/ ±1000dps/ ±2000dps

Table 3.2 - Specification of IMU ATR Promotion TSDN121. *To be precise the sensors also contain a magnetometer and a barometric pressure sensor, but they have not been used and their information are not reported in this table.*

The sensors were placed on the following body segments:

- 2 IMUs on the right forearm: one distally (on the wrist) and the other more proximally (in the middle of the forearm). The IMUs reference numbers were respectively 09 and 10.
- 2 IMUs on the right arm: one distally (close to the elbow) and the other more proximally (in the middle of the arm). The IMUs reference numbers were respectively 11 and 13.
- 1 IMU on the upper trunk (C7). The IMU reference number was 14.

- 1 IMU on the right roller ski. The IMU reference number was 15.

The IMUs were placed on only one side of the athlete because the symmetry of the pushing gesture was assumed. Two IMU sensors were placed on the same upper limb segment to consider the influence of a different sensors' position on the detection of the cycle events. The sensors were attached to the subjects two times during the experiment because firstly they were aligned with the body segments frames and then they were rotated. However, the position did not change. This procedure is performed to assess the influence of the sensors' orientation on the cycle events identification.

When the sensors were aligned to the body segments, their y axis was approximately parallel to the longitudinal axis of the segment to which they were fixed. The Y axis of the forearm and arm sensors pointed toward the hand considering a zero flexion at the elbow joint while the Y axis of the sensor on the upper back pointed towards the head. The sensors' z axis was approximately orthogonal to the segment surface. For the sensors on the upper limb, furthermore, the z axes were ensured to point approximately in the medio-lateral direction of the subjects' body during a hypothetical poling gesture (Figure 4). In the rotated configuration each sensor was simply clockwise rotated of approximately 45 deg around the z axis (Figure 5).

During the measurement, the IMUs recorded the 3D linear acceleration (range: ±16 g) and the 3D angular velocity (range: ±2000 dps) with a sampling frequency of 500 Hz. The signals were collected with SensorController.

The IMUs were enveloped in a plastic film and firmly attached to body segments with adhesive tape as showed in Figure 4 (sensors aligned with the body segments)Figure 5 (sensors rotated).

Figure 4 - IMUs placed on a subject in the "aligned" configuration.

Figure 5 - IMUs placed on a subject in the "rotated" configuration.

3.3 Acquisition protocol

The protocol consisted of a total of 12 trials, among which 6 trials were done with the sensors aligned with the body segment and then the same 6 trials were executed with the sensors rotated. Each trial lasted approximately 30 seconds counted starting since the treadmill reached a constant velocity. The recovery time between each trial was 2 minutes, except for the one between the 6th and the 7th trial that was longer because the sensors had to be detached from the subjects and reattached rotated to prepare the "rotated" configuration. The recovery intervals were necessary to prevent fatigue. The protocol was designed to explore 3 different speed and two distinct treadmill inclinations, for each of the two IMUs orientation conditions described in the previous paragraph. In particular, in the 3 first trials the treadmill was kept flat (1 deg) and the treadmill speed was increased through the 3 trials, passing from slow, to middle, and high speed. In the next 3 trials the treadmill inclination was increased to reach 6 deg and the speed is once again increased through the 3 trials (slow, middle, high speed). The last 6 trials followed the same inclination and speed pattern of the previous 6 trials, but the sensors were clockwise rotated of 45 deg around their z axis. Since the activity intensity reasonably differ from male and female subjects, the velocities for the two treadmill inclinations (1 deg and 6 deg) were appropriately chosen for each participant with the help of a coaching expert to ensure that the subjects did not struggle to perform the task avoiding unusual body movement which could impair the measurements. The table below (Table 3.3) reports the treadmill speed and inclination for each trial of each subject.

Trial number	Speed	Subject	Treadmill speed (km/h)	Treadmill inclination (deg)	IMUs orientation
1	low	A	10	1	Aligned with body segment
		B	10		
2	medium	A	15	1	
		B	15		
3	high	A	20	1	
		B	20		
4	low	A	8	6	
		B	6		
5	medium	A	10	6	
		B	8		
6	high	A	12	6	
		B	10		
7	low	A	10	1	Rotated clockwise of 45 deg around the z axis of the sensor
		B	10		
8	medium	A	15	1	
		B	15		
9	high	A	20	1	
		B	20		
10	low	A	8	6	
		B	6		
11	medium	A	10	6	
		B	8		
12	high	A	12	6	
		B	10		

Table 3.3 - Details about the trials performed by each subject.

3.4 Acquisitions for data Calibration

The pole force sensors offset was corrected before the measurements, recording a null force and compensating the corresponding bias. The actual calibration of the piezoelectric sensor was done at the VTT MIKES in Kajaani.

Concerning the IMUs, a static calibration allowed the correction of the accelerometer's bias, sensitivity, and axes misalignment, while only the bias and the acceleration sensitivity were corrected for the gyroscopes [24]. The calibration procedure consisted of two parts. The first part was done before the beginning of the measurement protocol and the second part was done at the end of the measurement protocol. Both the first and the second part of the calibration procedure involved 6 static acquisitions consisting in placing the IMUs in 6 different positions orienting each axis of the sensors once time parallel and once time antiparallel to the gravity. In particular, all the sensors were put on a plane surface with an axis aligned with the gravity and pointing upwards, then a static acquisition (at least 5 seconds) was recorded from all the sensors. The sensors were then placed again on the same surface with the axis that before was pointing upwards always aligned with the gravity but this time pointing downwards, and another static acquisition is performed. The same process is repeated for all the sensor axes leading to collect a total of 6 recordings for each sensor. The signals acquired during the static measurements are used in post processing to correct the above-mentioned errors implementing the accelerometers and gyroscopes mathematical models as described in Ferraris et al. [24]. The mathematical models which allow the IMUs calibration are further discussed in the data analysis chapter.

4 Data analysis

All the data acquired during the measurements were processed in MATLAB software (The MathWorks Inc.). The 1st trial (sensors aligned with the body segments, speed: 10 km/h, inclination: 1 deg) recorded with the second subject was excluded by the analysis because the data concerning the force signals were missing. However, this did not mean the loss of a recording in those speed and inclination conditions for the second subject because the trials in which the sensors are rotated are recorded in the same conditions of the trials in which the sensors are aligned with the body segments and therefore the 7th trial (sensors rotated with the body segments, speed: 10 km/h, inclination: 1 deg) compensated the loss of the 1st trial.

The data analysis can be divided in 6 macro section:

1. Preliminary steps:
    - The IMUs measurement system is synchronized with the Coachtech system.

- The beginning of the treadmill constant speed is identified to exclude the poling cycles that happens before that moment.
    - The acquisition errors of the IMUs signals are corrected through a mathematical model of the IMUs signals errors and processing the signals acquired during the static calibration procedure.
2. Cycle events identification:
    - The poles hits and lifts of reference are identified from the force signals.
    - Three cycle events identification methods from the IMUs signals are proposed: one based on the acceleration norm, one based on the angular velocity norm and a last one based on the fusion of the two previous methods.
3. Wrong cycles identification: description of an algorithm to identify automatically mistakes in the identification of the cycles performed with one of the IMUs-based identification methods proposed, through a comparison with the reference cycles identification (the one based on the force signals).
4. Ski inclination evaluation:
    - The alignment of the ski sensor frame with the ski frame is described.
    - The ski inclination is evaluated with a method based on the ski sensor angular velocity integration around the ski mediolateral axis.
    - The ski inclination is assessed with a method based on the use of the ski IMU as an inclinometer.
5. Ski velocity and displacement calculation: the ski velocity and displacement are calculated integrating the ski IMU linear acceleration along the ski longitudinal axis.
6. Features extraction from the IMUs signals: some variables are calculated from the IMUs acceleration signals and angular velocity signals to investigate their relationship with different treadmill inclinations and speeds.

4.1 Preliminary steps

The first phase of the data analysis involved some preliminary steps to prepare the signals to the following phases where they are used to identify the cycle events, or they are processed to calculate other variables.

4.1.1 Data preparation

The norm of the acceleration and angular velocity signals from all the sensors was calculated for each trial recorded. All the cycle events identification algorithms work with the signals norm because this allows to be independent form the sensor orientation on the body. This fact can be seen plotting the signal norm superimposed to the absolute values of the signal components along the 3 sensor axis and calculating the contribute of each component to the signal norm with a cross correlation between each component (the absolute values) and the signal norm. The cross correlation is then normalized dividing by the maximum value of the signal norm autocorrelation. In the case of the wrist sensor linear acceleration, when the sensor is aligned with the body segment the main contribute is brought by the X component because the sensor X axis lays on the sagittal plane (in which the poling gesture mainly happens) and is approximately parallel to the pole longitudinal axis for most of the poling cycle (Figure 6). When the sensor is rotated the Y axis now contributes more to the signal norm, however the signal norm pattern does not differ that much from the case when the sensor was aligned (Figure 7). The norms in the case aligned and rotated are obviously slightly different because they show different trials and therefore a variability in the signal is expected. These observations highlight how the single components patterns are sensitive to the sensors rotation while the norms patterns do not change due to the sensors rotation. Analogue comments can be done for the angular velocity norms and its components along the sensor axes (Figure 8,Figure 9).

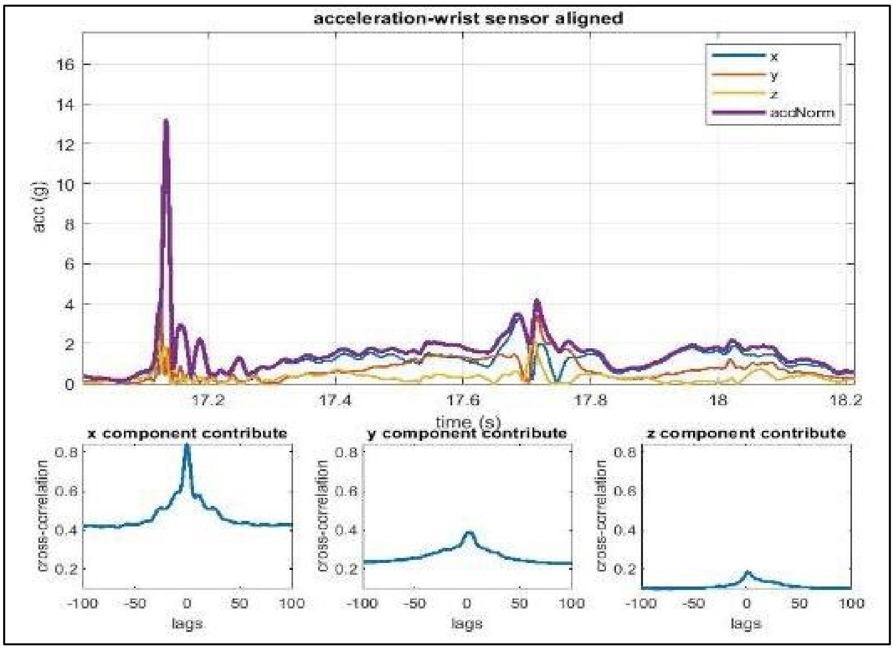

Figure 6 - Acceleration norm and components contributes. Sensor aligned. *(Top) - The acceleration norm from the wrist sensor is superimposed to the absolute value of the single components along the sensor axes. The sensor is in the condition aligned with the body segment. The plot shows a single cycle, and, on the left, it is possible to notice the spike caused by the pole hit while in the middle there is the peak caused by the pole lift. (Bottom)- The contribute of the components to the signal norm.*

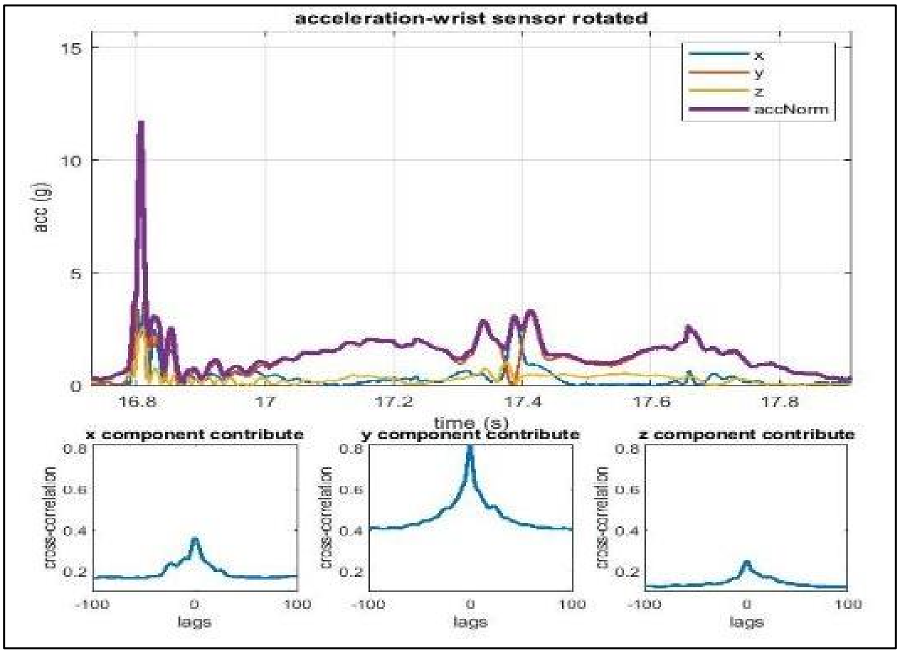

Figure 7 - Acceleration norm and components contributes. Sensor rotated. *(Top) - The acceleration norm from the wrist sensor is superimposed to the absolute value of the single components along the sensor axes. The sensor is in the condition rotated. The plot shows a single cycle, and, on the left, it is possible to notice the spike caused by the pole hit while in the middle there is the peak caused by the pole lift. (Bottom)- The contribute of the components to the signal norm.*

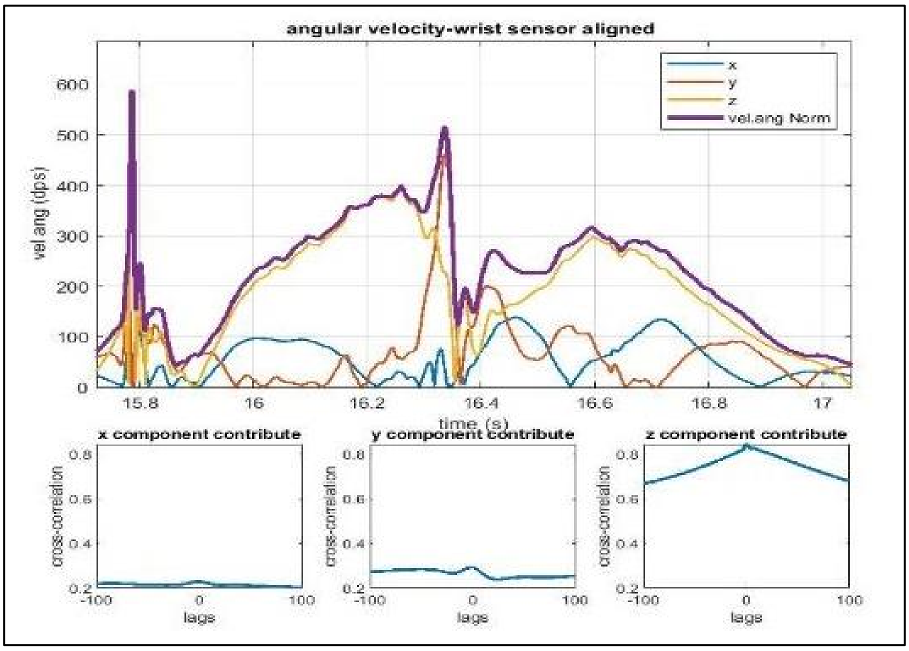

Figure 8 - Angular velocity norm and components contributes. Sensor aligned. *(Top)- The angular velocity norm from the wrist sensor is superimposed to the absolute value of the single components along the sensor axes. The sensor is in the condition aligned with the body segment. The plot shows a single cycle, and, on the left, it is possible to notice the spike caused by the pole hit while in the middle there is the peak caused by the pole lift. (Bottom)- The contribute of the components to the signal norm.*

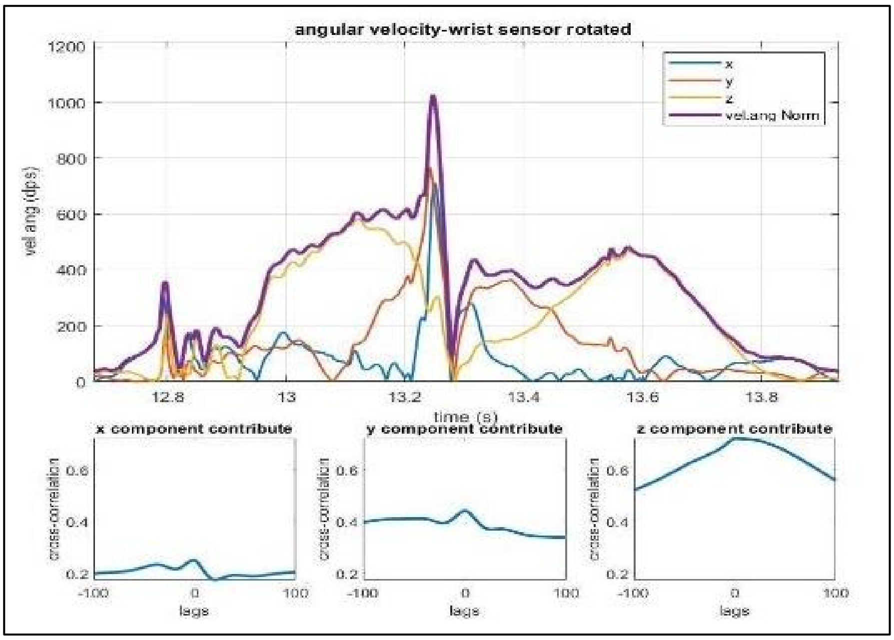

Figure 9 - Angular velocity norm and components contributes. Sensor rotated. *(Top)- The angular velocity norm from the wrist sensor is superimposed to the absolute value of the single components along the sensor axes. The sensor is in the condition rotated. The plot shows a single cycle, and, on the left, it is possible to notice the spike caused by the pole hit while in the middle there is the peak caused by the pole lift. (Bottom)- The contribute of the components to the signal norm.*

In the literature, the acceleration and angular velocity signal acquired with IMUs while skiing are often low pass filtered in the range of 1-4 Hz to yield the principal poling movement in the sagittal plane [16],[14],[19]. A spectral analysis was therefore conducted on the acceleration and angular velocity signals to verify if a filtering to prepare the signals to the successive cycle events identification was necessary.

The power spectral density (PSD) of the acceleration components along the 3 sensor axes was calculated for the wrist sensor and for all the trials where the sensors were aligned with the body segments (the first 6 trials). The PSD was calculated for each component with the Welch's method (500 samples hamming window, 50% overlap) with a theorical resolution of 1 Hz (calculated as the sampling frequency divided by the window length). The signal mean value was subtracted to the signal before performing the spectral analysis. The PSD square is then calculated and normalized dividing by its maximum value (this is done for each component) (Figure 10).

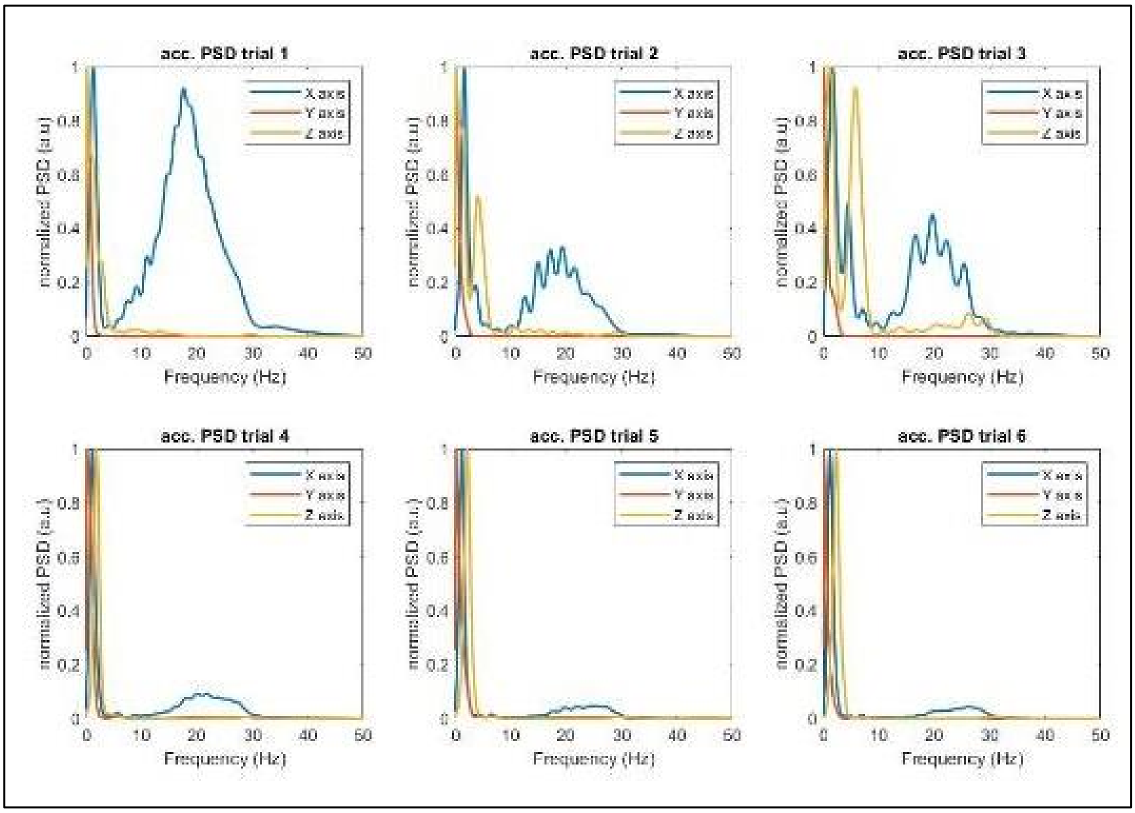

Figure 10 - Wrist sensor acceleration PSD. *The PSD is calculated for the condition "sensors aligned with the body segments", only for the wrist sensor. The first 3 trials are the ones when the treadmill is flat (1 deg) while the other 3 trials are the ones when the treadmill is inclined (6 deg).*

Analysing the normalized PSD for each trial it is possible to notice that the frequencies related to the poling gesture are mainly below 5 Hz; however it is also evident a peak, especially for the x component, between 10 Hz and 30 Hz, which is probably related to the high frequencies caused by the sensor vibration during the pole hit. Moreover, for the trial performed at 1 deg treadmill inclination (1st, 2nd and 3rd trials) there are some frequency components between 5 and 10 Hz while in the treadmill inclined condition they are there but less evident. The angular velocity PSD was calculated in the same way described above for the linear acceleration (Figure 11).

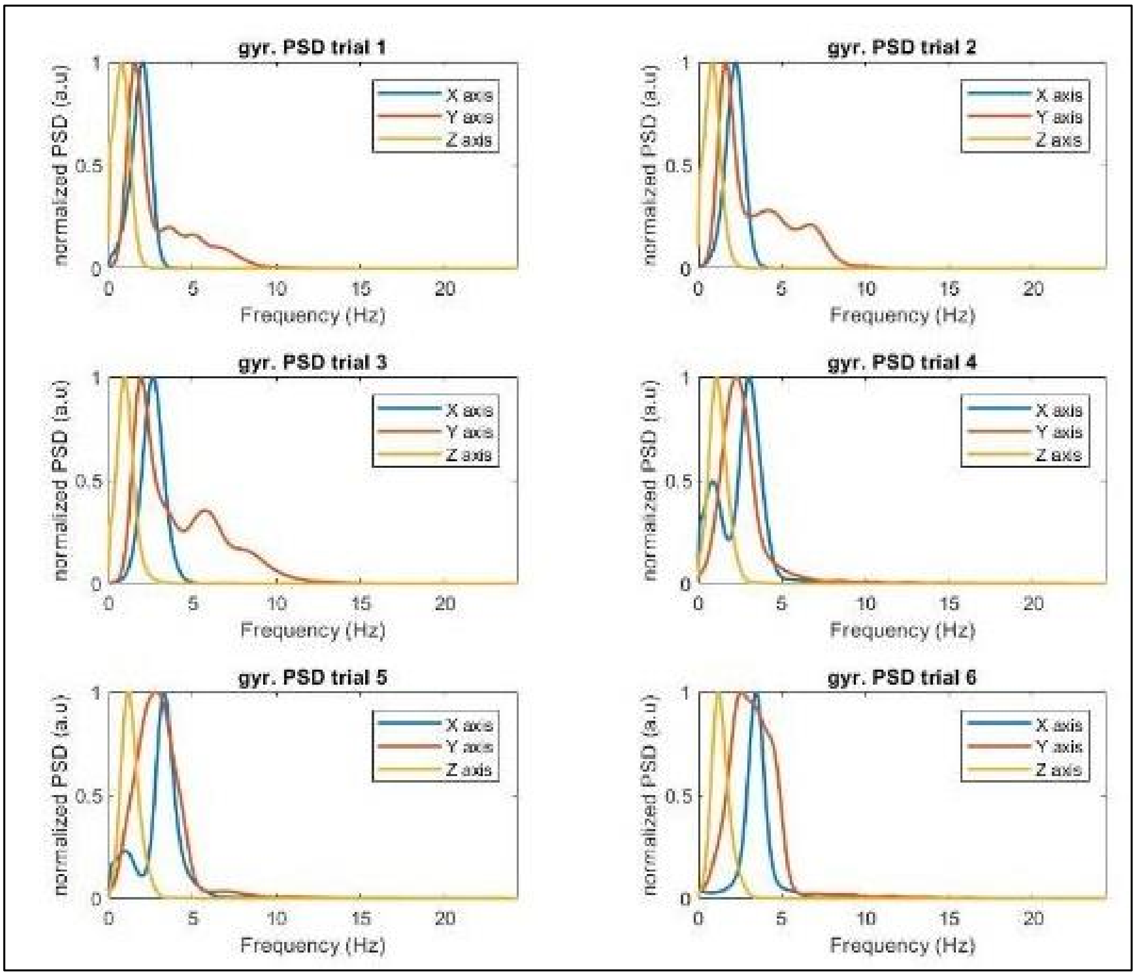

Figure 11 - Wrist sensor angular velocity PSD. *The PSD is calculated for the condition "sensors aligned with the body segments", only for the wrist sensor. The first 3 trials are the ones when the treadmill is flat (1 deg) while the other 3 trials are the ones when the treadmill is inclined (6 deg).*

Also for angular velocity most of the frequencies components are below 5 Hz, but this time there is not an evident peak at 20 Hz suggesting that the gyroscopes is less sensitive to the poles impacts. In the first 3 trial (1 deg treadmill inclination) there are some frequencies components between 5 Hz and 10 Hz for the Y component, while in the trials where the treadmill is inclined these components appear but less evident. From the picture that shows the angular velocity norm superimposed to the components along the sensor axes for the condition in which the sensor is aligned with the body segment (Figure 8), it is possible to notice that the peak after the spike caused by the pole hit is actually a fast rotation around the y axis (red signal contribute). This contribute is the one that has probably the frequencies components between 5Hz and 10Hz. This was verified filtering at 5 Hz and noticing the loss of the peak caused by that fast rotation around the y axis (Figure 12).

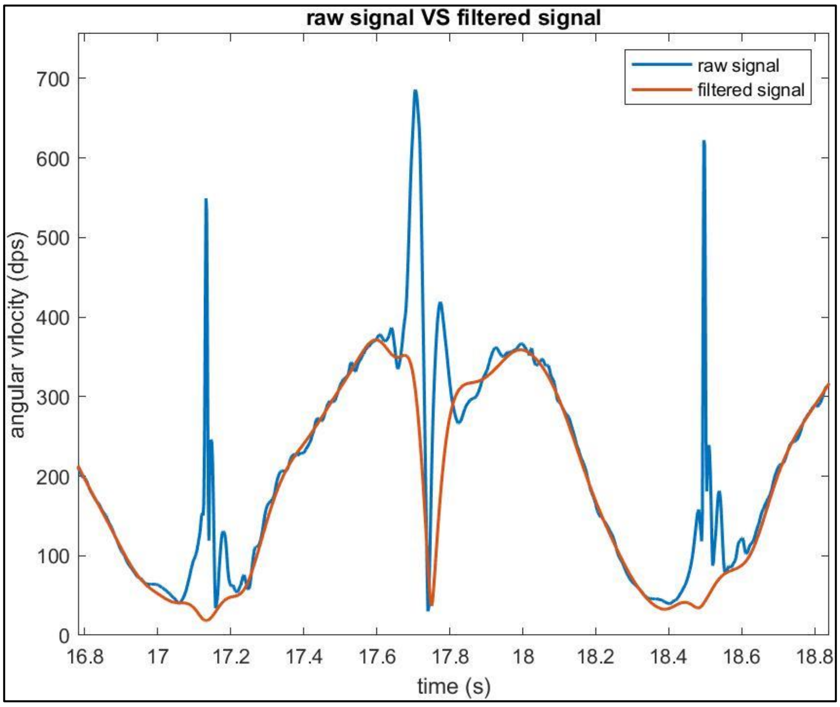

Figure 12 - Influence of a low pass filter on the wrist sensor angular velocity norm. *On the left and on the right there are the spikes caused by the pole hits (raw signal) and in the middle there is the peak associated to the lift. The red signal is the one low pass filtered (2nd order) with cutting frequency at 5 Hz. In this filtered signal the peak in the middle is attenuated.*

The analysis of the acceleration and angular velocity PSD (Figure 10, Figure 11) and of the pictures showing the signals norms superimposed to the signals components along the axes of sensing when the sensors are aligned with the body segments (Figure 6, Figure 8) suggest that:

- The gyroscope is less sensitive to the poles impacts and this is traduced in a very low PSD at high frequency and it is also noticeable from the ratio between the peak caused by the pole hit and the rest of the signal in the angular velocity norm (Figure 8). This ratio is clearly smaller than the corresponding one in the acceleration norm signal (Figure 6).
- The components between 5 Hz and 10 Hz in the angular velocity along the Y axis are probably caused by the fast rotation around the longitudinal axis of the wrist sensor (Figure 12).
- The last observation suggests that the frequencies components in the acceleration between 5 Hz and 10 Hz are again caused by the fast rotation around the Y axis that are traduced in a variation along the z and x axis acceleration.

From all these observations the following thoughts raised:

- Filtering the signals with a high pass filter at 20 Hz could highlight only the components related to the poles impact and help in the hits detection.
- Since the main poling gesture frequency components are mainly below 5 Hz it could be possible filter the signals at 5 Hz or even lower to obtain a smoothed pattern of the poling gesture filtering out faster movements; however some movements during the poling cycles like fast twist of the wrist along the forearm mediolateral axis which have frequency components higher than 5 Hz could contribute importantly to the signals norm pattern used to identify the pole lifts, therefore it may be better identify the lifts events directly from the raw signals avoiding any filtering.

4.1.2 Synchronization of the IMUs system with the reference system

The signals acquired with the Coachtech system (videos, pole forces and treadmill speed) were automatically synchronized among them and the IMUs data from the 6 sensors were aligned among them. However, the signals acquired with Coachtech and the IMU signals were not synchronized, hence the reason a synchronization was needed. The fact that the two systems were not synchronized is visually showed reporting the force signals acquired with Coachtech and the acceleration norm calculated from the acceleration components of the wrist sensor (Figure 13).

To perform the synchronization, a hit on the ground with the right pole was performed at the beginning of each trial. The hit caused a spike in the force signal and in the wrist sensor acceleration norm. The samples corresponding to these spikes were identified with a peak analysis and were set as the start samples for both the IMUs signals and the force signals resulting in an alignment of the two signals starts. To also align the end of the signals from the two different systems (which now start at the same time) the IMUs signals were cut so that they had the same length of the corresponding force signals (Figure 14).

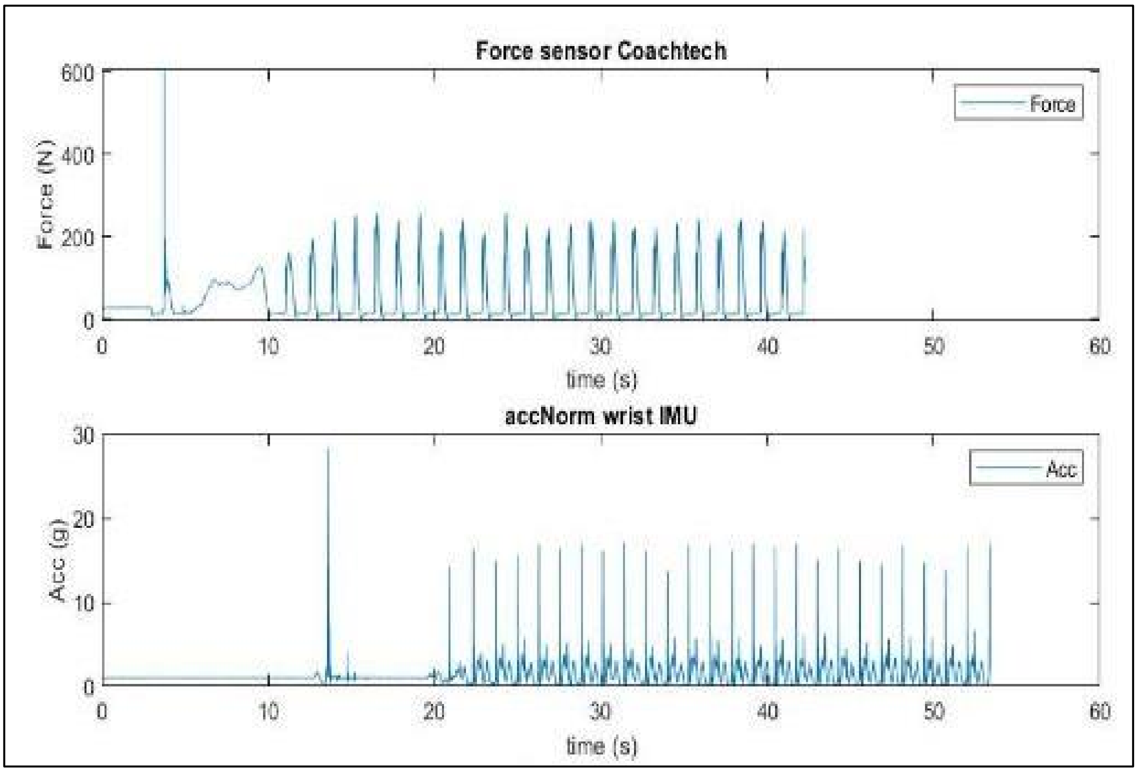

Figure 13 - Acquisition systems not synchronized. *The force signal from the Coachtech system and the wrist sensor acceleration norm from the IMUs system are not synchronyzed. It's evident from the first spike in both the signal which is not aligned.*

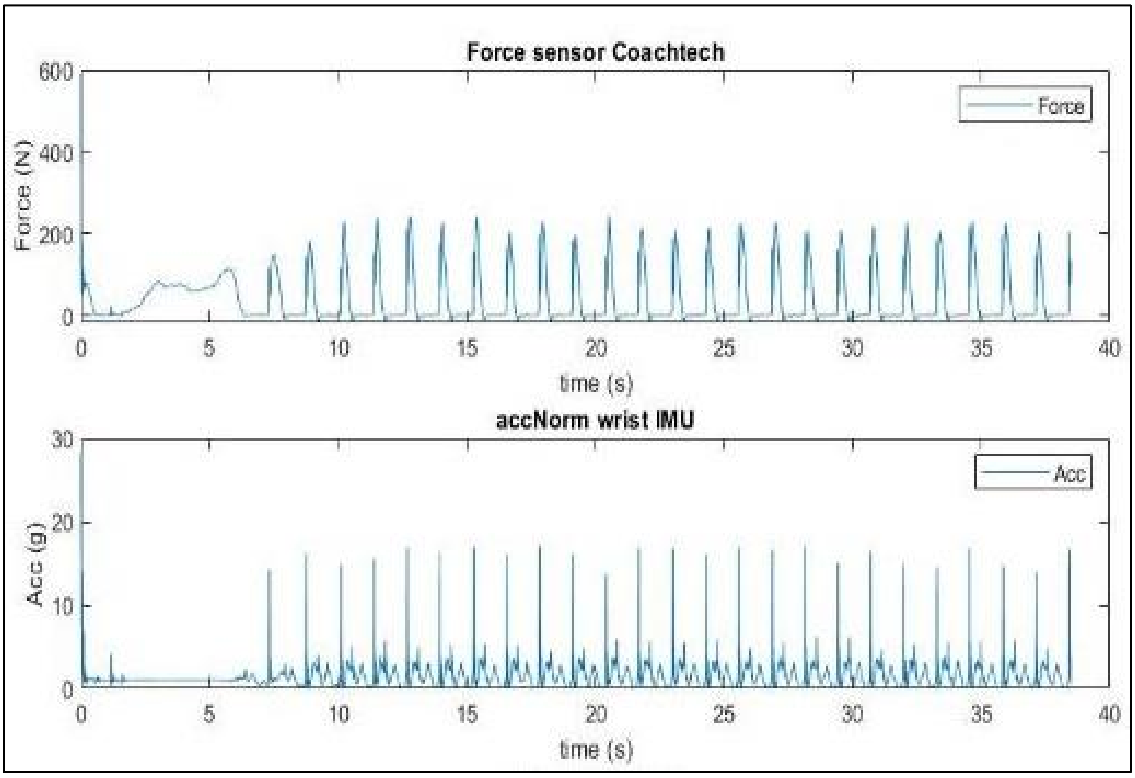

Figure 14 - Acquisition systems synchronized. *The force signal from the Coachtech system and the wrist sensor acceleration norm from the IMUs system are now synchronyzed. The spikes due to the pole hit at the beginning of thetrial are now aligned and the signals have the same number of samples.*

The peak analysis to identify the first spike in the signals was performed as described below:

- For the force signals: the peaks that are at least as high as the 20% of the maximum value in the signal are selected and the first peak identified is set to be the spike caused by the synchronization pole hit.
- For the wrist acceleration norm signal: the peaks that are at least as high as the 40% of the maximum value in the signal and that are away from each other at least 600 ms are selected and the first peak identified is set to be the spike caused by the synchronization pole hit.

4.1.3 Identification of the beginning of the treadmill's constant speed

The treadmill takes a few seconds to reach the desired speed. In this period the skier starts skiing and performs some poling cycles that are recorded by the IMUs (Figure 15).

However, this few cycles need to be excluded from the analysis because performed at a speed that is not the one selected at the beginning of the trial and the cycle parameters calculated from these cycles would not be representative of that particular trial. To recognize the sample corresponding to the beginning of the treadmill constant speed the first peak that is at least as high as the 90% of the maximum signal was identified.

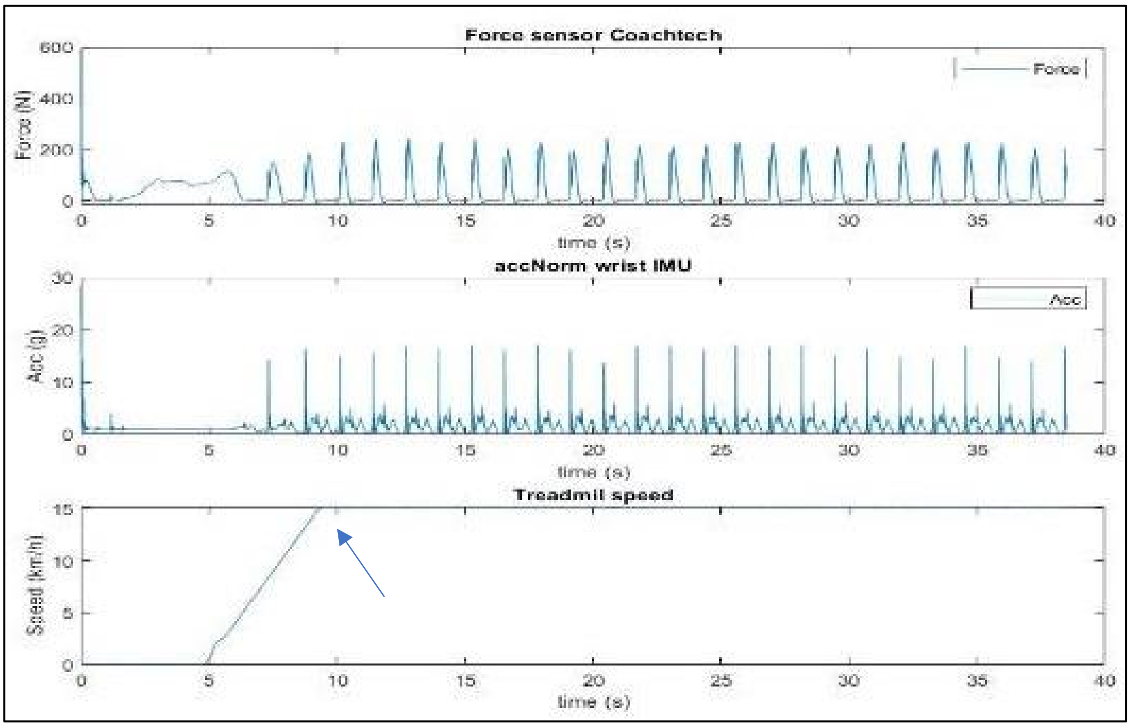

Figure 15 - Beginning of the treadmill constant speed. *The arrow shows the beginning of the treadmill constant speed in the speed signal. Comparing the speed signal with the force signal and the wrist sensor acceleration norm, some cycles are clearly before the beginning of the constant speed.*

4.1.4 IMUs calibration

When the IMUs signals are used to identify some particular pattern or some particular instants (i.e. spikes, peaks) to relate them to some kind of event (i.e. pole hit, pole lift) a calibration is not always performed [13]. On the other hand, a calibration is important to reduce the drift errors when the IMUs signals are integrated to study the sensors linear velocity and displacement (linear acceleration integration) or the sensor rotation (angular velocity integration) [25]. In this study the IMUs signals were integrated only in two occasions: (1) to calculate the ski velocity and displacement integrating respectively one and two times the acceleration signal of the ski IMU along the ski longitudinal axis, and (2) to calculate the ski inclination on the treadmill integrating the ski angular velocity around the ski medio-lateral axis. The static calibration was performed to evaluate the influence of a calibration on the drift errors when the signals were integrated.

The IMUs calibration was performed similarly to Ferraris et al 1995 [24]. In this paper, the authors present some mathematical models of the signals acquired with an IMU, which consider the most common acquisition errors. In particular, the above-mentioned models allow to correct the accelerometer offset, sensitivity and axes misalignment and the gyroscope offset, sensitivity, axes misalignment and acceleration sensitivity. However in this study, for the angular velocity model was considered only the part of the model which allows to correct the offset because correcting the axes misalignment and the sensitivity would have required also some acquisition rotating the sensors around each axes and calculating the rotation angles integrating the angular velocity, and this would have made the procedure more complicated without remarkable advantages since the main source of drift (the calibration here is done to reduce the drift) is brought by the offset error [11].

Accelerometer model

As reported in Ferraris et al 1995 [24], a 3D accelerometer can be described by the Eq.1 where u_a is the output vector of the 3D accelerometer containing the acceleration sensed by the 3 sensor axes, K_a is the diagonal matrix of the scale factors (to correct the acceleration sensitivity), R_a is the orientation matrix (to correct the axes misalignment), a is the vector of the real 3D sensor acceleration and b_a is the vector of the senso offset. If the Eq.1 is written expressing a which is what we seek (Eq.2), the unknown variables to calculate are K_a, R_a, b_a because u_a is known since is the one acquired with the sensor.

$$u_a = K_a \cdot R_a \cdot a + b_a \tag{1}$$

$$a = R_a^{-1} \cdot K_a^{-1} \cdot (u_a - b_a) \tag{2}$$

The accelerometer offset can be estimated defining U_{a+} (Eq.3) as the matrix which contains the outputs of the 3D accelerometer when each of the 3 axes is parallel to g and points up, grouped into columns and U_{a-} (Eq.4) as the matrix which contains the outputs of the 3D accelerometer when each of the 3 axis is parallel to *g* and points down, grouped into columns.

$$U_{a+} = K_a \cdot R_a \cdot g + B_a \tag{3}$$

$$U_{a-} = K_a \cdot R_a \cdot (-g) + B_a \tag{4}$$

In the equations (Eq.3, Eq.4) *g* is the gravity magnitude, B_a is a 3x3 matrix containing the bias estimation of each accelerometer obtained in the different positions (used to define U_{a+} and U_{a-}) and the terms of interest for this study are on the diagonal and they are the bias for each axis when they are parallel to the gravity. Defining U_{as} as the sum of U_{a+} and U_{a-},

$$U_{as} = U_{a+} + U_{a-} \tag{5}$$

B_a can be expressed as:

$$B_a = \frac{1}{2} U_{as} \tag{6}$$

Remembering the definitions of U_{a+} and U_{a-} and defining U_{aD} as the difference between U_{a+} and U_{a-}

$$U_{ad} = U_{a+} - U_{a-} \tag{7}$$

U_{aD} can be written as:

$$U_{aD} = 2gK_a \cdot R_a \tag{8}$$

Inverting this equation (Eq.8) is possible to obtain:

$$K_a \cdot R_a = \frac{1}{2g} U_{aD} \tag{9}$$

Remembering that the rows of Ra are unit vectors (R_a is an orientation matrix) K_a can be expressed as:

$$\begin{bmatrix} K_{a,\sigma}^2 \\ K_{a,\mu}^2 \\ K_{a,\tau}^2 \end{bmatrix} = diag[(K_a \cdot R_a)(K_a \cdot R_a)^T]\frac{1}{2g}U_{aD} = \frac{1}{4g^2}diag[U_{aD} \cdot U_{aD}^T] \tag{10}$$

$$K_a = \begin{bmatrix} K_{a,\sigma} & 0 & 0 \\ 0 & K_{a,\mu} & 0 \\ 0 & 0 & K_{a,\tau} \end{bmatrix} \tag{11}$$

Since now K_a is known, expressing R_a from the Eq.9 is possible to also obtain R_a.

Gyroscope model

A 3D gyro can be described by the equation:

$$u_g = \omega + b_g \tag{12}$$

Where u_g is the output vector of the 3D gyro, ω is the vector of the real 3D angular velocity and b_g is the sensor bias. Writing the equation (Eq.12) as:

$$\omega = u_g - b_g \tag{13}$$

is possible to obtain the actual 3D angular velocity ω if the bias b_g is calculated.
The gyro bias can be obtained considering that if we are in a steady condition then:

$$u_g = b_g \tag{14}$$

However, the gyro bias has also a drift over time and should be written as:

$$b_g(t) = b_{g0} + b_{g1}t \tag{15}$$

where b_{go} is the gyro output during a steady condition before the experiment and b_{g1} is the output during the steady condition after the experiment.

4.2 Cycle events identification

The cycle events (poles hits and poles lifts) are essential to calculate the cycle spatio-temporal parameters because they mark respectively the beginning and the end of each cycle phase (paragraph 1.1). The identification of the cycle events was firstly performed based on the force signals to obtain the reference events and then they were calculated based on the IMUs signals to obtain the hits and the lifts that will be compared with the reference events to evaluate the accuracy and the precision of the IMU-based identification. To identify the cycle events from the IMUs signals three methods were developed:

- Acceleration norm-based method
- Angular velocity norm-based method
- A "fusion" method which merges the identification of the previous two methods.

These three algorithms were developed analysing the signals from the wrist sensor, but they were implemented for all the sensor on the upper limb to evaluate the robustness of the algorithm to different positions.

4.2.1 Cycle events identification from the reference system

The force signal represented the reference signal to identify the cycle events (poles hits and lifts). When the poles hit the ground a spike rises in the force signal, then a force is exerted while the poles are in contact with the ground (push phase) that allows the athlete to generate propulsion, then when the poles are lift from the ground a null force is expected. However, the piezoelectric sensor embedded in the poles grip was sensitive also to the pole inertial force so that the fast rising of the arms was traduced as a negative force in the force signal.

In the force raw signals, a bias was evident, highlighting problems during the force bias correction that was performed before the trials (see protocol chapter) (Figure 16). This bias was then compensated considering that during the periods when the poles does not touch the ground the force recorded should be zero. In particular, a window between each negative peak and each spike in the force signal was selected. All these windows were associated to the moments when the poles do not touch the ground. The mean value over all the identified windows was considered the bias and was therefore subtracted to the raw force signals to obtain the unbiased signals (Figure 17).

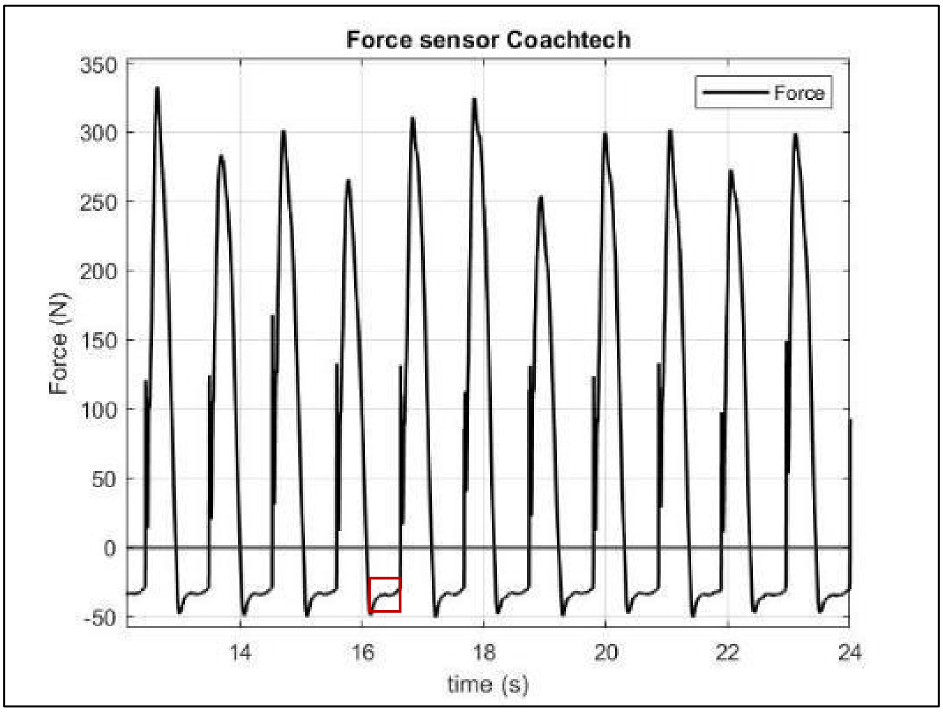

Figure 16 - Force raw signal in which is evident a bias. *In the force signals recorded is evident a bias since the force should be positive. The red rectangle highlights a period where the poles do not touch the ground and the force is expected to be zero.*

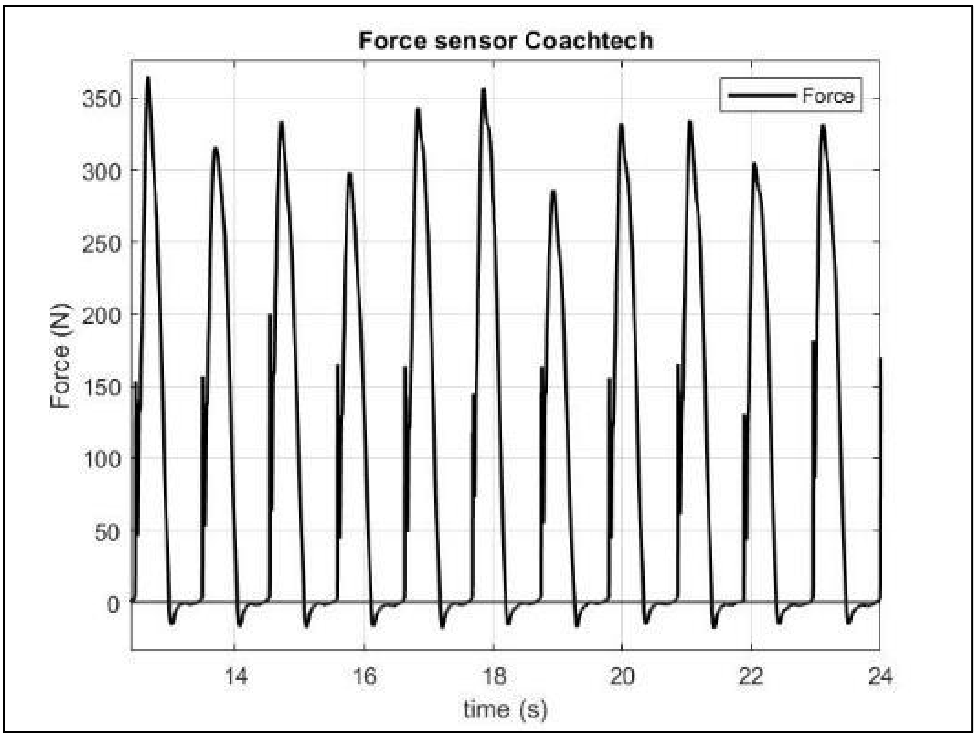

Figure 17 - Force signal unbiased. *The bias in the force signal is corrected. It is possible to see that the zero line lies on the periods where the force is expected to be zero. The negative values in the force are caused by the inertia during the sudden rising of the poles at the end of each poling cycle.*

Once the bias was corrected, an approximative identification of the cycle events (hits and lifts) was performed as follow:

- Firstly, the negative peaks in the signal were identified: the force signals considered as a function of time is translated over the zero values adding the signal minimum value, then the signal is overturned with respect to the zero line. The samples corresponding to the negative peaks are identified recognizing all the peaks in the overturned signal which are at least as high as the 90% of the signal maximum value, that are away from each other at least 680 ms. These negative peaks were associated to the pole lifts.
- Secondly, the spikes caused by the pole impacts were identified: in the force signal, a window between each negative peak previously identified, is selected and the first peak which is at least as high as the 20% of the maximum value of the force signal in that window is considered the spike of interest and is associated to a pole hit.

The above described identification was considered an approximative identification because the actual hit is expected to be at the bottom of the spike and not on the top and the negative peaks are actually caused by the sudden rising of the poles which happens slightly after the actual pole lift. A more accurate cycle events identification was therefore performed starting from the raw identification as described below:

- Hits fine identification:
    - A window in correspondence of each raw hit identified is defined with the upper limit as the sample corresponding to the raw hit and the lower limit 170 ms before the same raw hit sample.
    - The signal in this window is smoothed with a moving window which calculate the average over 12 samples each sliding step. The smoothing decreases the variability in the part where the force is expected to be zero.
    - The difference of each pair of samples in the window defined above is calculated and they represent the signal increment each 2 ms (the sampling frequency was 500 Hz).

- The first increment which is higher than the 99 percentiles of the all increments is considered the sample at the bottom of the spike.

- Lifts fine identification:
    - A window is defined between each pair of raw events (raw hit and raw lift).
    - The samples closer to zero in each of these windows are considered the actual lifts.

The raw and more accurate cycle events identification is shown for a few cycles (Figure 18) and for a cycle (Figure 19) in the pictures below.

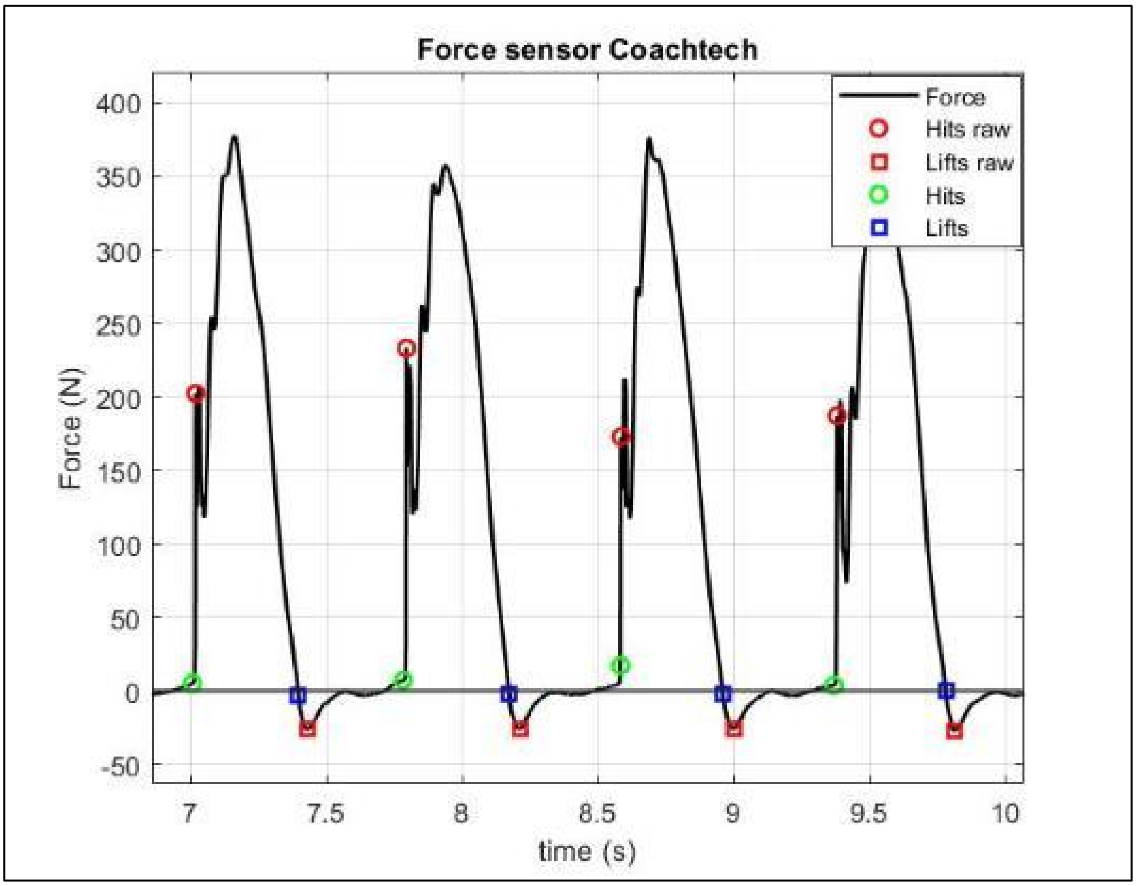

Figure 18 - A few cycle events identified from the force signal.

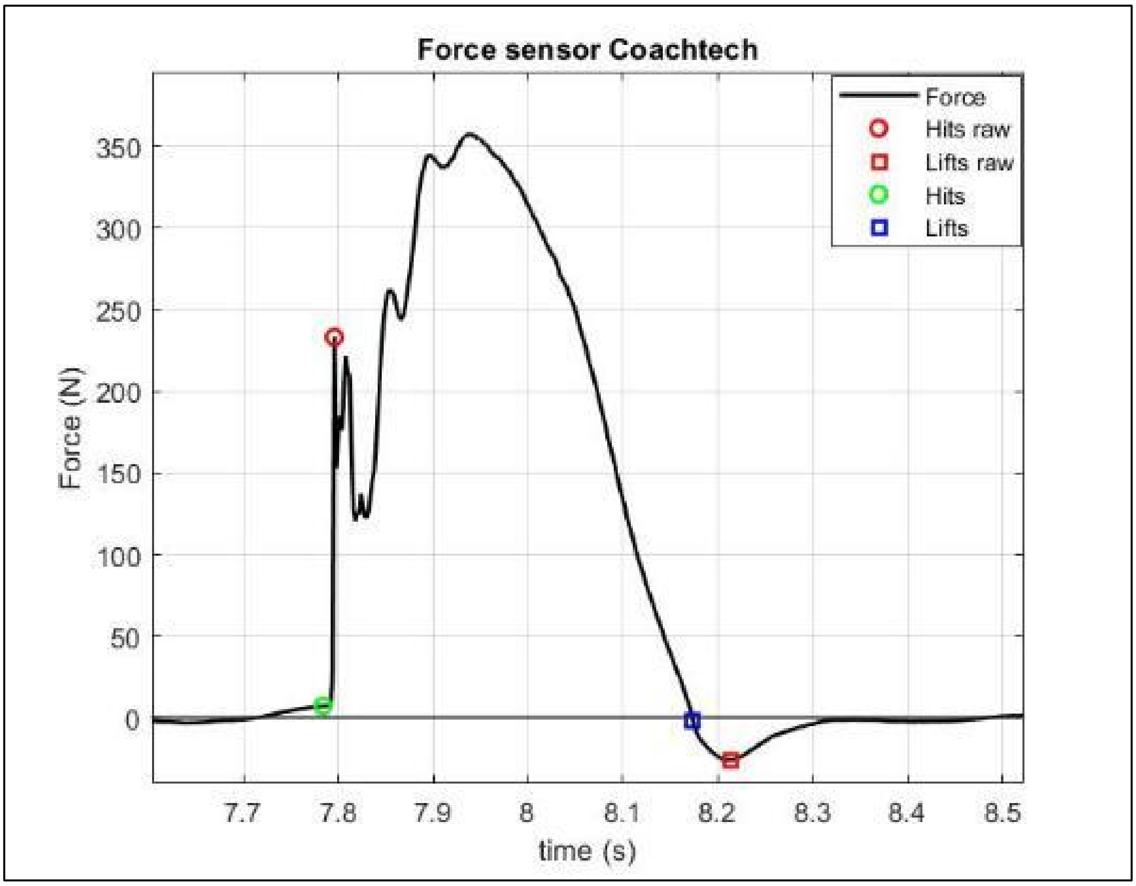

Figure 19 - Cycle events identification from the force signal: macro on a single cycle.

4.2.2 Cycle events identification from the IMUs system

Different algorithms have been developed to find the optimum strategy to identify the cycle events from the IMUs signals. An algorithm uses the acceleration norm similarly to how described in Fasel et al. 2015 [7]. In this article [7], the poles cycle events identification is validated for this method for a sensor applied on the pole and for a diagonal stride skiing technique. Another algorithm inhere tested is based on the angular velocity norm. A third algorithm evaluated in this thesis merges the identifications from both the angular velocity norm and the acceleration norm, in particular, it identifies the hits from the acceleration norm and the lifts as the mean of the lifts identified by the acceleration method and the angular velocity method.

Acceleration norm-based method

When the pole hits the ground it provokes a spike in the acceleration norm signal due to the sensor vibration during the impact, while when the pole is lifted from the ground the acceleration norm shows a peak caused by the sudden rising of the arm.

The cycle events identification performed with this method is described below.

Hits identification

The raw signals are filtered with a high pass filter to highlight only the high frequency related to the pole ground impacts (Figure 20,Figure 21). A second order high pass filter with a cutting frequency at 20 Hz is therefore applied to the acceleration components and the acceleration norm is calculated again using the filtered components (Figure 20).

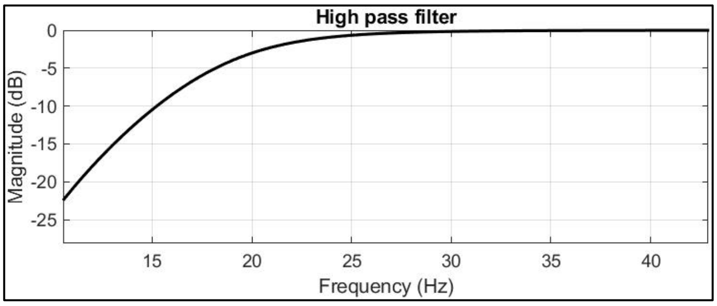

Figure 20 - Acceleration high pass filter mask. *The attenuation in dB, as function of the frequency is reported.*

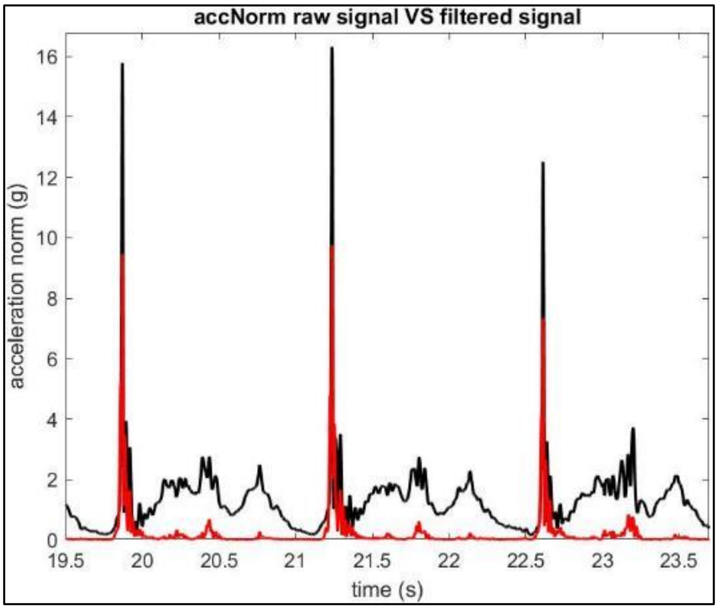

Figure 21 - Effect of the high pass filter on the acceleration norm. *The acceleration norm filtered (red) is superimposed to the raw signal (black).*

The hits peaks in the filtered acceleration norm (red signal in Figure 21) are identified with a peak analysis which selects all the peaks that are at least as high as the 10% of the maximum value assumed by the filtered signal and that are at least 680 ms away from each other (Figure 22).

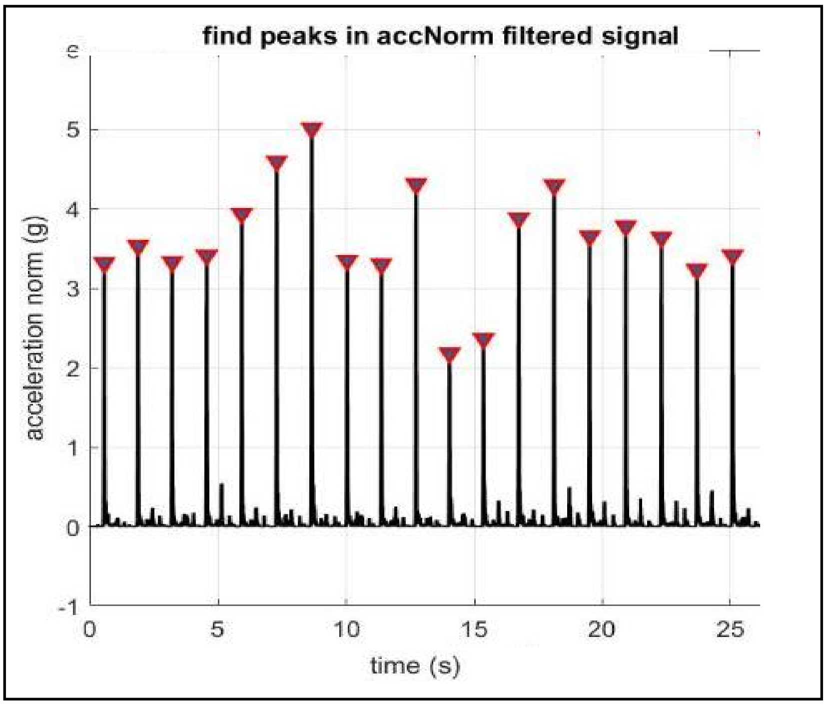

Figure 22 - Hits identification in the filtered acceleration norm. *The peaks corresponding to the pole hits are identified in the high pass filtered acceleration norm.*

The peaks base, which correspond to the hits, is identified working with the raw acceleration norm, considering a window for each peak, with the sample 10 ms away from the hit peak as upper limit and the signal sample 20 ms away from the same hit peak as the lower limit. In this window the signal is smoothed with a 5-sample sliding window. The increment for each sample is then calculated and the first increment which is higher than the 88 percentiles of all the increments is considered to be the peak base.

Lifts identification

A window between each pair of hits previously identified is selected in the raw signal. Each of these windows is large the 80% of the time interval between two consecutive hits and is centred in this interval. The highest peak in each of these windows is considered the pole lift instant (Figure 23).

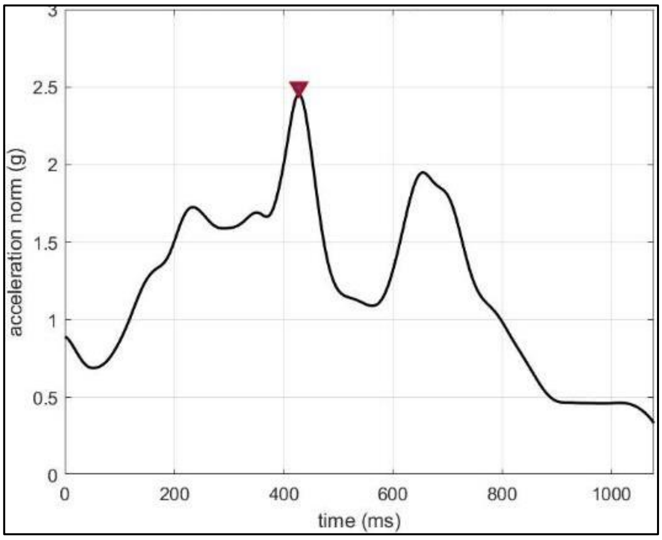

Figure 23 - Lift identification between two hits. *The peak corresponding to the pole lift is identified in a window between two hits. The higher peak in this window is the one associated to the pole lift.*

The cycle events are identified for all the trials and for all the sensors on the upper limb, and the algorithm developed allows to visualize the acceleration norm and the cycle events selecting a subject, a sensor and a trial. An example of the automatic events identification for a few cycles (Figure 24) and for a single cycle (Figure 25) are showed below.

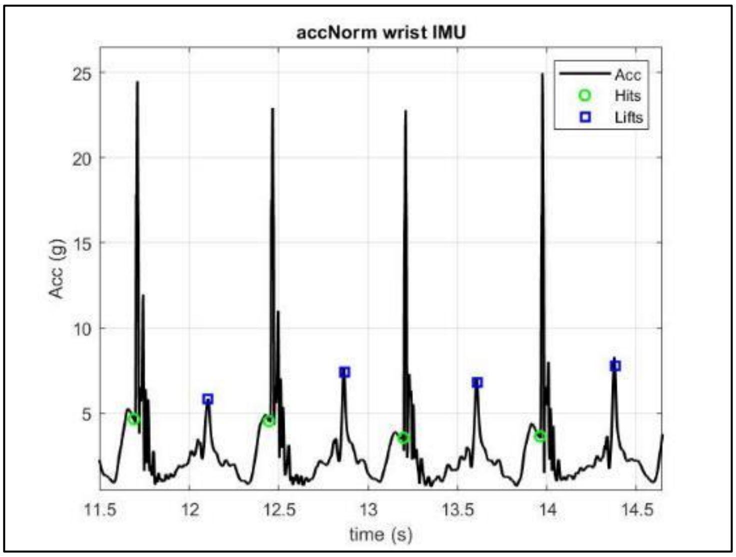

Figure 24 - Cycle events identification with the acceleration norm-based method: macro on a few cycles. *The cycle events identification algorithm identifies the pole hits and lifts and plot them on the acceleration norm signal.*

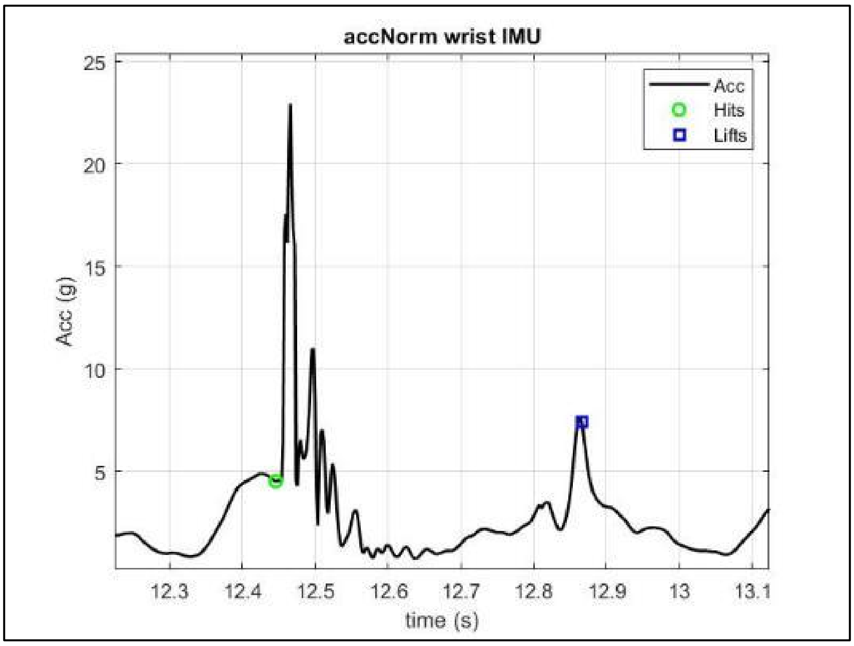

Figure 25- Cycle events identification with the acceleration norm-based method: macro on a single cycle.

Angular velocity norm-based method

When the pole hits the ground, it provokes a spike also in the angular velocity norm even if it is less evident than in the case of the acceleration norm. When the pole is lifted from the ground if we would look only at the absolute value of the angular velocity component around the mediolateral axis we would expect the signal have a minimum approximately in zero. However, but we are working with the angular velocity norm, which keeps into account all the components and in proximity to where the above mentioned minimum would be expected, in the signal from the wrist sensor, there is a peak instead, caused by a fast twist of the forearm around its longitudinal axis (Figure 8, Figure 9, Figure 26). In the signals from the other sensors (for example arm distally) there is still a peak in the signal but is related to the max angular velocity reached during the pushing phase which happens before the pole lift (Figure 26). However, as said before the algorithms where developed starting from the wrist sensor signals and then applied to the other sensors to investigate the robustness of the algorithm to different positions.

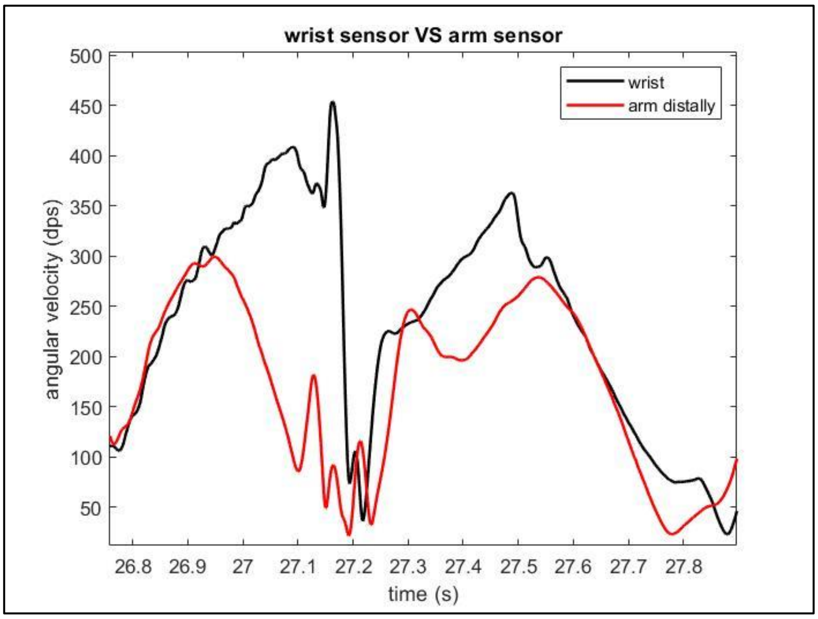

Figure 26 - Wrist and arm sensor angular velocity norm comparison. *The signal from the wrist sensor (black) has a peak related to a fast wrist twist around the forearm longitudinal axis. The signal from the arm does not have this peak because obviously the wrist twist is not sensed by a sensor on the arm. There still a peak in the signal from the arm sensor, that is however probably related to the maximum angular velocity during the pushing phase.*

The cycle events identification performed with this method is described below.

Hits identification

The raw signals are filtered with a high pass filter to highlight only the high frequency related to the pole ground impacts. A second order high pass filter with a cutting frequency at 20 Hz is therefore applied (Figure 27,Figure 28) .

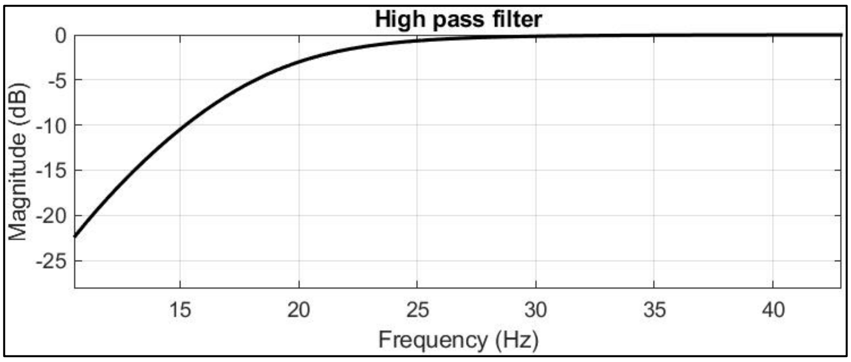

Figure 27- Angular velocity high pass filter mask. *The attenuation in dB, as function of the frequency is reported.*

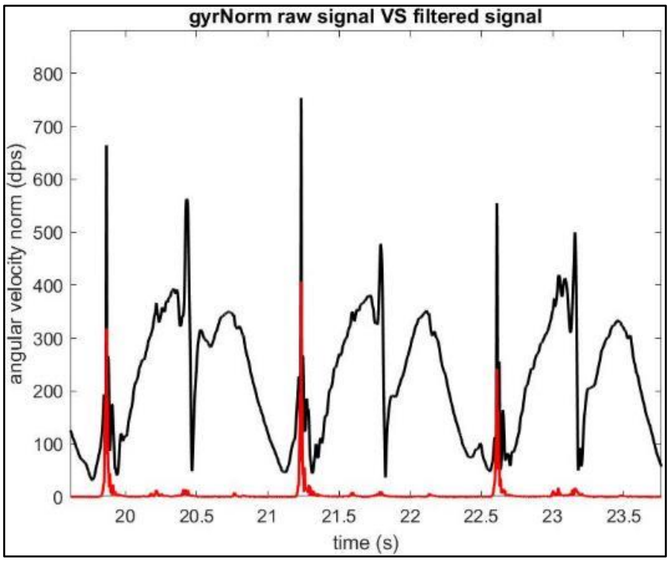

Figure 28 - Effect of the high pass filter on the angular velocity norm. *In black the unfiltered signal. In red the high pass filtered signal.*

The hits peaks in the filtered signals are identified with a peak analysis which selects all the peaks that are at least as high as the 10% of the maximum value assumed by the filtered signal and that are at least 680 ms away from each other (Figure 29).

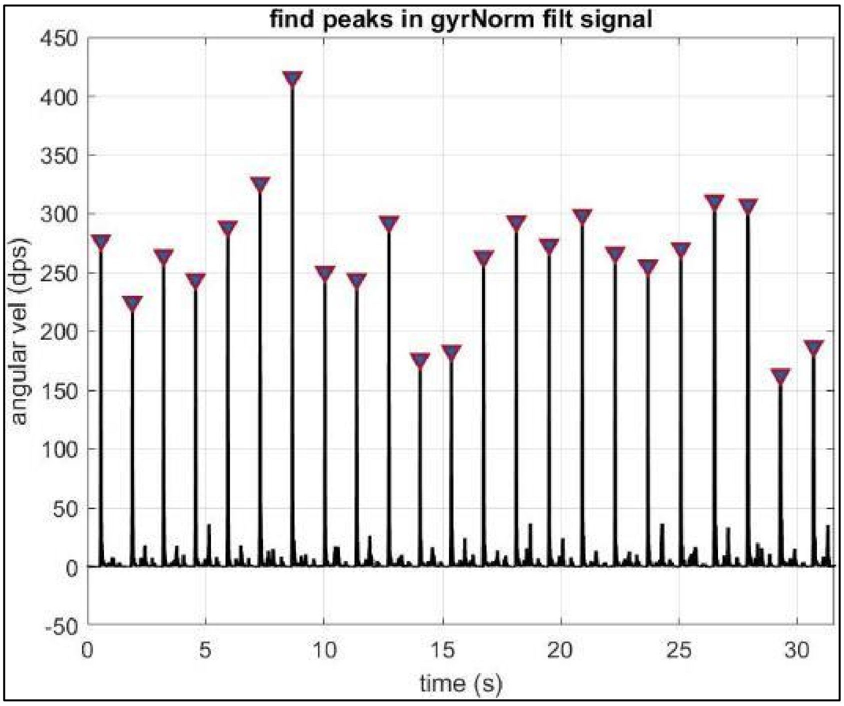

Figure 29 - Hits identification in the filtered angular velocity norm. *The peaks corresponding to the pole hits are identified in the high pass filtered signal.*

Lifts identification

A window between each pair of hits previously identified is selected in the angular velocity raw signal. Each of these windows is large the 80% of the time interval between two consecutive hits and is centred in this interval. The peaks that have a prominence of at least 100 dps and that are at least 440 ms away from each other are identified in each window and the first peak of them is selected to be the pole lift. (Figure 30).

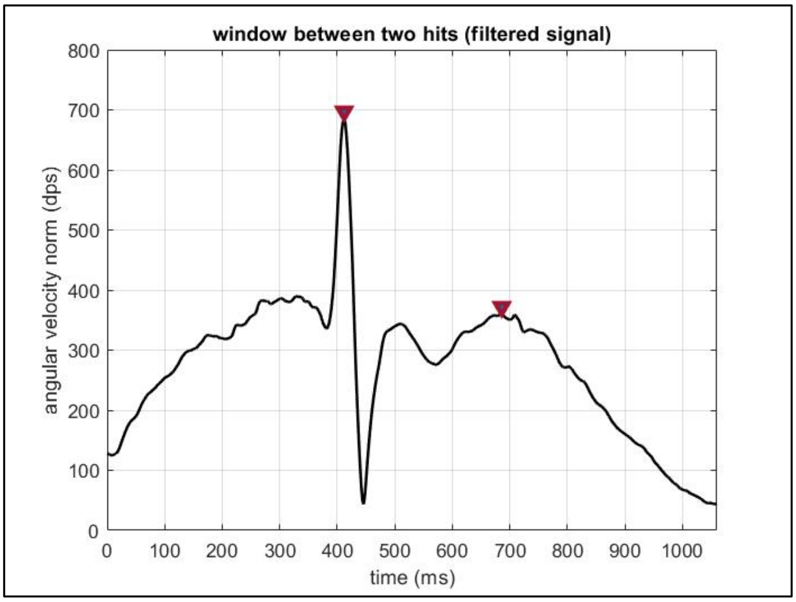

Figure 30- Lift identification between two hits in the raw angular velocity norm. *The peak analysis identifies two peaks. The first one is selected as pole lift.*

The cycle events are identified for all the trials and for all the sensors on the upper limb, and the algorithm developed allows to visualize the angular velocity norm and the cycle events selecting a subject, a sensor and a trial. An example of the automatic events identification for a few cycles (Figure 31) and for a single cycle (Figure 32) are showed below.

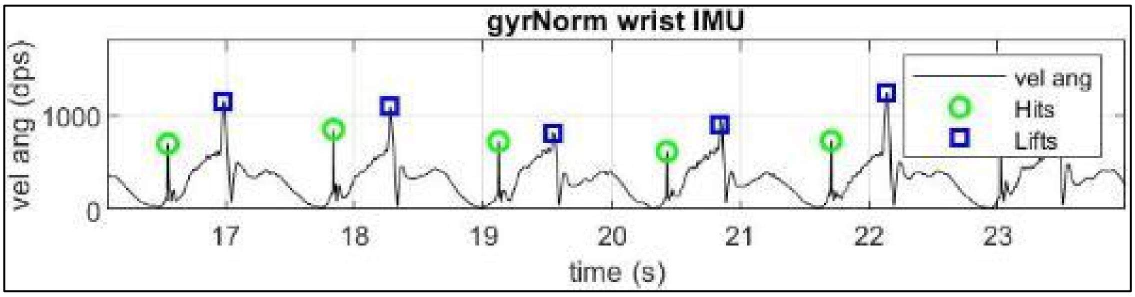

Figure 31 - Cycle events identification with the acceleration norm-based method: macro on a few cycles.

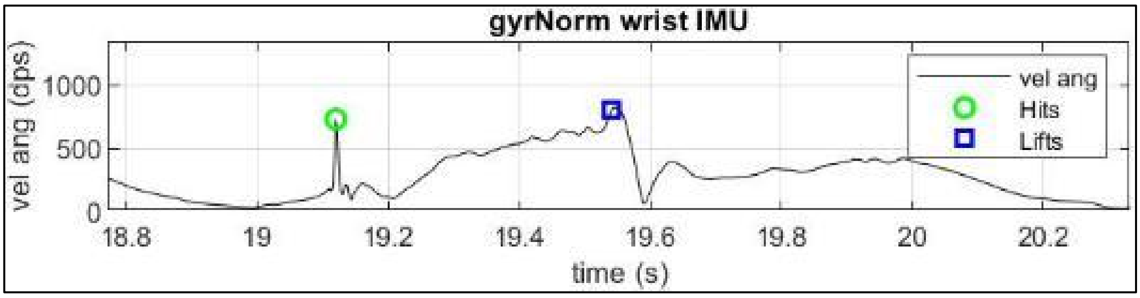

Figure 32 - Cycle events identification with the acceleration norm-based method: macro on a single cycle.

Fusion method

This method includes two versions and was developed considering the two previous methods performances (see the results chapter) and in particular after the following observations:

- The identification of the hits with the acceleration norm-based method is more precise than the one based on the angular velocity norm.
- The angular velocity norm-based method (from the wrist sensor) identifies the pole lifts more precisely than the acceleration norm-based method.
- The acceleration norm method tends to overestimate the lift identification (identify the lifts slightly later than the reference system) while the angular velocity norm-based method is inclined to underestimate the lift instants (identify the lifts slightly later than the reference system) especially when the treadmill is inclined and with the sensor placed more proximally on the upper limb.

Therefore, this method merges the identifications of the two previous methods as described below:

- First version:
    - The hits are recognized in the same way of the acceleration norm-based method.
    - The lifts are recognized in the same way of the angular velocity norm-based method.
- Second version:
    - The hits are recognized in the same way of the acceleration norm-based method.
    - Each pole lift instant is defined as the mean of the lift identified by the acceleration norm-based method and the corresponding lift identified by the angular velocity norm-based method.

4.3 Wrong cycles identification

The cycles detection based on the force signal is considered as the reference. A visual inspection of the identification plot based on the force signal (Figure 33) for each trial of each subject has been done to ensure the correspondence between the cycles performed in the reality and the ones detected by the algorithm. Since from these force signal plots is relatively easy to notice a possible mistake in the identification, a further check based on the video recording was considered unnecessary.

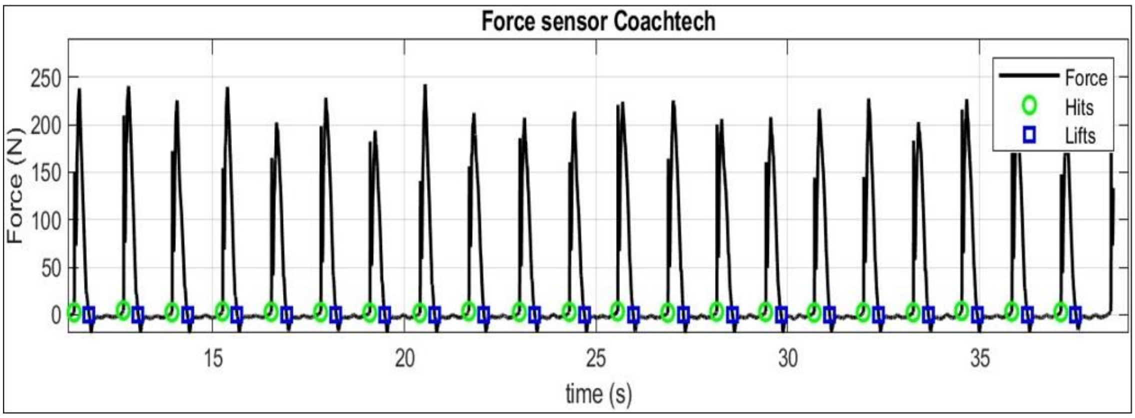

Figure 33 – example of cycle events identification based on the force signal. *The events identified represents the reference events. This type of plot can be visualized for each trial of each subject and it makes easy to identify an error in the events detection.*

Concerning the IMUs signals, the algorithms used to recognise the pole hits and the pole lifts can make mistakes in the identification. In particular, these mistakes can be missing cycles or overestimated cycles (identify a cycle when there is not) (Figure 34). The recognition of these mistakes is necessary to calculate the percentage of cycles correctly detected by the algorithms and to pair the cycles identified by the reference system with the ones identified from the IMUs signals. The correct cycles pairing is essential to calculate the time errors in the cycle events identification (i.e. $Time\_hit_{reference} - Time\_hit_{IMU}$).

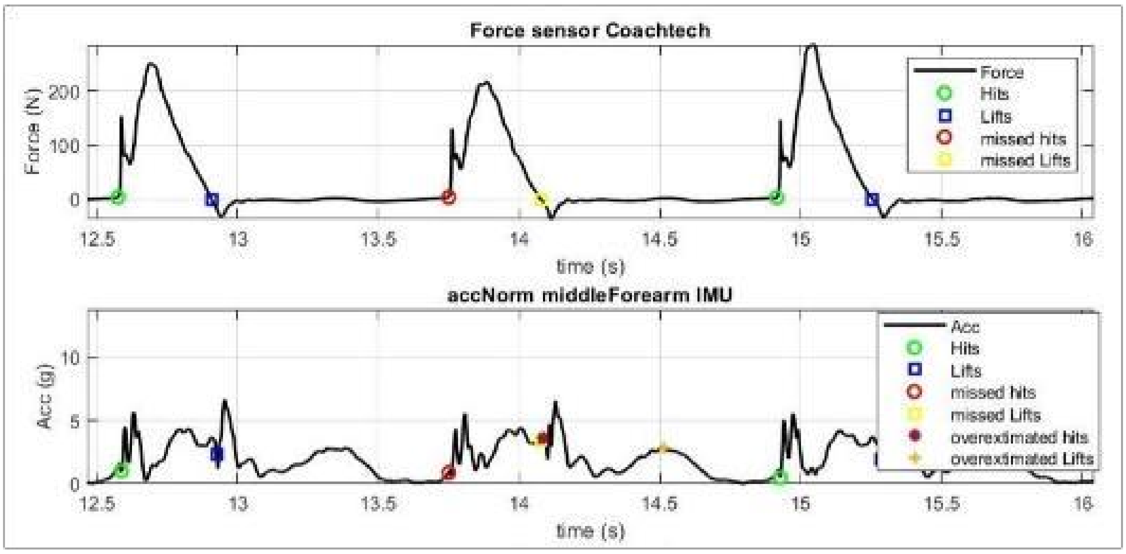

Figure 34 – Example of wrong cycles recognition. *The algorithm automatically highlights the cycles missed by the identification methods based on the IMU signals, in the reference signal and in the IMU signal. The overestimated cycles are represented only in the IMU signal. In this example a missed cycle is followed by an overestimated cycle and to be precise the overestimation is the cause of the missed cycle, but there could be cases when these two errors are not paired.*

4.3.1 Algorithm description

The hits and lifts identification methods based on the IMUs signals start from the hits identification and then they identify the lifts between each pair of identified hits, ensuring a lift recognition between two hits (paragraph 4.2.2). In other words, only the hits are needed to identify a cycle and hence the wrong cycles algorithm can be designed working on the hits solely.

For each hit identified with the reference system (force signal), the wrong cycles algorithm looks for a match among the hits identified with the IMUs system checking if the temporal difference between the two events is less than 80 ms. If this condition is not satisfied that cycle is considered missed. A similar logic is applied to find out the overestimated cycles, but this time the algorithm checks a match for each hit identified from the IMU signals among the reference hits. The threshold difference between the two hits is still 80 ms (Figure 35). The 80 ms threshold was chosen considering that it was short enough to not include another event identification (lift of the same cycle or hit of another cycle) and long enough to include the max inaccuracy of the hits identification that was indeed of a few milliseconds.

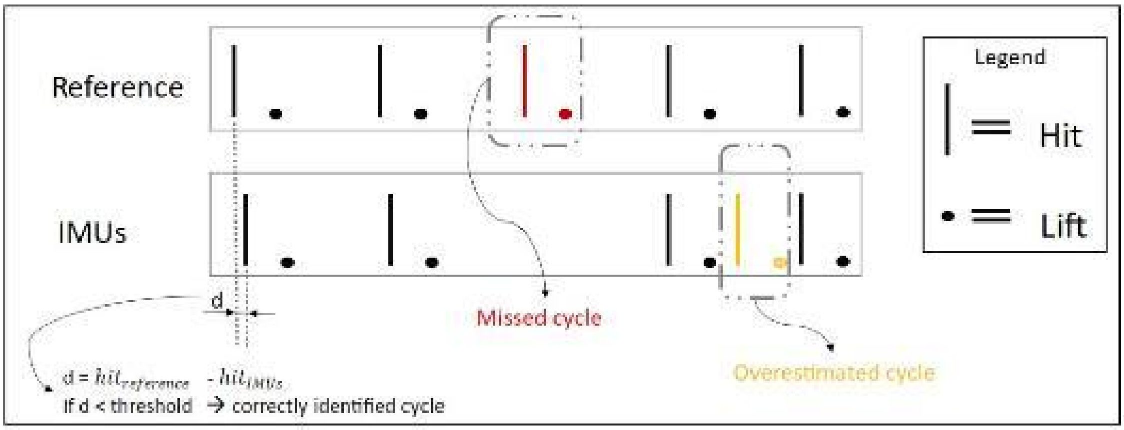

Figure 35 - The scheme shows the logic behind the wrong cycles identification algorithm. *Checking a match for each hit identified in the force signal within a 80 ms window in the IMU signal allows to define the missed cycles. The overestimated cycles are found considering the hits identified in the IMU signals and looking for a match among the reference hits. If there is no correspondence within 80 ms the cycle is considered overestimated.*

4.4 Cycle parameters

The cycle temporal parameters cycle time, pushing time, recovery time, pushing phase and recovery phase (Paragraph 1.1) were calculated based on the cycle events identified and excluding the wrong cycles recognized.

These parameters were calculated both for the gold standard system and for the IMUs (with the three cycle events identification methods), and for all the sensors on the upper limb.

4.5 Relationship between IMUs signals and skiing speed or terrain inclination

The cycle parameters (cycle time, poling time, recovery time) calculated from the cycle events (pole hits and pole lifts) and from the ski velocity and displacement (cycle speed and cycle length) are used to evaluate the performance and are related to different skiing conditions such as skiing speed and track steepness (paragraph 1.1). The measured IMU signals (linear acceleration and angular velocity) their self can be influenced by different skiing conditions. It would be interesting to identify other parameters calculated from the IMUs signals that vary with skiing speed and/or terrain inclination. In this study, some parameters have been therefore calculated from the acceleration and angular velocity signals to explore their sensitivity to different speed and inclination conditions. In particular, the parameters calculated for both the acceleration signals and angular velocity signals were the following:

- Mean value: the mean value over each poling cycle.
- Integral: the time integral over each cycle. It represents the velocity variation when the linear acceleration is integrated, and it represents the angular variation when the angular velocity is integrated.
- Lift peak: the value assumed by the signal in correspondence to the identified lift for each cycle.

These parameters have been calculated for all the trials and for all the sensors placed on the upper limb and their relationship with skiing speed and terrain inclination is evaluated.

4.6 Ski inclination

All the cycle parameters (cycle time, poling time, recovery time, cycle speed, cycle length) are sensitive to different ground steepness [26]. In the double poling technique, the skis are always kept on the soil and their inclination corresponds to the ground inclination. It would be therefore interesting to be able to calculate the skis inclination and this study attempted to do that as described below.

The ski inclination has been calculated in two different ways, one that involves the angular velocity integration around the ski medio-lateral axis and the other that involves the use of the ski IMU as an inclinometer measuring the gravity components along the 3D accelerometer axes. The angular velocity integration is a method often used to calculate an IMU pose over time in dynamic conditions, but it is affected by drift errors. Drift errors during the integration that are usually managed reducing the sensor's measuring errors with a good calibration and implementing some kind of drift reduction algorithm [25],[11],[27]. The method based on the use of the accelerometer as an inclinometer is usually implemented in conditions where the motion studied is quasi-static and the acceleration sensed by the IMU is therefore almost entirely due to the gravity allowing an easy identification of the gravity components [28]. This method is interesting because it does not involve an integration and, therefore, a drift error. However, it is avoided in dynamic conditions because in this case the acceleration sensed by an IMU has some components related to the gravity and other components related to the sensor actual acceleration, and the separation of these two components is not a simple issue [25] [28]. However, calculating the ski inclination using accelerometer as inclinometer could be useful in this study because the ski motion during a general trial being performed on a treadmill is a dynamic movement that happens principally in one direction and the ski inclination in average could be considered constant. This means that the gravity component could be separated from the sensor acceleration component with an appropriate filter.

In both the methods, the ski sensor must be aligned with the ski frame because the sensor inclination is calculated directly form the signals. However, in order to evaluate the ski inclination, it is necessary to know the relative orientation between the ski and the sensor.

The two methods to calculate the ski inclination were applied to the calibrated and to the uncalibrated signals to assess the calibration efficacy in reducing the drift for the method based on the angular velocity integration and also to evaluate the usefulness of the calibration for a drift free method like the one that uses the accelerometer as an inclinometer.

4.6.1 Sensor alignment

The sensor frame alignment with the frame of the object on which the sensor is placed (i.e: body segment, ski) is a common procedure that is done before studying the sensor attitude, and in the literature is sometimes called functional calibration [29],[30]. A method to align a sensor placed on a ski with the ski frame is proposed by some authors [7],[31]. In these papers the authors say that is possible to align the sensor on the ski with the ski frame using the ski principal direction of motion. In another paper, Fasel et al. 2017 [29], describes a functional calibration to align some IMUs with the body segments in alpine skiing and they made public the scripts to perform this functional calibration [32]. Performing a functional calibration of the sensors placed on the skiers body is not necessary for the purposes of this study because these sensors are utilized to identify the pole events using the norm of the signals which is independent from the sensors orientation (paragraph 4.1.1). However, the mathematical methods used to align the sensors with the body segments can be useful to align the ski sensor with the ski frame. In particular, the author made use of quaternions to express the orientation of the sensor axes with respect to the segment axes and then converted the quaternions in rotational matrices to rotate the sensor axes and align them with the body segment axes. The same mathematical methods are implemented in this study to align the ski sensor axes with the ski frame, which is defined by the detection of the principal ski movement during the poling cycles and by the detection of the gravity component during a static measurement with the ski placed on a plane surface. The ski sensor alignment is further described below.

The sensor axes must be aligned with the ski frame to know the ski inclination. A static measurement before the trials allows the alignment of a sensor axis with the gravity which is perpendicular to the ski if this is kept on a plane surface. The detection of the principal movement direction during each trial allows to align another sensor axis with the ski longitudinal axis (Figure 36). Therefore, it is possible to completely align the sensor to the ski.

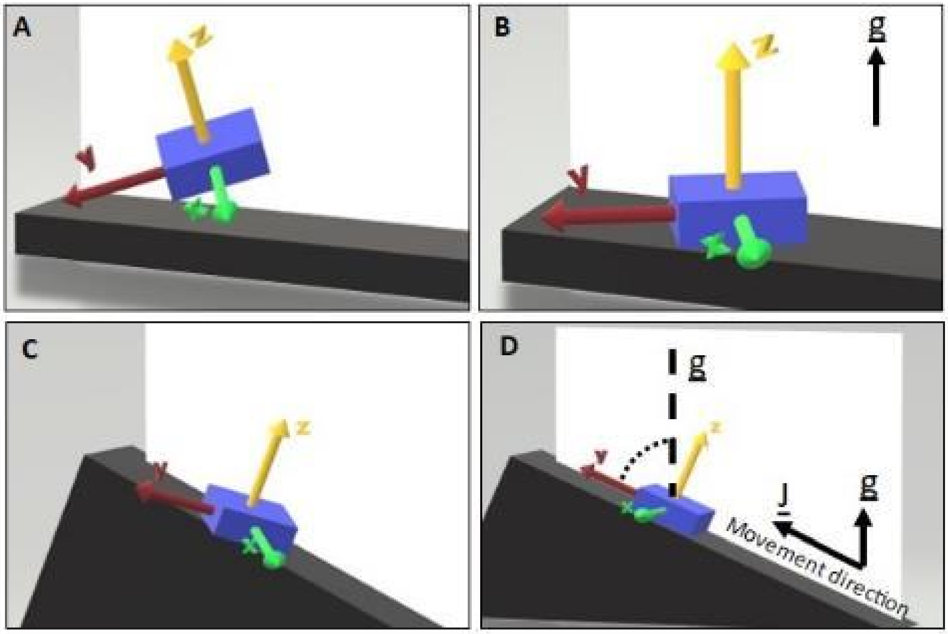

Figure 36 – Sensor alignment steps. *(A) The sensor is placed on the ski and the exact axes orientation is unknown. (B) Thanks to a static acquisition (only gravity sensed) the z axis can be aligned with the gravity force vector. If the ski is on a plane surface and the ski can be considered parallel to the ground, the z axis is now orthogonal to the ski surface. (C) In each trial the z axis will be now perpendicular to the inclined surface, but the other two axes can be rotated in any direction on the surface. (D) Considering that during a trial the skis are kept parallel and they move along a specific direction, it is possible to align the y axis with the principal direction of movement.*

In detail, when the sensor is steady it measures only the gravity acceleration, hence it is possible to calculate the angle between one sensor axis (V_1) and the gravity acceleration (V_2) with the formula:

$$\theta = \arccos\left(\frac{V_1 \cdot V_2}{|V|_1 |V|_2}\right) \tag{16}$$

Then the vector perpendicular to the plane defined by V_1 and V_2 is calculated as:

$$V_{normal} = \frac{V_1 \times V_2}{|V_1 \times V_2|} = \begin{bmatrix} a_i & a_j & a_k \end{bmatrix} \tag{17}$$

It is now easy to define the rotational quaternion (Eq.18) and to express the rotational matrix from the rotational quaternion (Eq.19). This makes possible to align a sensor axis with the gravity vector (Eq.20).

$$q = \left[\cos\left(\frac{\theta}{2}\right); \quad \sin\left(\frac{\theta}{2}\right) a_i; \quad \sin\left(\frac{\theta}{2}\right) a_j; \quad \sin\left(\frac{\theta}{2}\right) a_k\right] \tag{18}$$

$$R = \begin{bmatrix} q_1^2 + q_2^2 - q_3^2 - q_4^2 & 2q_2q_3 - 2q_1q_4 & 2q_2q_4 + 2q_1q_3 \\ 2q_2q_3 + 2q_1q_4 & q_1^2 - q_2^2 + q_3^2 - q_4^2 & 2q_3q_4 - 2q_1q_2 \\ 2q_2q_4 - 2q_1q_3 & 2q_3q_4 + 2q_1q_2 & q_1^2 - q_2^2 - q_3^2 + q_4^2 \end{bmatrix} \tag{19}$$

$$signal_{aligned} = signal \cdot \mathrm{R}' \tag{20}$$

The principal movement direction, expressed in the form of a vector referred to the ski sensor axes, is identified with principal component analysis (pca) on the ski acceleration signals along each axis filtered with a 2nd order low pass filter to smooth them. It is then possible to use the equations above (Eq.16-20) to align another sensor axis with the main direction of motion, considering this time V_1 as the new axis that must be aligned and V_2 as the vector calculated with the pca. The gravity contribution in the acceleration used in the pca must be compensated to obtain a realistic result of the principal movement direction. To remove the gravity, the acceleration signals along each axis have been filtered with a second order filter at 0.1 Hz to yield the only gravity and then these components have been subtracted to the acceleration signal that will be used to compute the pca. It has been decided to low pass filter at 0.1 Hz to yield the gravity components after a spectral analysis of the ski sensor acceleration (the PSD is calculated in the same way described for the acceleration and angular velocity of the wrist sensor in the chapter 3.2.2). The accelerations along the longitudinal and mediolateral ski axes have frequency components mainly between 0.5 Hz and 3 Hz, while the acceleration along the axis normal to the ski has some higher components due to the vibrations of the skies on the treadmill (Figure 37). Filtering at 0.1 Hz should allow to obtain mainly the components related to the gravity and since it's still sensitive to slow changes within a period of 10 s (1/0.1Hz) this should allow to use this method outside to sense the changes in the track inclination even if with a low time resolution (fast changes not detectable).

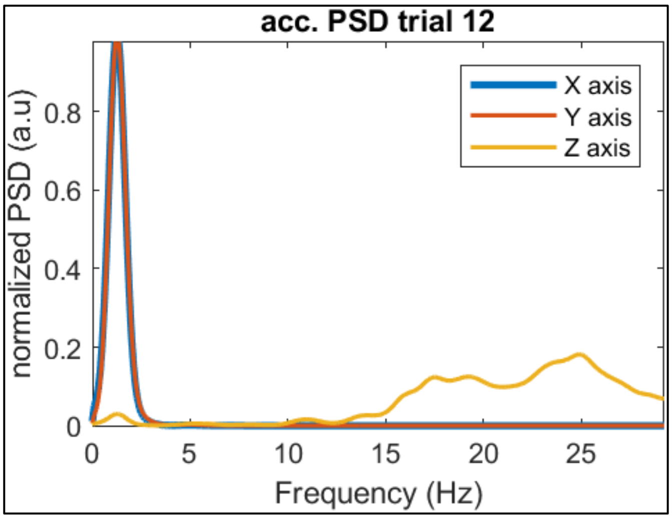

Figure 37 - Ski sensor acceleration PSD. *The PSD is calculated for the ski sensor acceleration for the 12th trial of the first subject in which the sensor is rotated on the ski, the treadmill is inclined of 6° and the treadmill speed is 12 km/h.*

The processing steps on the ski sensor acceleration to align the ski sensor axes with the ski sensor frame are described with a scheme below (Figure 38).

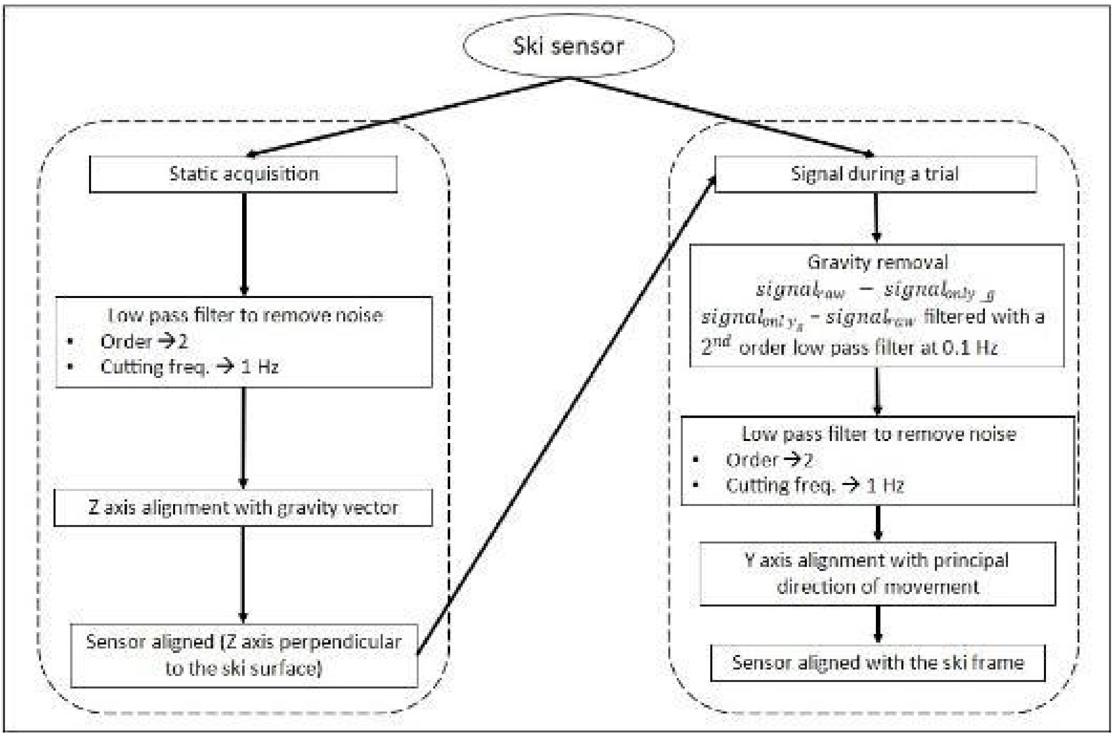

Figure 38 –Processing steps on the ski IMU acceleration to align the sensor with the ski frame. *The left branch reports the sensor's z axis alignment with the gravity vector. The right branch describes the alignment of the sensor's y axis with the principal direction of movement. The last step in the left branch is connected to the first step in the right branch to remark that the signal used to align the y axis is already aligned with gravity.*

4.6.2 Inclination calculation

Once the ski sensor is aligned with the ski frame it is possible to calculate the ski inclination using the two methods: angular velocity integration and accelerometer as inclinometer.

The angular velocity integration was done considering the sensor medio-lateral axis and assuming the boundary condition are known. In this case the initial inclination was set to be the treadmill inclination at the beginning of each trial. The signal was integrated from the beginning to the end of the trial by a trapezoidal integration to obtain the instantaneous inclination for the duration of the trial. The mean value of the instantaneous inclination was then calculated to obtain the average ski inclination to compare with the reference inclination (the treadmill inclination).

Considering the second method (accelerometer as inclinometer), the ski sensor acceleration components were filtered with a low pass filter with cutting frequency at 0.1 Hz and the output was assumed to be only the gravity components of the signal (Figure 37). The knowledge of the gravity components allows to calculate the sensor axes inclination with respect to the gravity direction implementing the following equation:

$$\theta = \arccos\left(\frac{v \cdot V_1}{|V|_1}\right) \tag{6}$$

Where *v* is the versor of the axis which the angle θ with the gravity direction is calculated and V_1 is the gravity vector extrapolated with the low pass filter at 0.1 Hz.

4.7 Ski velocity and displacement

After the ski sensor alignment described in the previous paragraph was performed, the ski instantaneous velocity and ski displacement were calculated integrating with a trapezoidal integration the ski sensor acceleration along the ski longitudinal axis one and two times, respectively, for the entire duration of the trial. The treadmill velocity is added to the instantaneous ski velocity to obtain the relative speed between the skis and the treadmill. The displacement is obtained integrating this relative speed. Before the integration the acceleration signal is filtered with a second order low pass filter at 4

Hz to keep all the frequencies related to the poling movement but removing the noise at higher frequencies (Figure 37). The g components are removed from the acceleration signal, which is integrated with the same principle adopted during the sensor alignment, therefore filtering the signal with a low pass filter with cutting frequency at 0.1 Hz and subtracting it from the acceleration which will be integrated. The instantaneous speed is then averaged from the moment in which the treadmill reach the constant speed till the end of the trial, to allow the comparison with the reference skis average speed (the treadmill velocity for that particular trial). The displacement obtained integrating the ski velocity over the entire trial is the overall displacement for that trial. To obtain the cycle length the ski velocity was integrated over each cycle detected by the wrist sensor with the acceleration norm-based cycle events identification method. Another calculation of the cycle length was performed multiplying the cycle time of each cycle detected by the wrist sensor with the acceleration norm-based cycle events identification method with the average ski velocity for each corresponding cycle. The average ski cycle velocity for each cycle is calculated averaging the ski instantaneous speed over each cycle.

5 Statistical analysis

The errors in the identification of the cycle events were calculated as differences between the reference cycle events time instants (the pole hits and pole lift identified from the force signals) and the time instants of the events identified by the IMUs-based cycle events identification methods. These errors were calculated for the identifications performed by all the sensors on the upper limb (2 on the arm and 2 on the forearm). Then, the cycle temporal parameters calculated from the reference cycle events were compared with the cycle temporal parameters calculated from the cycle events identified with the IMUs-based identification methods. The normality of the cycle events identification errors and of the cycle parameter, was assessed with a Lilliefors test (significance level of 5 %) and since most of the distributions were not normally distributed the results were reported as median and interquartile range. Regarding the distribution of the time differences in the cycle events identified by the reference system and by the IMUs-based methods, the median and the interquartile ranges of these distributions were considered respectively as accuracy and precision [7],[33].

The agreement between the reference identification method and the IMUs-based identification methods were also assessed with a Bland Alman analysis [34] of the cycle temporal parameters. The Bland Altman analysis was adapted to a non-normal distributed data reporting the median instead of the mean value and calculating the 97.5 percentile and the 2.5 percentile as limits of agreement [35],[36]. Both the limits of agreement and the medians are reported with their confidence interval at 95% confidence level (grey bands). The confidence intervals were calculated with the bootstrap method [37].

The results about the ski inclination and ski velocity calculated with the IMU-based method were qualitatively compared with the treadmill speed and inclination.

6 Results and discussion

The results of the previously described analysis are reported and discussed in this section. They are organized as follow:

1. Influence of the sensor position in detecting the cycle events:
    - The percentage of missed cycles for each cycle events identification method is showed for each sensor on the upper limb.
    - The performance of the cycle identification methods for the different sensors on the upper limb is compared in terms of accuracy and precision in detecting the pole hits and the pole lifts.
    - The cycle temporal parameters calculated starting from the IMUs-based cycle events identification methods are qualitatively compared for the different sensor positions on the upper limb.
2. Sensitivity of the cycle events identification methods to different subjects:
    - The pole hits and pole lifts identification accuracy and precision for the two different subjects that took part to the experiment, are compared.
3. Influence of the sensor orientation in detecting the cycle events:

- The performance of the cycle events identification methods for the two sensors orientation conditions (sensors aligned with the body segment and sensors rotated) is compared in terms of accuracy and precision in detecting the pole hits and the pole lifts.

4. Comparison of the cycle events identification methods:
    - The temporal cycle parameters calculated starting from the cycle events identified with the IMUs based methods are compared with the same cycle parameters calculated starting from the cycle events identified with the reference system.
    - The cycle events identification methods are compared in terms of accuracy and precision in detecting the cycle events and in calculating the temporal parameters.
    - The agreement of each of the three IMUs-based identification methods with the reference identification method is evaluated with a Bland Altman analysis for each temporal cycle parameter.
5. Relationship between IMUs signals and skiing speed or terrain inclination:
    - The results about the relationship between the IMUs signals and skiing velocity and inclination are reported and discussed.
6. Performance of the methods to calculate the ski inclination:
    - The performance of the method based on the integration of the angular velocity around the ski medio-lateral axis is qualitatively evaluated and compared with the performance of the inclinometer-based method.
    - The inclinometer-based method performance is qualitatively evaluated comparing the inclination results with the known treadmill inclination.
7. Performance of the ski velocity and displacement calculation:
    - The results regarding the ski velocity and displacement calculated integrating the ski sensor linear acceleration along the ski longitudinal axis are discussed.

All the results about the cycle events identification methods have been obtained starting from the IMUs signals calibrated and then uncalibrated, to evaluate a possible difference in the methods performance introduced by the calibration. Since no differences in the performances were noticed, concerning the cycle events identification methods, only the results obtained from the calibrated signals will be reported.

In the paragraph about the IMUs-based cycle events identification methods, two versions of the “fusion” cycle events identification method were introduced. However, after a first evaluation of the results, the results about the 2nd version of this method (the one which identifies a lift as the mean of the corresponding lifts identified by the acceleration norm-based and angular velocity norm-based methods) were considered not particularly relevant with respect to the other “fusion” method version and therefore they are not reported in the following paragraphs.

6.1 Influence of the sensor position in detecting the cycle events

The cycle events identification methods based on the IMUs signals were developed starting from the wrist sensor signals and then applied also to the other sensors on the upper limb. Analysing the performance of the methods when applied to sensors placed on different position on the upper limb allows to understand the robustness of the identification methods developed. If an algorithm is robust it will have similar performances for the different sensor positions. This analysis also allows to identify the better position on the upper limb to place the sensors to study the cycle parameters.

6.1.1 Missed cycles

The total number of cycles identified by the reference system (the one based on the force signal) were 550. This count includes the cycles detected in all the trials performed by both the subjects.

The missed cycles percentage for each sensor indicates the algorithms ability to detect the cycles. The algorithm based on the acceleration norm could detect all the cycles with the wrist sensor and missed 30 cycles with the signals form the other sensors (Figure 6.1, left panel). The algorithm based on the angular velocity norm missed a total of 47 cycles considering all the sensors and 13 of the missing cycles were from the wrist sensors (Figure 39). However, overall the number of missed cycles was relatively small considering both the algorithms and all the sensors suggesting that the cycles identification (purely in terms of cycles recognition) with the methods developed was not too influenced by the sensor position on the upper limb. Since the cycles identification is based on the pole hits, the missed cycles for the “fusion” method (the one which merges the identification from the other two methods) are not reported because are the same of the acceleration norm-based method (the two methods identify the hits in the same way).

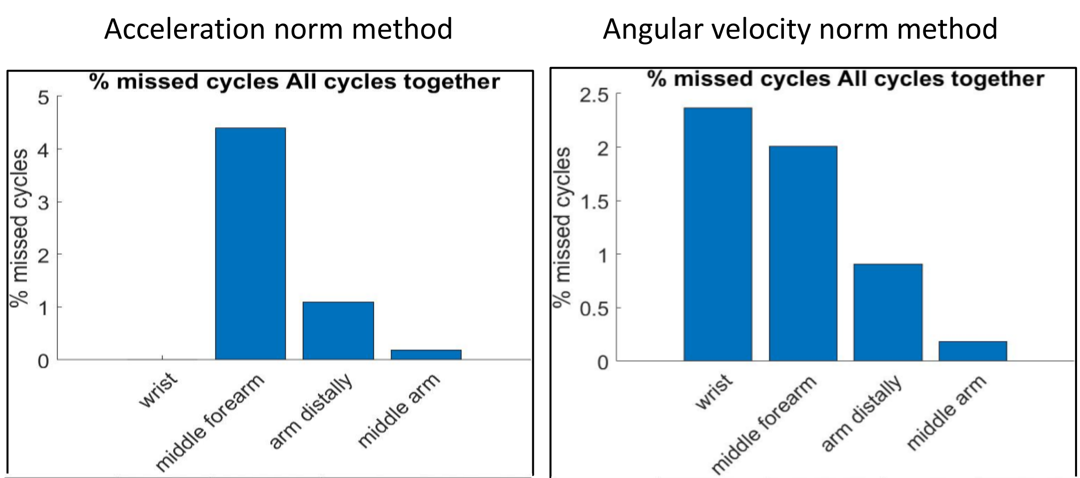

	tot cycles	missed cycles	percentage of missed cycles
wrist	550	0	0
middle foreamr	550	24	4.4
arm distally	550	6	1.1
middle arm	550	1	0.2

	tot cycles	missed cycles	percentage of missed cycles
wrist	550	13	2.4
middle foreamr	550	11	2
arm distally	550	5	0.9
middle arm	550	1	0.2

Figure 39 - Missed cycles percentage. Sensor position influence. *The bar plots show the percentage of missed cycles for each sensor and for the acceleration norm-based method (on the left) and for the angular velocity norm-based method (on the right). In the tables under the graphs are reported also the number of missed cycles.*

6.1.2 Errors in detecting the cycle events

Figure 6.2 and 6.3 report the error in identifying pole hits and lifts. The bar plots show the errors (median and interquartile range) in the detection of the pole hits (Figure 40) and pole lifts (Figure 41) for each sensor and for the identification method based on the acceleration norm and for the one based on the angular velocity norm. Since the “fusion” method identifies the hits as the acceleration norm-based method and the lifts as the angular velocity norm-based method the “fusion” method cycles events are not showed.

The acceleration norm-based method could detect the pole hits with the wrist sensors accurately (the median error is just a few milliseconds) and precisely (the interquartile range is small). The median error is small also for the sensor placed on the middle forearm and on the arm distally, while is greater for the sensor on the middle of the arm (Figure 6.2). The imprecision (interquartile range) of the pole hits detection rises for the sensors placed more proximally than the wrist sensor.

The hits identification based on the angular velocity norm is in general less accurate than the one based on the acceleration norm (greater mean error and greater interquartile range). The wrist sensor provides the best performance with both methods, while the other sensors are less precise and less accurate (especially the ones on the arm).

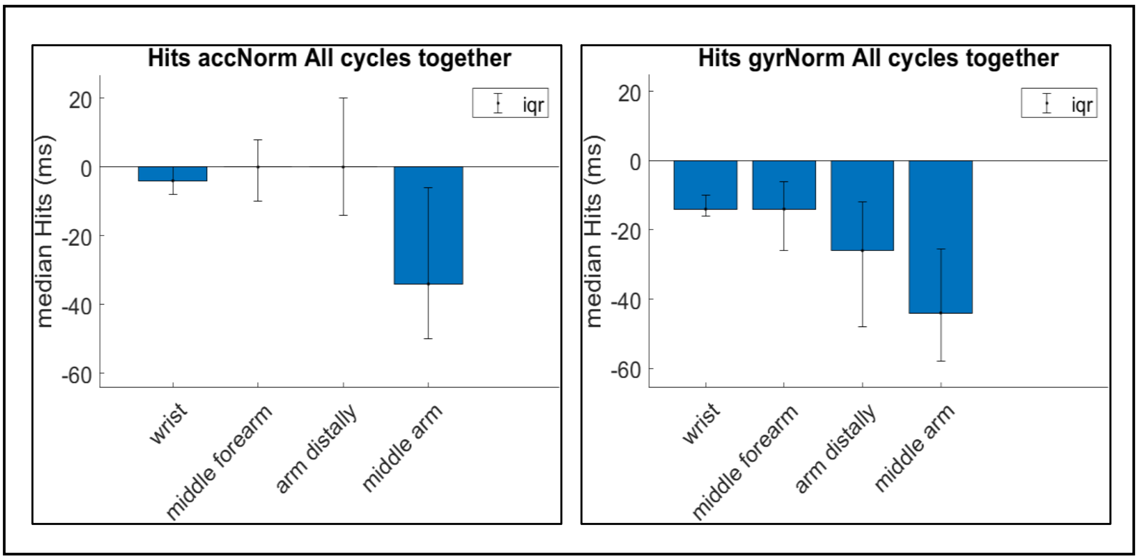

Figure 40 - Errors in detecting the pole hits. Sensor position influence.

Regarding the pole lifts recognition, the acceleration norm-based method identifies the lifts with a similar accuracy with all the sensors. Among all the sensors, the wrist sensor is the one with less dispersion of the data, while the other sensors are less precise, especially the ones on the arm.

The angular velocity norm-based method identifies accurately and precisely the lifts with the wrist sensor, but the other sensors show a relevant imprecision and in the case of the sensor on the middle of the arm also a low accuracy.

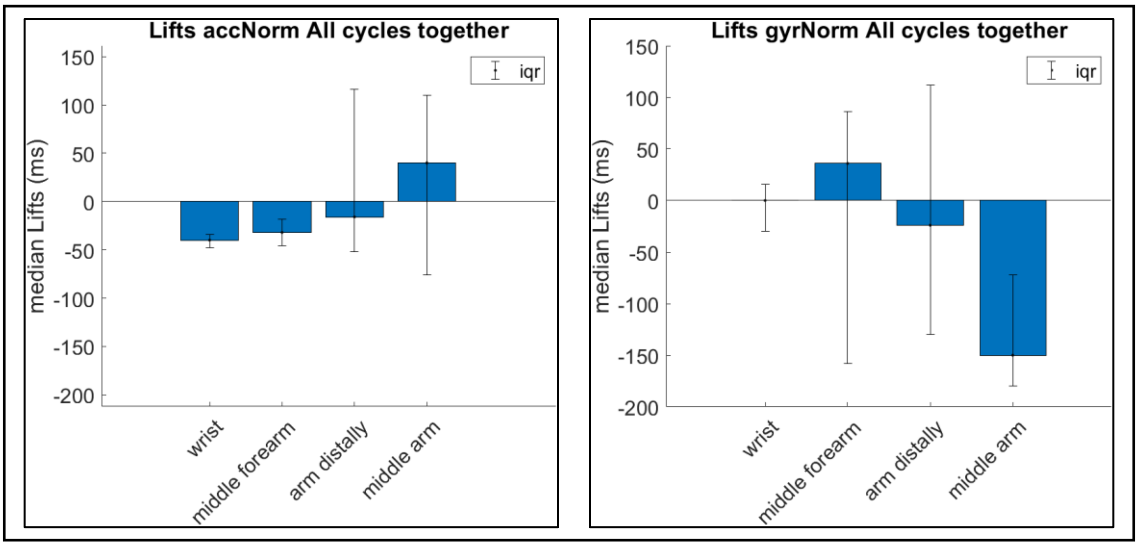

Figure 41 - Errors in detecting the pole lifts. Sensor position influence.

6.1.3 Cycle temporal parameters

The cycle temporal parameters (cycle time, pushing time, recovery time) are defined starting from the cycle events and the performance in calculating these parameters from the IMUs signals is therefore strongly related to the performance in detecting the cycle events showed above. However, the cycle temporal parameters are reported because they are useful to better understand which sensor (position on the upper limb) performs good enough to be used for a cycle temporal parameters analysis. The resting time is not showed because showing cycle time and pushing time, the resting time is complementary, and it does not bring more useful information to assess the methods effectiveness in calculating the cycle parameters. The cycle parameters reported are grouped by different treadmill velocity and inclination. The cycles of the trials in which the sensors are aligned with the body segments are considered together with the cycles in which the sensors are rotated because this analysis is not intended to assess differences between aligned and rotated. Also the cycles from different subjects are considered together, and for this reason the values assumed by the parameters are not representative for a particular subject in that particular condition, but the aim of this study was to inspect the influence of different skiing conditions in calculating the cycle parameters and not the influence on the parameters themselves. The results about the cycle time calculated with the “fusion” method are not reported because are the same of the acceleration norm-based method since the cycle time is a parameter defined only by the pole hits.

Overall, all the sensors and both the identification methods agree with the reference system in the cycle time calculation (Figure 42).

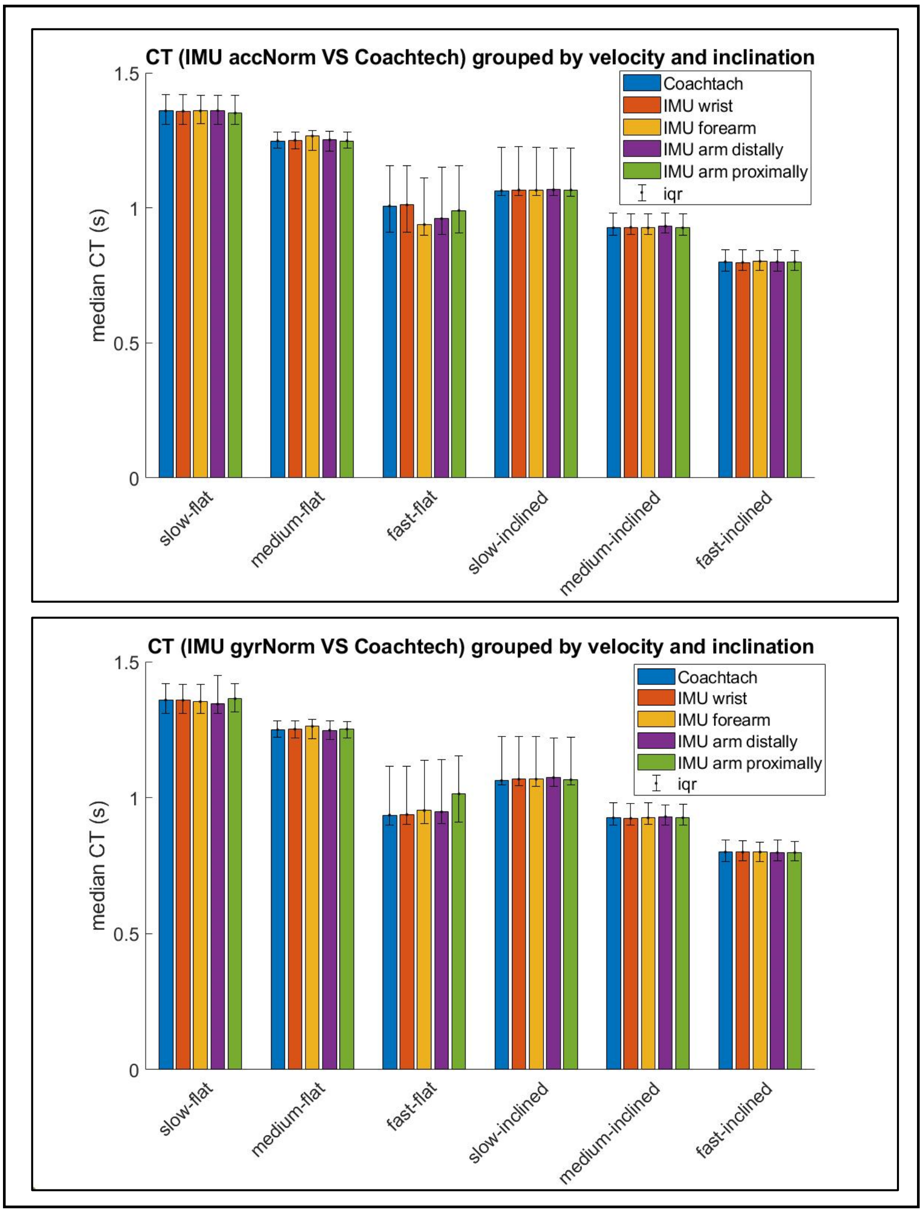

Figure 42 - Cycle time (acceleration and angular velocity methods). Influence of the sensor position.

For the acceleration norm-based method, the push time calculation quite agrees with the reference only for the 2 sensors on the forearm, while the performance of the other sensors (arm distally and arm proximally) changes a lot depending on the skiing condition considered and are generally worse in the conditions when the treadmill is inclined (Figure 43). For the angular velocity norm-based method and the fusion method the only sensor which is reliable for the push time calculation is the one on the wrist (Figure 43, Figure 44).

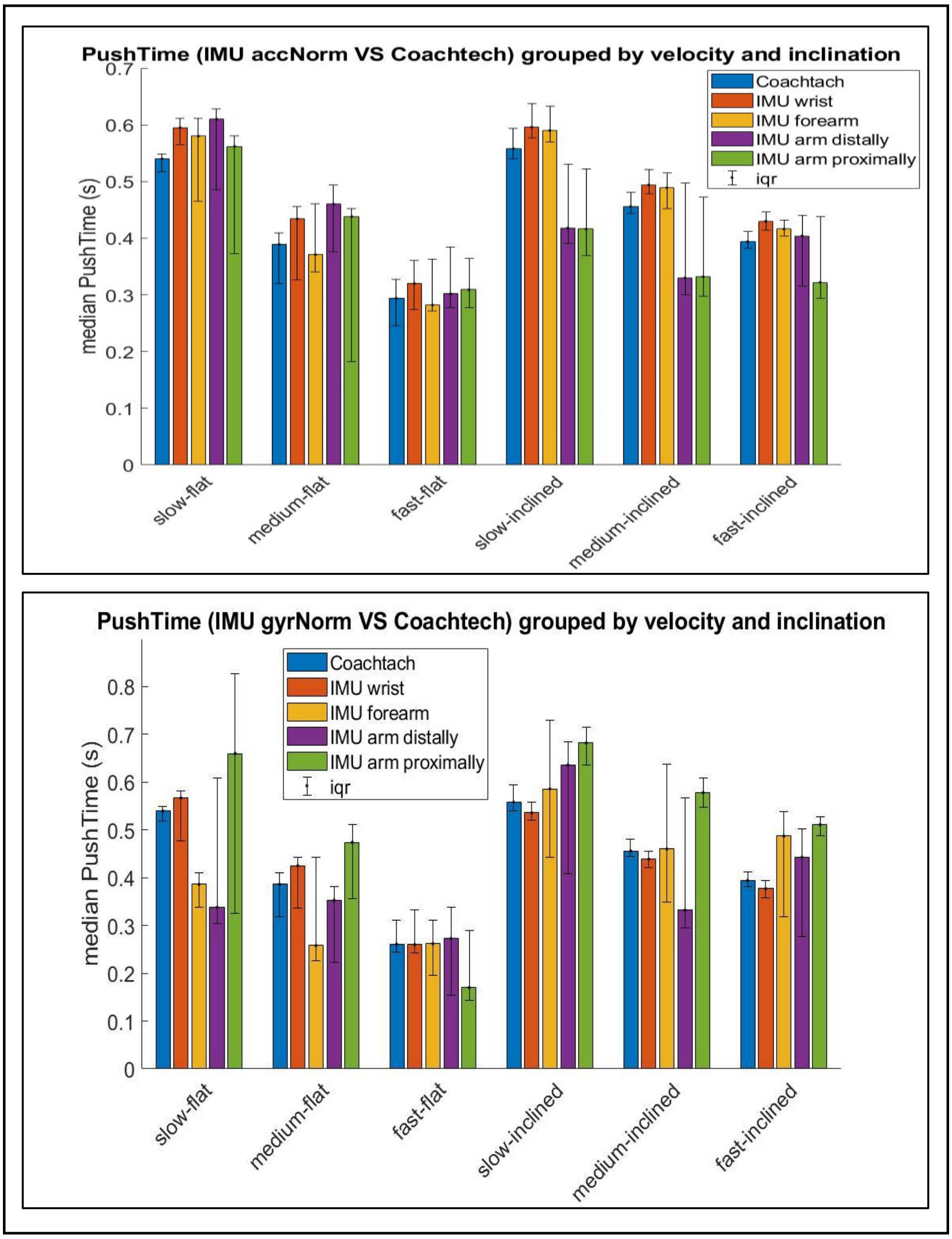

Figure 43 - Push time (acceleration and angular velocity methods). Influence of the sensor position.

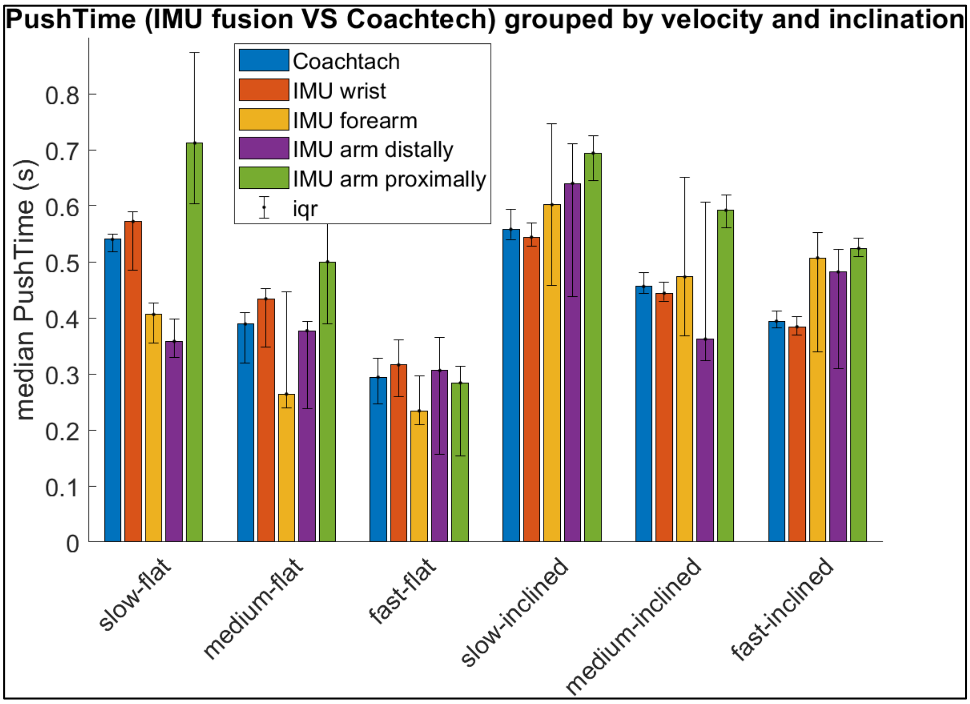

Figure 44- Push time (fusion method). Influence of the sensor position.

From the figures above (Figure 42, Figure 43, Figure 44), all the 4 sensors on the upper limb seem to be adequate to calculate the cycle time while only the wrist sensor seems to agree with the reference in calculating the push time. Since the 4 upper limb sensors agreement with the reference in calculating the cycle time is only assessed qualitatively, a quantitative evaluation is reported below (Table 6.1) in terms of accuracy and precision (median errors and interquartile range). The same is done for the pushing time (Table 6.2).

	CT absolute errors (ms)			
	Acc method		Gyr method	
	median	iqr	median	iqr
wrist	0	4	0	4
middle forearm	0	4	0	6
arm distally	0	10	0	14
middle arm	0	9	0	6

Table 6.1 - Cycle time errors. Influence of the sensor position.

	Push time absolute errors (ms)			
	Acc method		Gyr method	
	median	iqr	median	iqr
wrist	-38	16	14	44
middle forearm	-34	28	42	254
arm distally	-16	179	-1	251
middle arm	48	178	-116	99

Table 6.2 - Push time errors. Influence of the sensor position.

From the table above (Table 6.1) the accuracy for all the sensors in detecting the cycle time results to be better than 2 ms (the sampling period) and the worse imprecision is 14 ms for the sensor placed distally on the arm with the angular velocity norm method. Concerning the pushing time (Table 6.2), the wrist sensor has an accuracy better than 38 ms and the worse imprecision is 44 ms (angular velocity method), while the other sensors are very imprecise (large interquartile range).

Summing up the results showed in the pictures about the missed cycles (Figure 39), the pictures about the errors in detecting the pole events (Figure 40, Figure 41) and the pictures about the cycle temporal parameters (Figure 42, Figure 43, Figure 44, Table 6.1, Table 6.2), it is possible to deduce that:

- The signals from all the sensor are adequate to recognize the poling cycles.
- The wrist sensor, considering the overall accuracy and the precision in detecting poling cycles, is the one that shows the better performance for both the acceleration norm-based method and the angular velocity norm-based method. However, the acceleration norm-based method shows a similar performance also for the sensor on the middle of the forearm.
- The acceleration norm-based method identifies the hits more accurately than the angular velocity norm-based method.
- The angular velocity norm-based method identifies the lifts more accurately than the acceleration norm-based method when the wrist sensor is considered, but with the other sensors the acceleration norm-based method shows similar or better performance in the lifts identification than the angular velocity norm-based method.

- All the sensors and with all the methods developed, are adequate to calculate the cycle time.
- The push time (and rest time) are adequately calculated only with the 2 sensors on the forearm for the acceleration norm-based method and only with the wrist sensor for the angular velocity norm-based method and the fusion method.

From the results above, the wrist seems to be the best position to place the sensors to identify the cycle events with the methods developed. For this reason, the other results showed from now on will be relative to the wrist sensor only. The study wants, indeed, to investigate the better performances that can be obtained with the identification methods developed.

6.2 Sensitivity of the cycle events identification methods to different subjects

In order to be used with skiers, the identification methods are supposed to have similar performances for the subjects that took part to the experiment. The pictures show respectively the error in detecting the hits (Figure 45) and the lifts (Figure 46) with different identification methods and for the different subjects (on the left subject 1 and on the right subject 2). There is actually a difference in the performance depending on the subject, but considering the entity of the difference (a few milliseconds) and that the dispersion of the data is quite big (the interquartile range) these differences were not considered relevant enough to prevent to consider licit grouping all the trials from different subjects. However, the acceleration norm-based method seems less affected by a different subject while the angular velocity norm-based method seems more sensitive to this variable.

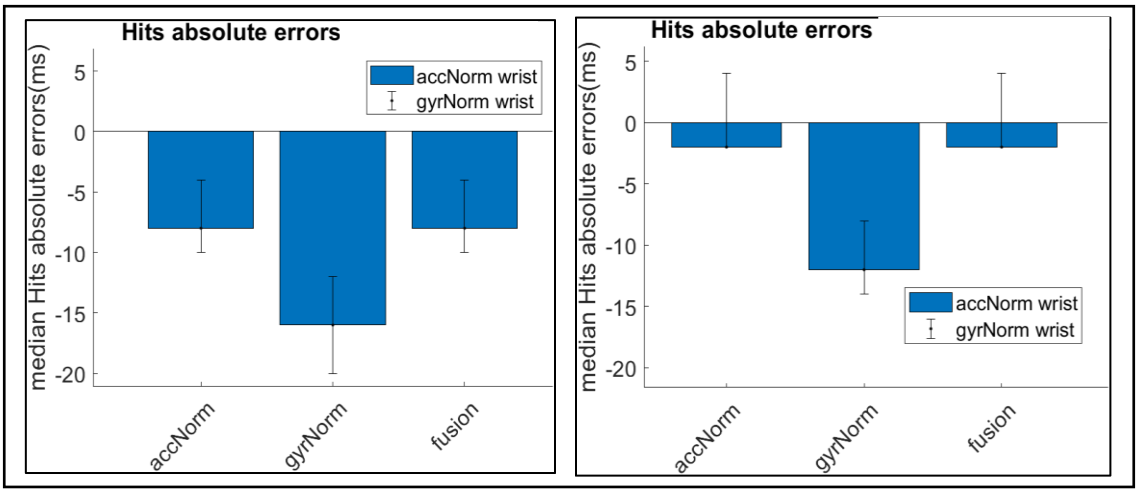

Figure 45 - Errors in detecting the pole hits. Subject sensitivity.

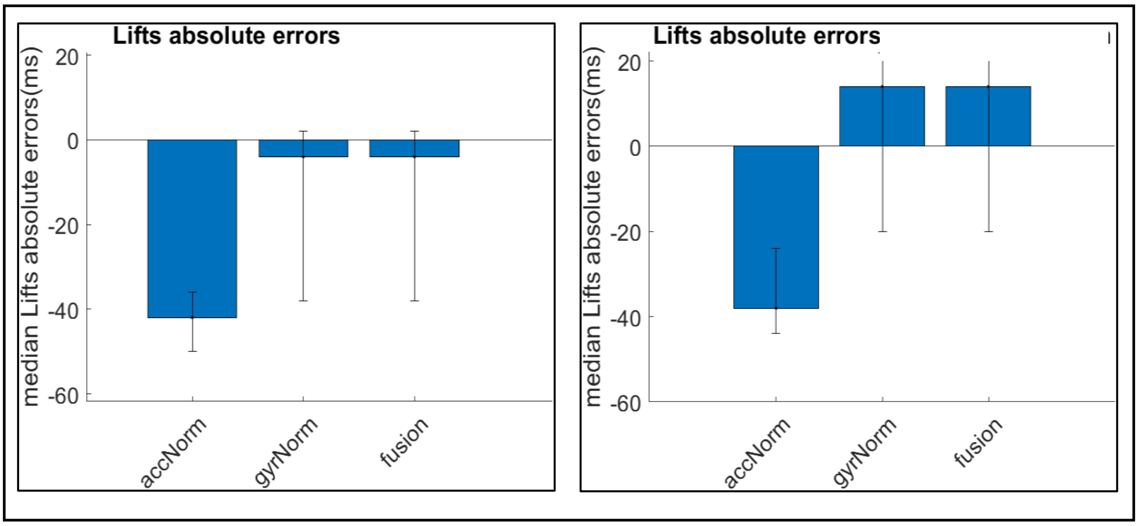

Figure 46 - Errors in detecting the pole lifts. Subject sensitivity.

6.3 Influence of the sensor orientation in detecting the cycle events

The identification methods worked using the norms of the signals to prevent to be sensitive to different orientation conditions (as described in method section). It is therefore expected that the performances at different orientation (sensors aligned with the body segments compared with sensors rotated) should be irrelevant. From the picture (Figure 47) it is possible to confirm this hypothesis since there are some differences in the medians from the two different sensor orientation condition but considering the large interquartile ranges (which moreover are intersected for the two orientation conditions) these differences are obviously not relevant. From now on, the results will consider the cycles from the trials with different sensor orientation conditions as independent.

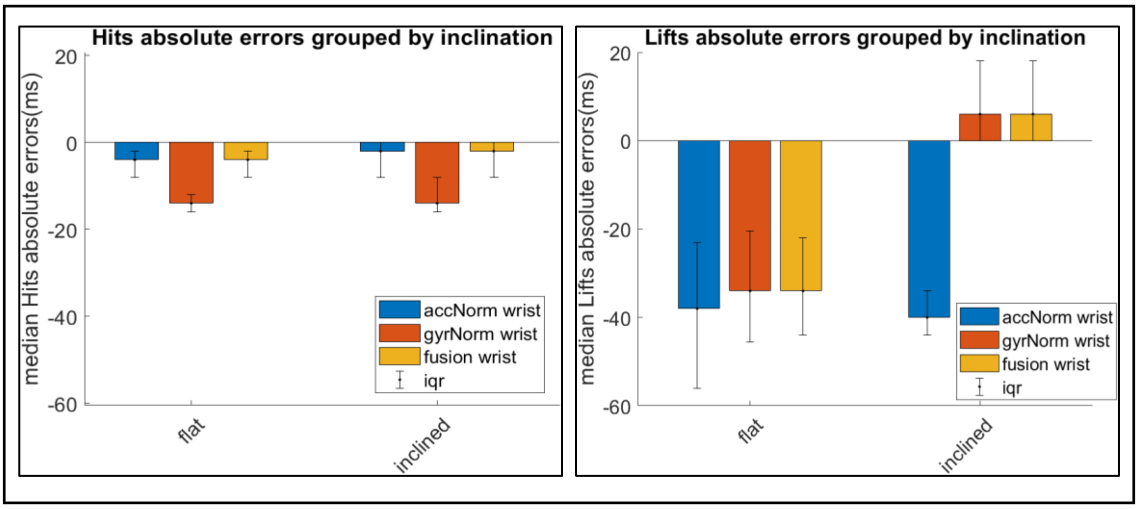

Figure 47 - Errors in detecting the pole events. Influence of the sensor orientation.

6.4 Comparison of the cycle events identification methods

In the previous paragraphs, the sensors position and rotation on the upper limb and the sensitivity of the IMUs-based cycle identification methods to different subjects have been assessed concluding that the wrist is the best position to place a sensor to detect the cycle events with the method developed and that the sensor orientation and different subjects do not strongly influence the cycle events identification performance. In this chapter, the 3 cycle events identification methods are therefore compared in terms of pole events and cycle parameters errors, considering only the wrist sensor and grouping the cycles from the trials, all together or grouping them based on different skiing speed and inclination to assess the influence of these skiing conditions in detecting the cycle events.

6.4.1 Cycle events and cycle temporal parameters errors

The cycle events and cycle parameters errors are showed, before grouping the cycles from all the trials together to have an overall understanding of the identification method performance, and then grouping the cycles depending on the treadmill inclination and speed. To read the errors when grouped by different skiing condition is important to better understand the real methods performances because when the cycles are grouped all together, different performances at different skiing conditions could compensate each other, resulting in an overall error that do not reflect the real performances of the method.

Analysing the results about the overall performance in detecting the pole events (Figure 48) is evident that the hits identification is very accurate and precise when performed by the acceleration norm-based method or the fusion method, and less accurate when performed by the angular velocity norm-based method. The pole lifts are identified more accurately by the angular velocity norm-based method and the fusion method but the errors dispersion is quite large while the accuracy of the acceleration norm-based method is worse but the dispersion of the errors is smaller.

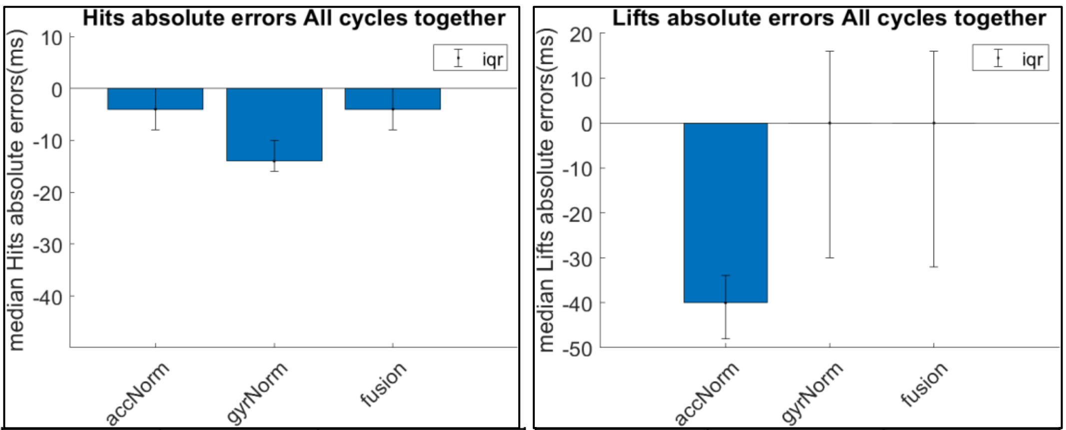

Acc method		Gyr method		Fusion method		Acc method		Gyr method		Fusion method	
median	iqr	median	iqr	median	iqr	median	iqr	median	iqr	median	iqr
-4	8	-14	6	-4	8	-40	14	0	46	0	48

Figure 48 - Cycle events errors. Cycle events identification methods comparison.

Analysing the pole hits errors for different skiing condition (Figure 49), the identification methods performances are similar for all the different skiing conditions, but the acceleration norm-based method and the fusion method seem to have better performances increasing the skiing speed.

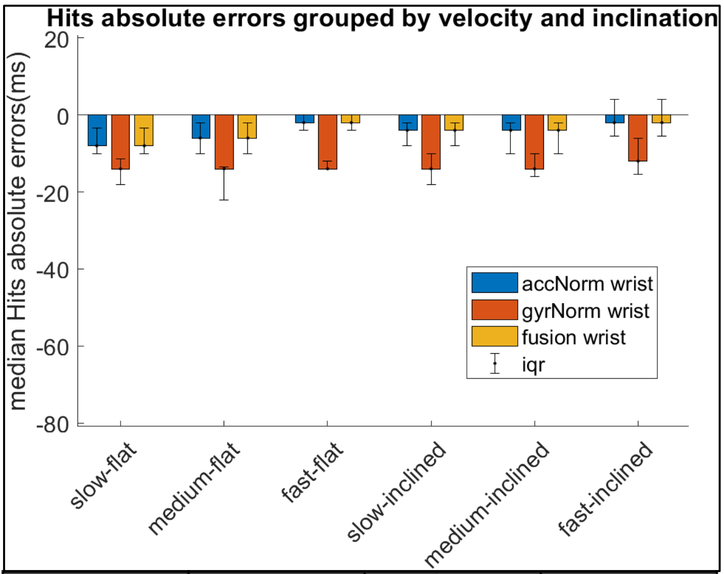

	Acc method		Gyr method		Fusion method	
	median	iqr	median	iqr	median	iqr
slow-flat	-8	7	-14	7	-8	7
medium-flat	-6	8	-14	9	-6	8
fast-flat	-2	4	-14	2	-2	4
slow-inclined	-4	6	-14	8	-4	6
medium-inclined	-4	8	-14	6	-4	8
fast-inclined	-2	10	-12	10	-2	10

Figure 49 – Pole hits errors in different skiing conditions. Cycle events identification methods comparison.

The pole lifts errors over different skiing conditions (Figure 50), show that the acceleration norm-based method improves the performance at higher speeds, while the angular velocity norm-based method and the fusion method have better performances in the inclination condition than the flat condition. One could notice that in some conditions the fusion method show a slightly different median error if compared to the angular velocity method and this should not happen since the lifts for the two methods are identified in the same way. However, this is justified because the cycle identified by the two methods is different (Figure 39) since the fusion method identifies the hits (and therefore the cycles) like the acceleration norm-based method.

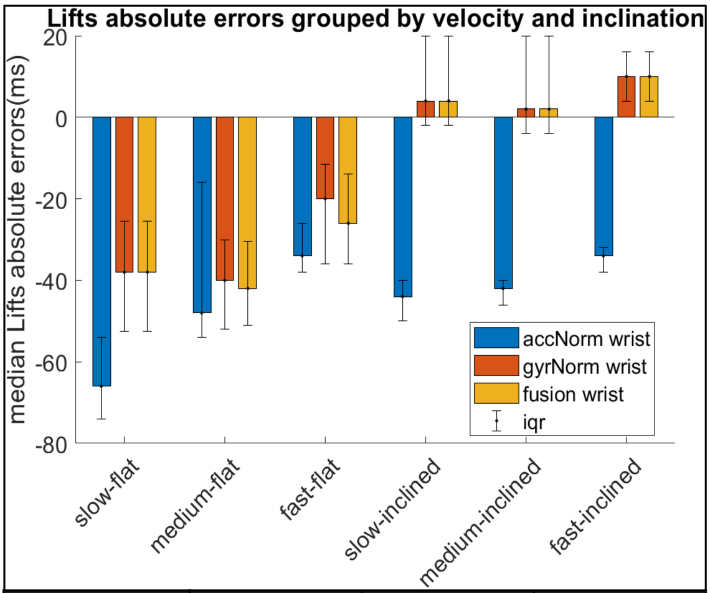

	Acc method		Gyr method		Fusion method	
	median	iqr	median	iqr	median	iqr
slow-flat	-66	20	-38	27	-38	27
medium-flat	-48	38	-40	22	-42	21
fast-flat	-34	12	-20	25	-26	22
slow-inclined	-44	10	4	22	4	22
medium-inclined	-42	6	2	24	2	24
fast-inclined	-34	6	10	12	10	12

Figure 50 – Pole lifts errors in different skiing conditions. Cycle events identification methods comparison.

The cycle time is calculated very accurately and precisely by all the methods (Table 6.3). Considering the relative errors, all the methods have an average imprecision smaller than the 0.4 %.

CT absolute errors (ms)					
Acc method		Gyr method		Fusion method	
median	iqr	median	iqr	median	iqr
0	4	0	4	0	4

CT relative errors (%)					
Acc method		Gyr method		Fusion method	
median	iqr	median	iqr	median	iqr
0.0	0.4	0.0	0.4	0.0	0.4

Table 6.3 - Cycle time absolute and relative errors. Cycle events identification methods comparison.

The overall accuracy in calculating the push time (Table 6.4) is better for the angular velocity norm-based method and for the fusion method than for the acceleration norm-based method; however, the dispersion of the errors is smaller for this one. The higher dispersion for the angular velocity method and for the fusion method is justified by the results showing the push time errors over different skiing conditions (Figure 51). The two methods, indeed, overestimate the parameter when skiing in a flat condition while underestimate the parameter when skiing in an inclined condition. The push time percentage errors (Figure 52) show that the angular velocity method and the fusion method commit in general errors between the 5% and the 10% while the acceleration norm-based method commits errors around the 10%.

Push time absolute errors (ms)					
Acc method		Gyr method		Fusion method	
median	iqr	median	iqr	median	iqr
-38	16	14	44	4	44

Push time relative errors (%)					
Acc method		Gyr method		Fusion method	
median	iqr	median	iqr	median	iqr
-8.7	3.9	3.1	10.7	1.1	11.5

Table 6.4 - Push time absolute and relative errors. Cycle events identification methods comparison.

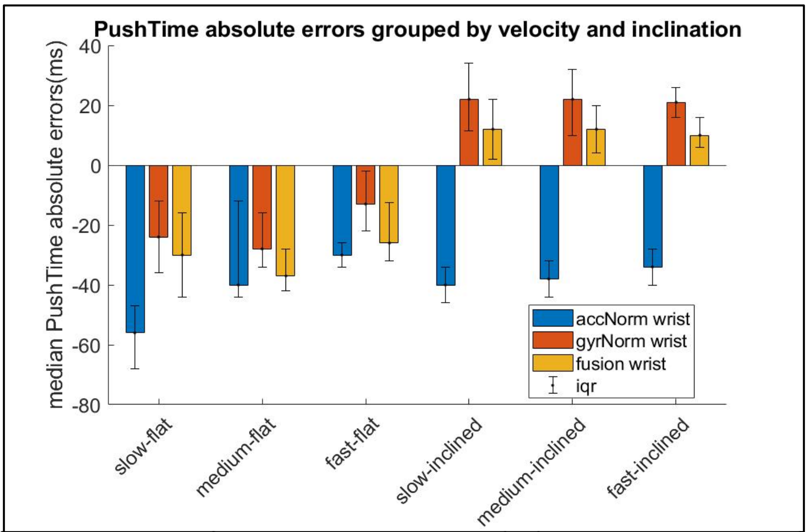

	Acc method		Gyr method		Fusion method	
	median	iqr	median	iqr	median	iqr
slow-flat	-56	21	-24	24	-30	28
medium-flat	-40	32	-28	18	-37	14
fast-flat	-30	8	-13	20	-26	20
slow-inclined	-40	12	22	22	12	20
medium-inclined	-38	12	22	22	12	16
fast-inclined	-34	12	21	10	10	10

Figure 51 - Push time absolute errors in different skiing conditions. Cycle events identification methods comparison.

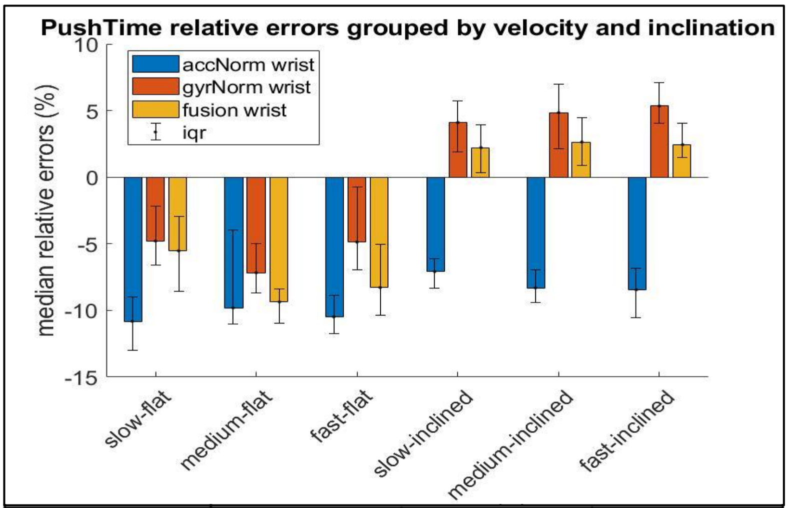

	Acc method		Gyr method		Fusion method	
	median	iqr	median	iqr	median	iqr
slow-flat	-10.8	4.0	-4.8	4.4	-5.5	5.6
medium-flat	-9.8	7.0	-7.2	3.7	-9.4	2.6
fast-flat	-10.5	2.9	-4.9	6.2	-8.3	5.3
slow-inclined	-7.1	2.2	4.1	3.8	2.2	3.6
medium-inclined	-8.3	2.5	4.8	4.9	2.6	3.6
fast-inclined	-8.5	3.7	5.3	3.1	2.4	2.6

Figure 52 - Push time relative errors in different skiing conditions. Cycle events identification methods comparison.

6.4.2 Cycle parameters Bland Altman analysis

The Bland Altman analysis has been performed for the cycle temporal parameter to evaluate the agreement of the IMUs-based cycle events identification methods with the force signal-based cycle events identification method (the reference one).

On the X axis of the Bland Altman graphs there are the reference values (the one calculated form the force signal-based identification) of the parameter of interest, while on the Y axis there are the percentual errors of the parameters of interest (absolute errors divided by the reference parameter value) [34]. The median error is reported in green and the limits of agreement in red. The representation of the median and the limits of agreement as the 97.5 percentile and the 2.5 percentile is suggested in literature as a modified Bland Altman analysis for non-normal distributed data [36],[35]. Both the limits of agreement and the medians are reported with their confidence interval at 95% confidence level (grey bands). The confidence intervals were calculated with the bootstrap method [37].

The information brought by the Bland Altman graphs is similar to the one brought by the bar plot of the errors reported in the previous paragraph, however this analysis allow to directly compare two methods (IMU vs reference) and to better assess the distribution of the errors and it also reports the confidence intervals for the median and the limits of agreement. The limits of agreement mark the range within stay the 95% of the errors and should not be confused with the interquartile range reported in the bar plots in the previous chapters or with the confidence intervals of the median value.
The cycle time Bland Altman graphs (Figure 53) show that the 95% of the errors are smaller than the 2% of the reference cycle times. The fact that the values are more spread for small reference values suggests that the variability in calculating the cycle time decreases for longer cycle times.

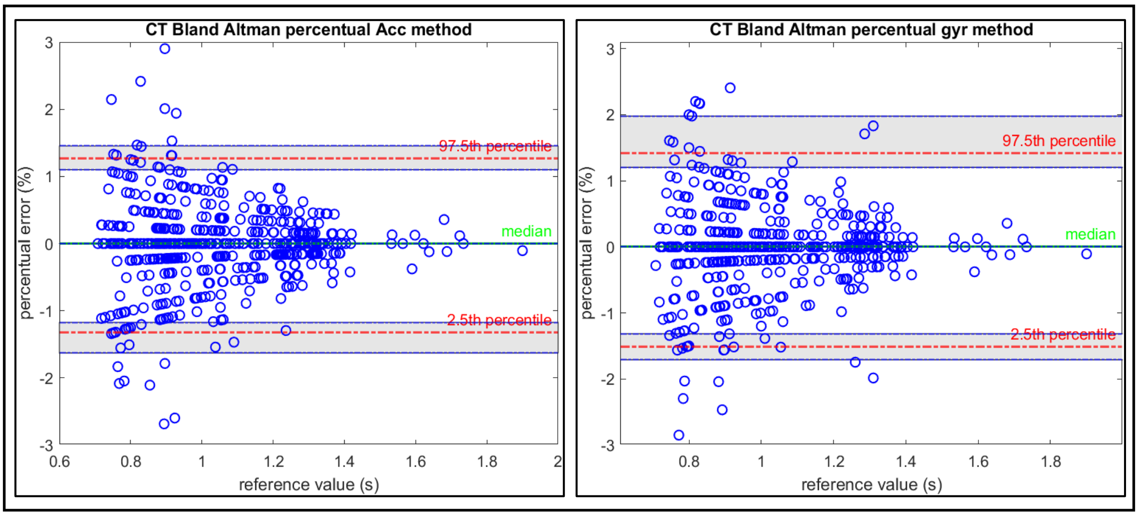

Figure 53 - Cycle time Bland Altman analysis.

The push time Bland Altman analysis of the acceleration and angular velocity method (Figure 54) show that the angular velocity method median error is smaller than the acceleration method median error but the dispersion of the data is greater in the angular velocity method.

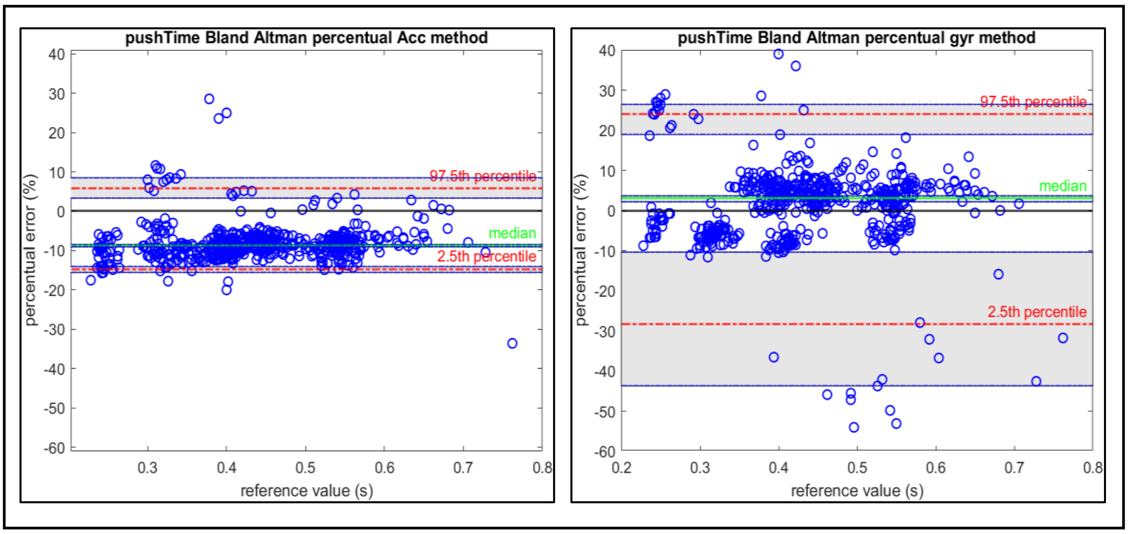

Figure 54 - Push time Bland Altman analysis for the acceleration and angular velocity cycle events identification methods.

The fusion method (Figure 55) is the one with the smaller push time median error but the data dispersion is similar to the one in the angular velocity method.

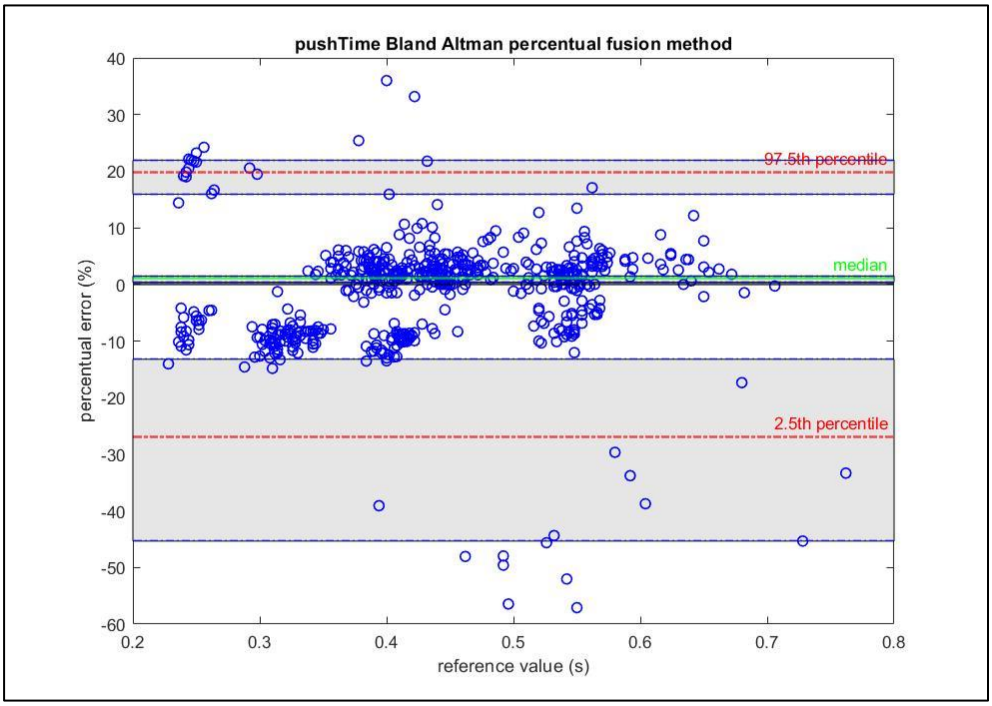

Figure 55 - Push time Bland Altman analysis for the fusion cycle events identification method.

6.5 Relationship between IMUs signals and skiing speed or terrain inclination

The parameters calculated directly from the IMUs signal norms (mean on the entire cycle, integral on the entire cycle, and pole lift peak) are reported grouped by different skiing speed and inclination.

The mean of the acceleration signal on the entire pushing cycle (Figure 56) seems a parameter sensitive to both the speed and the inclination. However, the skiing speed influences this parameter more than the inclination. In particular, this parameter value increases with higher skiing speeds and slightly increases in a more inclined condition.

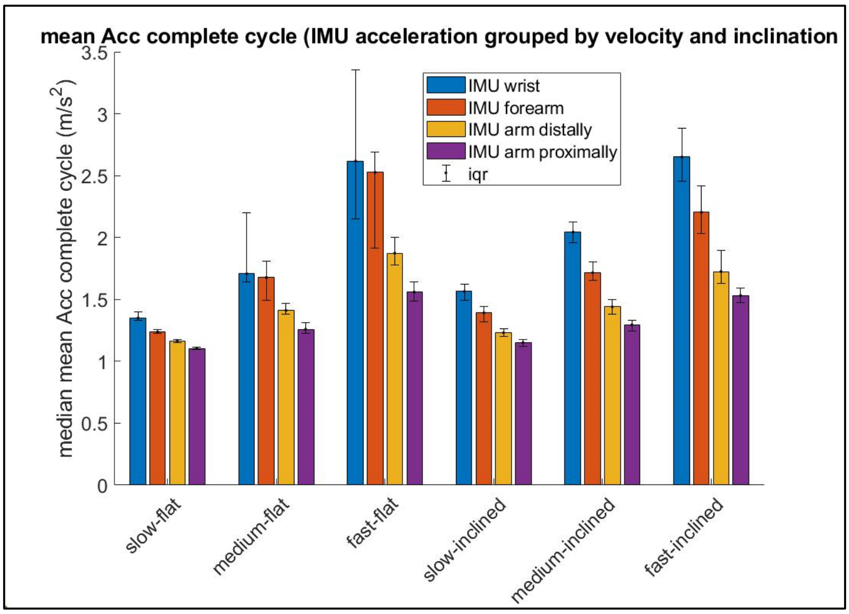

Figure 56 - Cycles mean acceleration over different skiing conditions.

The mean of the angular velocity signal on the entire pushing cycle (Figure 57) from the sensors on the forearm is more sensitive to different inclinations than to different velocities, while the angular velocity mean from the sensors on the arm are more sensitive to different velocities than to different inclinations. Specifically, the cycle angular velocity mean from the forearm sensors decreases in more inclined conditions and increase from a slow to a medium speed condition while it does not change from a medium to a fast condition. The cycle angular velocity mean from the arm sensors, instead, increases with higher speeds and slightly increases in a more inclined condition.

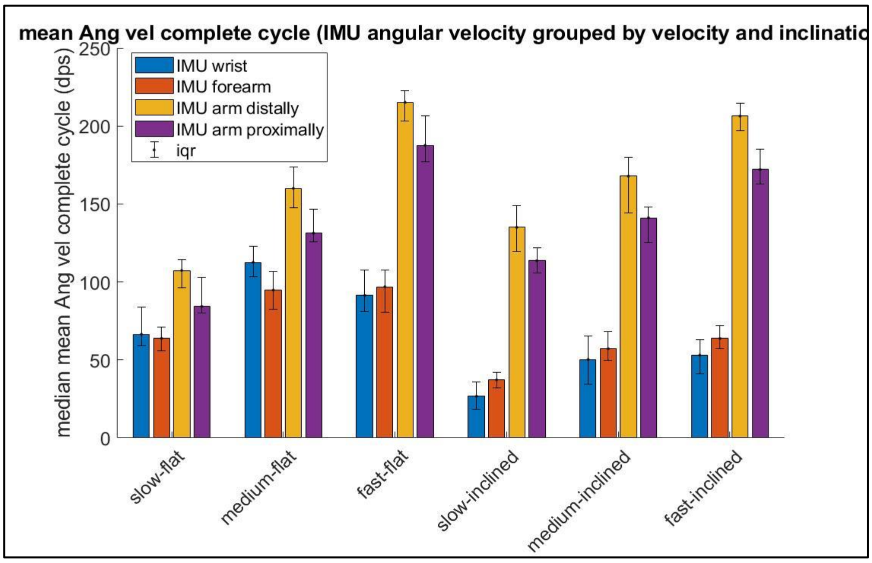

Figure 57 - Cycles mean angular velocity over different skiing conditions.

The mean of the acceleration signal on the entire pushing cycle (Figure 58) is a parameter sensitive to both different speeds and different inclinations. It increases at higher speeds, but it decreases in a more inclined condition.

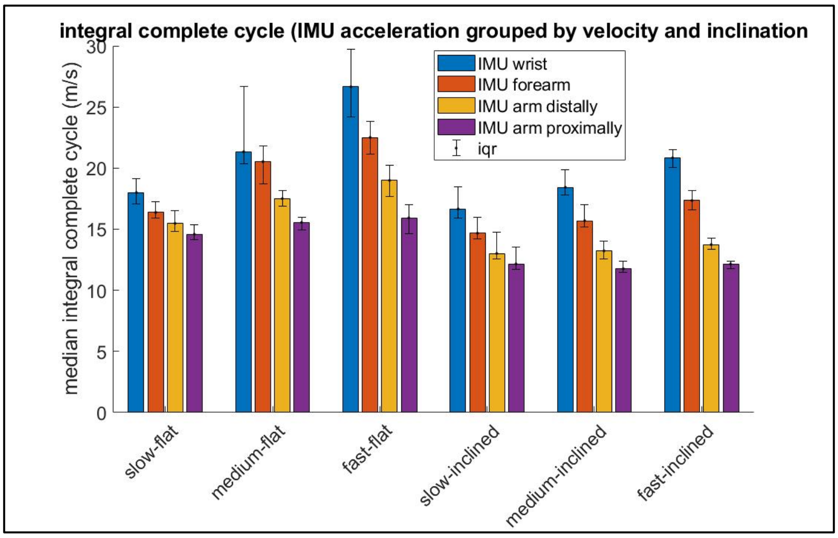

Figure 58 - Cycles acceleration integral over different skiing conditions.

The mean of the angular velocity signal on the entire pushing cycle (Figure 59) from the sensors on the forearm decreases in a steeper condition and increase from a slow to a medium speed condition but not from a medium to a fast speed condition. The same parameter, but from the sensors on the arm increases at higher speeds but only in a flat condition, while at a higher inclination the parameter value is generally lower than in the flat condition but it not sensitive to speed variations.

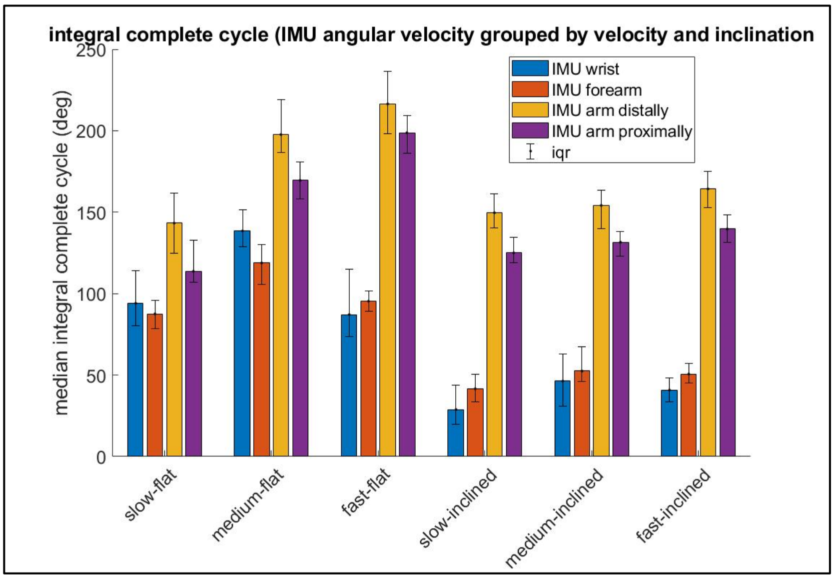

Figure 59 - Cycles angular velocity integral over different skiing conditions.

The acceleration pole lift peak (Figure 60) is particularly sensitive to the speed and it increases in faster skiing conditions, while it is less sensitive to the inclination.

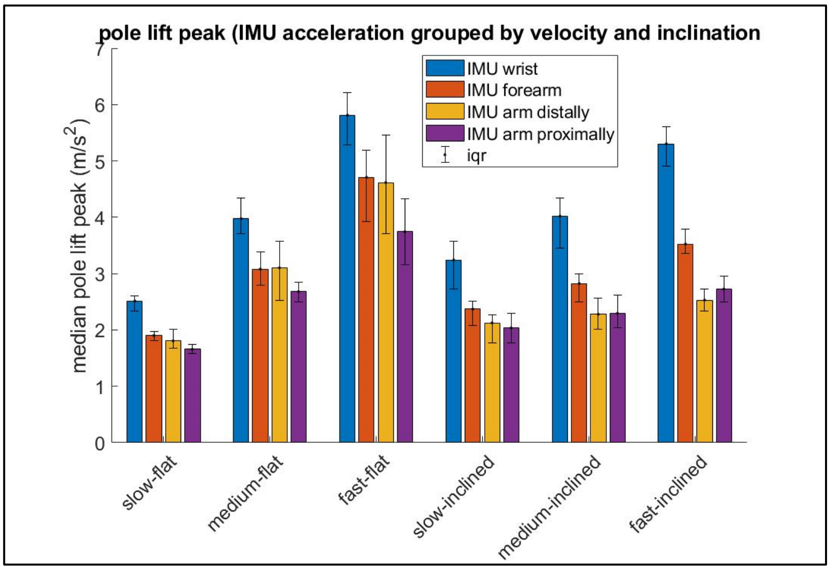

Figure 60 – Pole lift acceleration peak over different skiing conditions.

The angular velocity pole lift peak (Figure 61) from the wrist sensor show in general a decrement at a more inclined condition where it also increases at higher speeds, but in a flat conditions seems to increase from a slow to a medium speed condition but not from a medium to a fast condition. The same parameter from the other sensors is sensitive to both different inclination and speed conditions and, in particular, it increases at higher speed and decreases in a steeper condition.

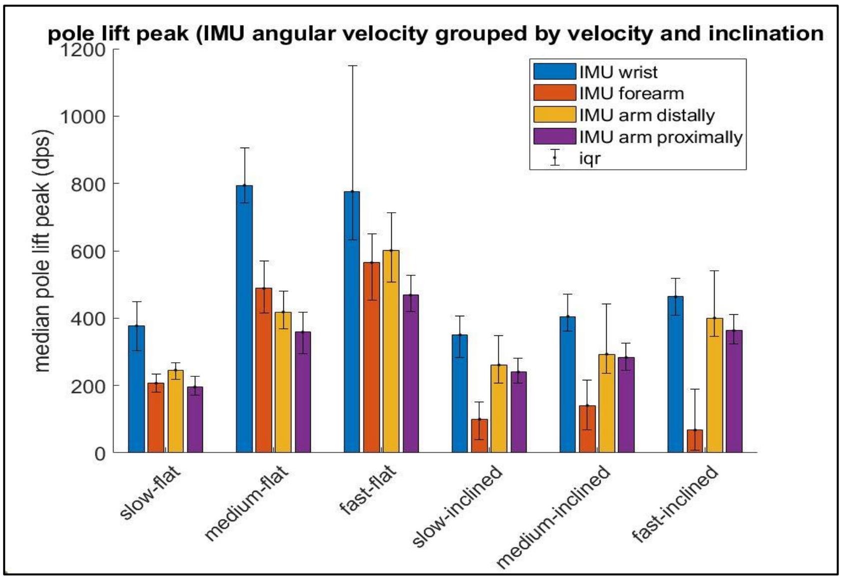

Figure 61 – Pole lift angular velocity peak over different skiing conditions.

6.6 Ski inclination

The ski inclination calculated integrating the angular velocity around the ski medio-lateral axis shows to be strongly affected by a drift error (Figure 62, Figure 63, Figure 64, Figure 65). The comparison between the integration of the calibrated and the uncalibrated signals (Figure 62) demonstrates that the gyro offset correction sorted an effect on the drift error, but it did not completely solved the problem. The fact that the entity of the drift errors in the calibrated signals changes a lot depending on which trial is analysed, suggests that the problem raised in the offset correction is that the offset was modelled as a linear function of time and the two samples (calibration acquisition) that define the modelled error were taken one at the beginning and one at the end of the experiment. The experiment lasted around 120 minutes for the first subject and around 90 minutes for the second subject. In the literature, the bias is usually corrected thanks to two static acquisitions at the beginning and at the end of each trail which last less than the entire experiment [38],[27]. The problem was probably, therefore that the offset is not linear over a long period of time, and this non-linearity is probably due to the change in the sensor temperature over time caused by the sensor heating after it is switched on. In the literature, is indeed reported that to minimize the drift error it is recommended to switch on the sensors at least 20 minutes before the experiment and wait till the sensor reach an equilibrium temperature [27]. Moreover, in the literature it is also reported that the drift linked to the gyroscope offset is strongly affected by the senso temperature change [27].

On the other hand, the ski inclination calculated with the method that used the ski IMU accelerometer as an inclinometer agrees with the treadmill inclination set at the beginning of each trial within a mean error of about 0.5 deg (Figure 66). This inclinometer-based method shows, therefore better results than the angular velocity integration method (Figure 62, Figure 63, Figure 64, Figure 65) because the gyroscope offset was not completely corrected.

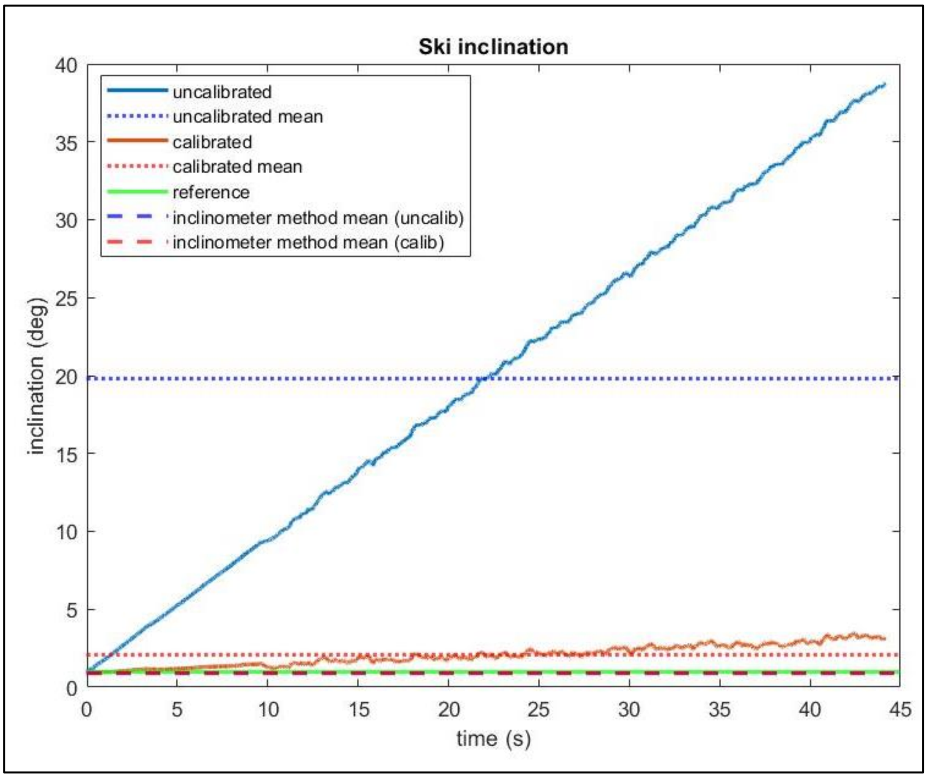

Figure 62 - Ski inclination calculated integrating the linear acceleration. First trial recorded from the first subject.

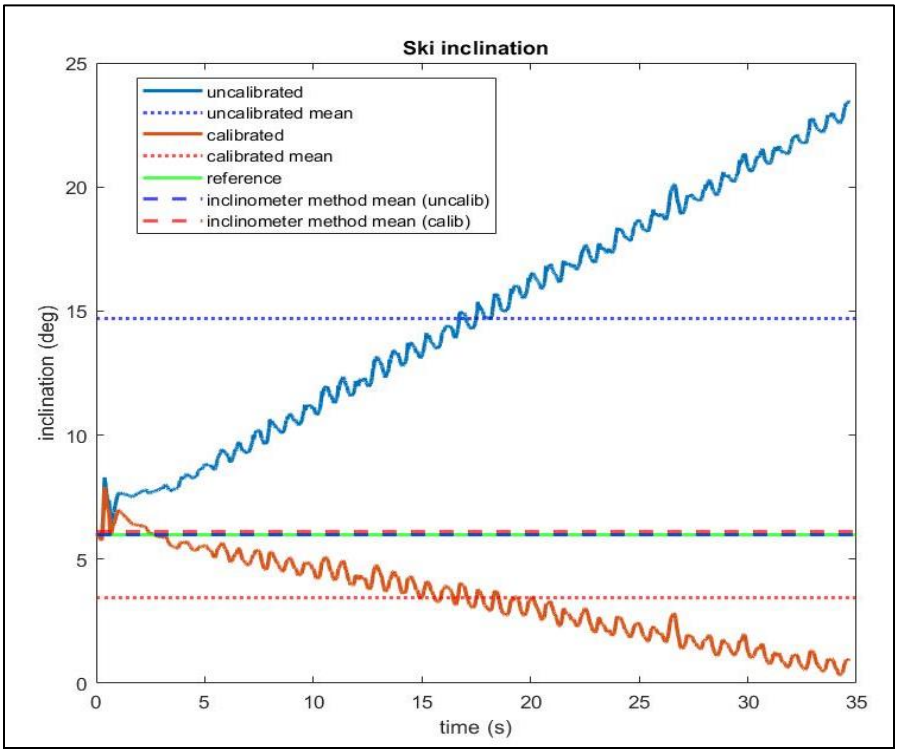

Figure 63 - Ski inclination calculated integrating the linear acceleration. Last trial recorded from the first subject.

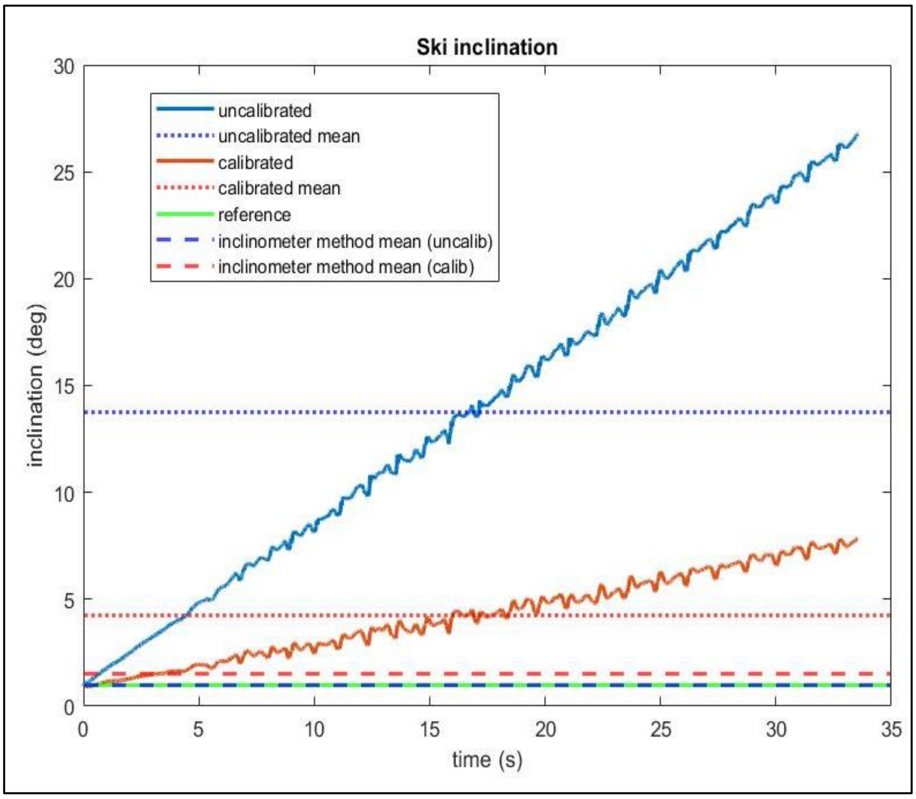

Figure 64 - Ski inclination calculated integrating the linear acceleration. First trial recorded from the second subject.

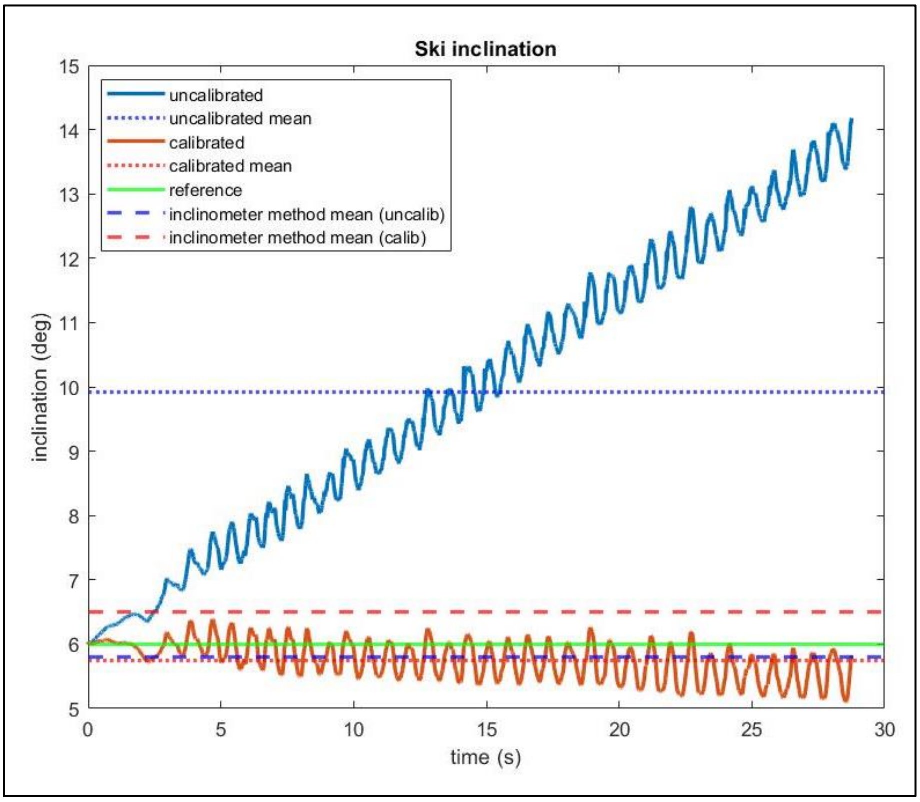

Figure 65 - Ski inclination calculated integrating the linear acceleration. Last trial recorded from the second subject.

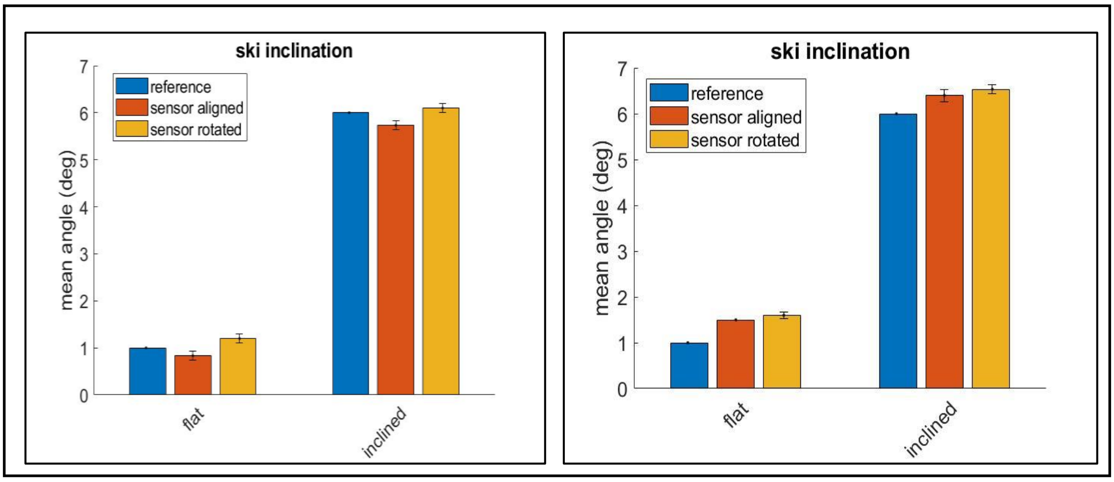

Figure 66 - Ski inclination calculation with the inclinometer method. *The results about the ski inclination calculated from the first subject are on the left, while the ones calculated from the second subject are on the right.*

6.7 Ski velocity and displacement

The ski velocity and displacement that were calculated integrating once and two times the sensor ski acceleration along the ski longitudinal axis are reported for the 10th trial of the first subject (Figure 67) and for the 2nd trial of the first subject (

Figure 68). These two trials have been chosen to show how the ski velocity and displacement sometimes agree quite well with the reference (Figure 67) and sometimes commits large errors (

Figure 68). However from both the trials it is possible to notice that the results from the calibrated and uncalibrated signals are very similar and that in the velocity and in the displacement there is not a noticeable trend over time that would indicate a drift error. This fact suggests that the filtering method used to remove the gravity components from the integrated acceleration worked well and that the disagreement between the results of reference and the results from the acceleration integration have another origin. It is therefore appropriate reflect on some issues to try to explain this disagreement:

- The treadmill speed is considered the reference speed, assuming that on average the ski speed is equal to the treadmill speed, but it is unknown how accurate this approximation is.
- The reference displacement for each cycle is calculated as the treadmill velocity multiplied by the cycle time, but it is unknown how accurate this approximation is.

The method developed to calculate the ski inclination involves a sensor alignment with the ski frame before the integration. If the alignment is not well performed the acceleration integration does not happen exactly along the ski longitudinal axis. However, this possible source of error should not be the principal source because the sensor alignment is performed at the beginning of the first 6 trials and again at the beginning of the last 6 trials, but not at the beginning of each trial, and there are good (Figure 67) and bad (

- Figure 68) performances (of the ski inclination calculation) for trials in which the sensor is aligned in the same way.
- The linear acceleration integration starts at the beginning of each trial when the athlete is steady on the treadmill (the initial velocity and displacement are

imposed to be zero). The treadmill instantaneous speed is then added to the instantaneous speed obtained by the integration for all the duration of the trial to obtain the relative speed between the ski and the treadmill.

All the above issues could contribute to the discrepancy between the reference results and the results based on the linear acceleration integration. However, the reference in this case is not exactly a reference since the ski velocity is not directly detected by a system but it is assumed to be on average the same of the treadmill.

To better asses the performance of the method used to calculate the ski velocity and displacement from the ski IMUs it would be therefore more appropriate compare the results with a marker-based stereo photogrammetric system which would calculate directly the ski velocity and displacement.

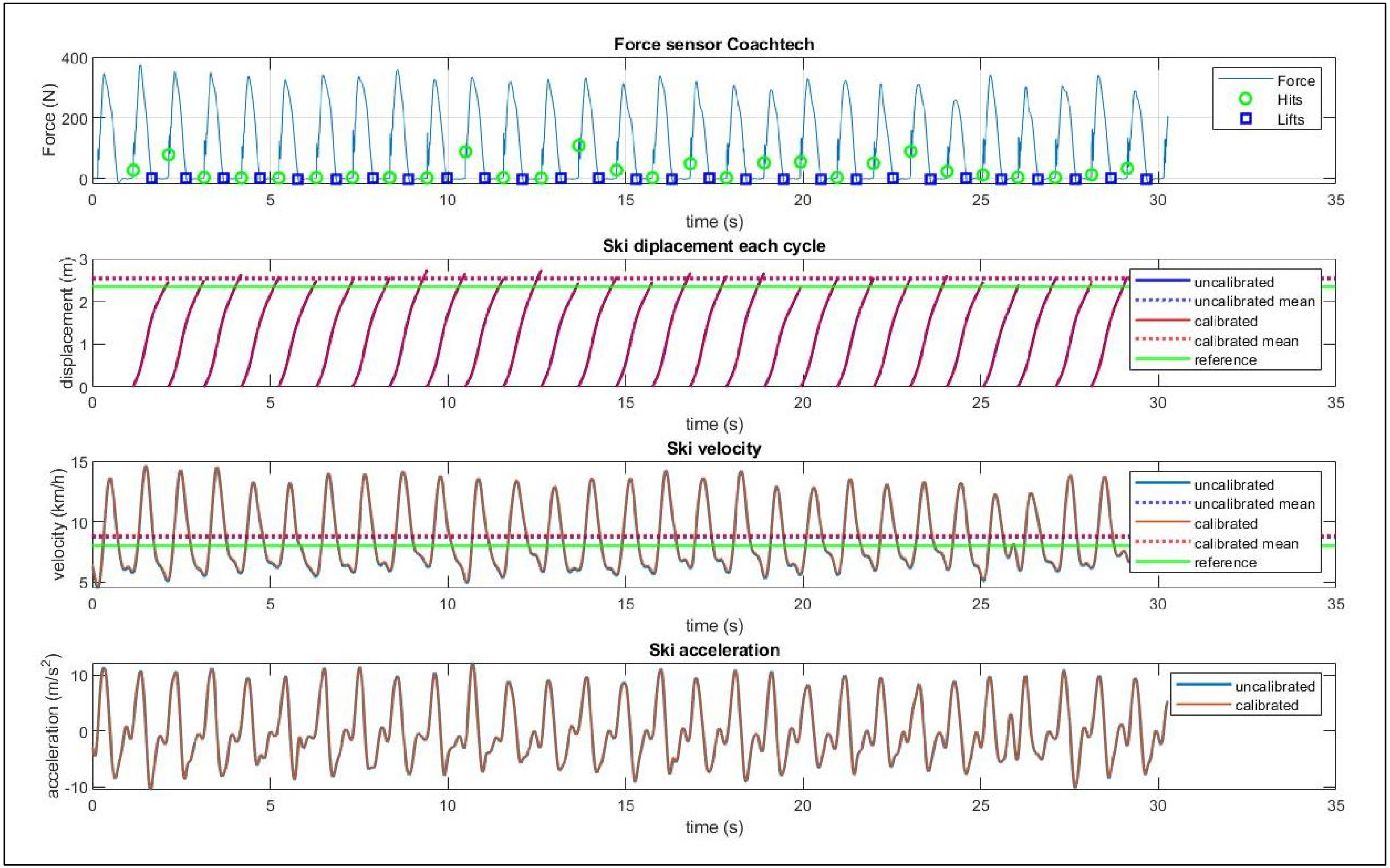

Figure 67 - Ski velocity and displacement. 10th trial acquired from the first subject.

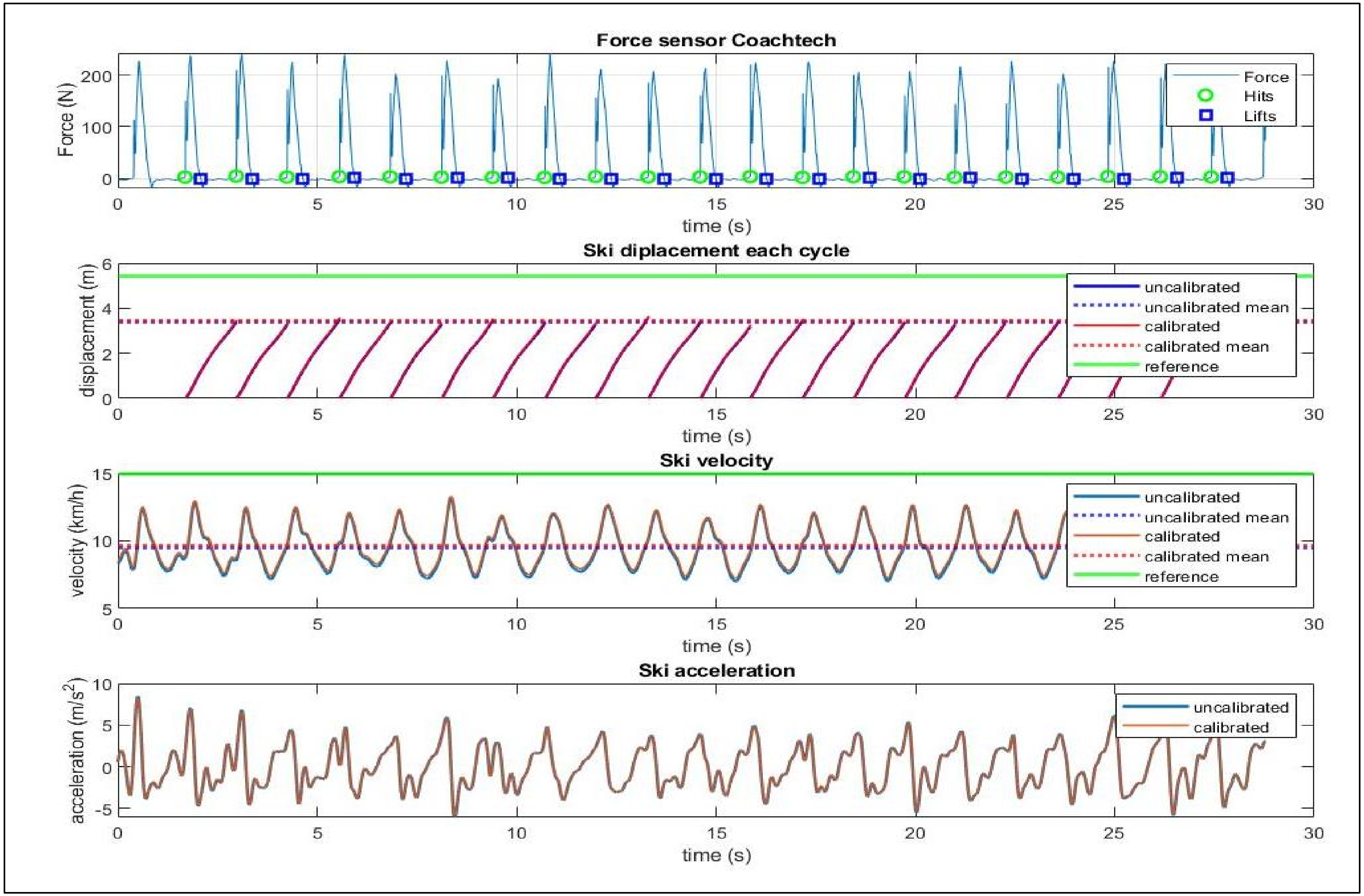

Figure 68 - Ski velocity and displacement. 2nd trial acquired from the first subject.

7 Conclusions

The principal purpose of this thesis was to elaborate on the calculation of the cycle parameters (cycle time, pushing time, recovery time, cycle length, cycle speed) in XC skiing double poling using IMU sensors and this motive led to the implementation of 3 IMU-based cycle events identification methods (for the computation of the cycle temporal parameters) and to the calculation of the ski speed with an IMU on the ski (for the computation of the cycle spatial parameter). A pole events acceleration norm-based method had already showed good results in detecting the pole hits and the pole lifts in previous studies [7], [16] with IMUs placed on the poles [7] or embedded in the poles [16], but in the studies where a sensor was placed on the wrist, only the pole hits were identified [13], [21], while a pole lifts identification was only proposed, but not reported [17]. The other two cycle events identification methods, the one based on the angular velocity norm and the “fusion” one, are novel methods, and they had a performance comparable with the method based on the acceleration norm. Moreover, as far as the author knows, the robustness of the cycle events identification algorithms to different positions on the upper limb had never been analysed before.

The possibility to calculate the ski inclination was also investigated, given its importance in contextualizing the cycle parameters. Regarding the cycle events identification methods, all the sensors on the upper limb, demonstrated to be adequate to identify the poling cycles with a null or a small amount of missed cycles, and to be capable to identify quite accurately the pole hits (error<44 ms) and, therefore, to provide a cycle time calculation consistent with the reference one (error<2 ms). However, the sensors placed more distally on the upper limb (in particular the wrist sensor), showed to provide in general a better performance. Considering, then, only the wrist sensor, the cycle events identification method based on the acceleration norm and the “fusion” one were the finest in detecting the pole hits with an overall accuracy of 4 ms and a precision of 8 ms, while the pole lifts were better identified by the angular velocity norm-based method and the “fusion” method with an overall accuracy smaller than 2 ms and a precision of 46 ms. However, considering the performances in different treadmill speed and inclination conditions, the angular velocity norm-based and the “fusion” methods, the lifts identification accuracy changes depending on the skiing conditions and show a better performance when the treadmill is inclined (error < 10 ms) with respect to a flat condition (error < 42). The accuracy and the precision of the cycle events identification methods in detecting the pole hits and the pole lifts, directly affect the cycle parameters calculation performance. The cycle time is calculated with a relative accuracy and a relative precision both smaller than the 0.4% of the reference value by all the cycle events identification methods. The acceleration norm-based method calculated the push time with a relative accuracy smaller than the 11% of the reference value in all the skiing conditions (treadmill speed and inclination). The angular velocity norm-based method and the "fusion" method calculated the push time with a relative accuracy smaller than the 10% of the reference value in the flat conditions and smaller than the 6% of the reference value in the inclined conditions.

Regarding the IMUs parameters (mean on a cycle, integral on a cycle and the pole lift peak value) calculated for the linear acceleration and the angular velocity of all the sensors on the upper limb showed to be strongly influenced by different skiing speed and terrain inclination suggesting the possibility to use them as indicators of different speed and inclination conditions or as parameters to asses performance. Specifically, the parameter "mean on a cycle" for the linear acceleration, appeared to be particularly sensitive to skiing speed variations, whereas the angular velocity integral seemed more influenced by treadmill inclination.

The ski inclination calculated integrating the ski sensor angular velocity around the ski medio-lateral axis was mainly considered to assess the efficacy of the IMUs calibration in reducing the drift errors due to the signal integration, and it proved, indeed, that the calibration performed, helped to reduce this type of error. However, the same results also highlighted a problem in the gyroscope bias correction which led to unsatisfactory performances even after the calibration. The ski inclination calculated with the inclinometer method seemed to agree with the treadmill inclination suggesting that the ski sensor alignment with the ski frame and the following filtering to extrapolate only the gravity components were successfully performed.

Concerning the skis speed and displacement calculated integrating the ski sensor acceleration along the ski longitudinal axis, the results did not show an evident trend suggesting an effective gravity components removal from the integrated acceleration signal, but the discrepancy of the results with the expected speed (the treadmill speed) depending on the trial, underlines a problem at some point during the procedure. However, it could be not appropriate to compare the ski speed calculated through the ski sensor acceleration integration with the treadmill velocity to assess the performance of the method.

7.1 Limits of the thesis and future perspective

A possible limitation was the small number of participants that took part to the measurements. Indeed, despite it was large enough to understand the overall behaviour of the methods developed in detecting the cycle events, it was insufficient for a validation of the methods. In future experiments would be interesting perform similar measurements, but with a larger number of subjects to ensure the validation of the cycle events identification methods proposed.

Regarding the inclinometer-based method to calculate the skis inclination, it seemed to be effective. However, the skis inclination was constant during each trial (excluding the movements due to the skis flexions related to the flexibility of the ski) and, therefore, the gravity components could be separated from the ski acceleration effectively. In order to implement this method outside on snow and along a real track, the ski inclination could not be considered constant anymore and the poor temporal resolution of the inclinometer method would not recognize fast inclination changes. However, it is speculated that the method could be appropriate also outside to provide an overall description of the terrain inclination in different sections of the track allowing to contextualize the cycle parameters calculation; nevertheless, additional studies are required to confirm it.

Concerning the ski velocity and displacement calculated by integrating the ski sensor linear acceleration, the gravity components were removed filtering the acceleration signal with a low pass filter to obtain only the gravity components to subtract to the acceleration signal that will be integrated. The operation of extraction of the gravity components (low pass filter of the acceleration) is the same followed in the inclinometer method for the ski inclination calculation and, therefore, the ski velocity and displacement evaluation has the same limits in terms of temporal resolution described above for the estimation of the ski inclination with the inclinometer method. The IMU-based ski velocity and displacement calculation method could be therefore not suitable in the present form to be used outside, or in situations in which the skis inclination changes, because the acceleration gravity components would not be adequately removed. Additional studies are required to test variation of the current approach to calculate ski velocity and displacement.

Bibliography

[1] T. M. Seeberg, J. Tjønnås, O. M. H. Rindal, P. Haugnes, S. Dalgard, and Ø. Sandbakk, "A multi-sensor system for automatic analysis of classical cross-country skiing techniques," *Sport. Eng.*, vol. 20, no. 4, pp. 313–327, 2017, doi: 10.1007/s12283-017-0252-z.

[2] Ø. Sandbakk and H. C. Holmberg, "A reappraisal of success factors for olympic cross-country skiing," *Int. J. Sports Physiol. Perform.*, vol. 9, no. 1, pp. 117–121, 2014, doi: 10.1123/IJSPP.2013-0373.

[3] J. Nilsson, P. Tveit, O. Eikrehagen, and J. Nilsson, "Cross-Country Skiing: Effects of speed on temporal patterns in classical style and freestyle cross-country skiing," *Sport. Biomech.*, vol. 3, no. 1, pp. 85–108, 2004, doi: 10.1080/14763140408522832.

[4] S. J. Lindinger, T. Stoggl, E. Müller, and H. C. Holmberg, "Control of speed during the double poling technique performed by elite cross-country skiers," *Med. Sci. Sports Exerc.*, vol. 41, no. 1, pp. 210–220, 2009, doi: 10.1249/MSS.0b013e318184f436.

[5] T. L. Stöggl and E. Müller, "Kinematic determinants and physiological response of cross-country skiing at maximal speed," *Med. Sci. Sports Exerc.*, vol. 41, no. 7, pp. 1476–1487, 2009, doi: 10.1249/MSS.0b013e31819b0516.

[6] H. C. Holmberg, S. Lindinger, T. Stöggl, E. Eitzlmair, and E. Müller, "Biomechanical analysis of double poling in elite cross-country skiers," *Med. Sci. Sports Exerc.*, vol. 37, no. 5, pp. 807–818, 2005, doi: 10.1249/01.MSS.0000162615.47763.C8.

[7] B. Fasel, J. Favre, J. Chardonnens, G. Gremion, and K. Aminian, "An inertial sensor-based system for spatio-temporal analysis in classic cross-country skiing diagonal technique," *J. Biomech.*, vol. 48, no. 12, pp. 3199–3205, 2015, doi: 10.1016/j.jbiomech.2015.07.001.

[8] F. Marsland, C. Mackintosh, J. Anson, K. Lyons, G. Waddington, and D. W. Chapman, "Using micro-sensor data to quantify macro kinematics of classical cross-country skiing during on-snow training," *Sport. Biomech.*, vol. 14, no. 4, pp.

435–447, 2015, doi: 10.1080/14763141.2015.1084033.

[9] S. J. Lindinger and H. C. Holmberg, “How do elite cross-country skiers adapt to different double poling frequencies at low to high speeds?,” *Eur. J. Appl. Physiol.*, vol. 111, no. 6, pp. 1103–1119, 2011, doi: 10.1007/s00421-010-1736-8.

[10] T. Stoggl, E. Muller, and S. Lindinger, “Biomechanical comparison of the double-push technique and the conventional skate skiing technique in cross-country sprint skiing,” *J. Sports Sci.*, vol. 26, no. 11, pp. 1225–1233, 2008, doi: 10.1080/02640410802027386.

[11] B. Fasel, “Drift Reduction for Inertial Sensor Based Orientation and Position Estimation in the Presence of High Dynamic Variability During Competitive Skiing and Daily-Life Walking THÈSE N O 7803 (2017) ÉCOLE POLYTECHNIQUE FÉDÉRALE DE LAUSANNE Benedikt FASEL,” 2017.

[12] C. Zoppirolli, K. Hébert-losier, H. Holmberg, and K. Hébert-losier, “Biomechanical determinants of cross-country skiing performance : A systematic review review,” *J. Sports Sci.*, vol. 00, no. 00, pp. 1–22, 2020, doi: 10.1080/02640414.2020.1775375.

[13] Y. Sakurai, F. Zenya, and Y. Ishige, “Automated identification and evaluation of subtechniques in classical-style roller skiing,” *J. Sport. Sci. Med.*, vol. 13, no. 3, pp. 651–657, 2014.

[14] F. Marsland, K. Lyons, J. Anson, G. Waddington, C. Macintosh, and D. Chapman, “Identification of cross-country skiing movement patterns using micro-sensors,” *Sensors*, vol. 12, no. 4, pp. 5047–5066, 2012, doi: 10.3390/s120405047.

[15] H. Myklebust, N. Nunes, J. Hallén, and H. Gamboa, “Morphological analysis of acceleration signals in cross-country skiing: Information extraction and technique transitions detection,” *BIOSIGNALS 2011 - Proc. Int. Conf. Bio-Inspired Syst. Signal Process.*, pp. 510–517, 2011.

[16] J. Bruzzo, N. C. Perkins, and A. Mikkola, “Embedded inertial measurement unit reveals pole lean angle for cross-country skiing,” *Sport. Eng.*, vol. 23, no. 1, 2020, doi: 10.1007/s12283-019-0316-3.

[17] Y. Sakurai, Z. Fujita, and Y. Ishige, “Automatic identification of subtechniques in

skating-style roller skiing using inertial sensors," *Sensors (Switzerland)*, vol. 16, no. 4, 2016, doi: 10.3390/s16040473.

[18] A. Nikkola, O. Särkkä, S. Suuriniemi, and L. Kettunen, "Pole force and inertial measurements to analyze cross-country skiing performance in field conditions," *Proc. Inst. Mech. Eng. Part P J. Sport. Eng. Technol.*, vol. 232, no. 4, pp. 323–333, 2018, doi: 10.1177/1754337118759359.

[19] F. Marsland, J. Anson, G. Waddington, H. C. Holmberg, and D. W. Chapman, "Macro-kinematic differences between Sprint and Distance cross-country skiing competitions using the classical technique," *Front. Physiol.*, vol. 9, no. MAY, pp. 1–8, 2018, doi: 10.3389/fphys.2018.00570.

[20] F. Marsland *et al.*, "Full course macro-kinematic analysis of a 10 km classical cross-country skiing competition," *PLoS One*, vol. 12, no. 8, pp. 1–15, 2017, doi: 10.1371/journal.pone.0182262.

[21] J. K. Baumgart, P. Haugnes, L. M. Bardal, S. Østerås, J. Kocbach, and Ø. Sandbakk, "Development of a Framework for the Investigation of Speed, Power, and Kinematic Patterns in Para Cross-Country Sit-Skiing: A Case Study of an LW12 Athlete," *Front. Sport. Act. Living*, vol. 1, no. July, pp. 1–9, 2019, doi: 10.3389/fspor.2019.00004.

[22] V. Ohtonen, O., Ruotsalainen, K., Mikkonen, P., Heikkinen, T., Hakkarainen, A., Leppävuori, A., & Linnamo, "Online feedback system for athletes and coaches," in *3rd International Congress on Science and Nordic Skiing*, 2015.

[23] "ATR-Promotions." https://www.atr-p.com/products/TSND121.html.

[24] U. Parvis, M., Ferraris, F., & Grimaldi, "Procedure for effortless in-field calibration of three-axis rate gyros and accelerometers." 1995.

[25] A. M. Sabatini, "Estimating three-dimensional orientation of human body parts by inertial/magnetic sensing," *Sensors*, vol. 11, no. 2, pp. 1489–1525, 2011, doi: 10.3390/s110201489.

[26] G. Y. Millet, M. D. Hoffman, R. B. Candau, and P. S. Clifford, "Poling forces during roller skiing: Effects of technique and speed," *Med. Sci. Sports Exerc.*, vol. 30, no. 11, pp. 1645–1653, 1998, doi: 10.1097/00005768-199811000-00014.

[27] B. Fasel and M. Erich, “Joint Inertial Sensor Orientation Drift Reduction for Highly Dynamic Movements,” vol. 22, no. 1, pp. 77–86, 2018.

[28] G. Ligorio and A. M. Sabatini, “A novel kalman filter for human motion tracking with an inertial-based dynamic inclinometer,” *IEEE Trans. Biomed. Eng.*, vol. 62, no. 8, pp. 2033–2043, 2015, doi: 10.1109/TBME.2015.2411431.

[29] B. Fasel, J. Spörri, P. Schütz, S. Lorenzetti, and K. Aminian, “Validation of functional calibration and strap-down joint drift correction for computing 3D joint angles of knee, hip, and trunk in alpine skiing,” *PLoS One*, vol. 12, no. 7, pp. 1–17, 2017, doi: 10.1371/journal.pone.0181446.

[30] J. Favre, R. Aissaoui, B. M. Jolles, J. A. de Guise, and K. Aminian, “Functional calibration procedure for 3D knee joint angle description using inertial sensors,” *J. Biomech.*, vol. 42, no. 14, pp. 2330–2335, 2009, doi: 10.1016/j.jbiomech.2009.06.025.

[31] J. Chardonnens, J. Favre, F. Cuendet, G. Gremion, and K. Aminian, “A system to measure the kinematics during the entire ski jump sequence using inertial sensors,” *J. Biomech.*, vol. 46, no. 1, pp. 56–62, 2013, doi: 10.1016/j.jbiomech.2012.10.005.

[32] B. Fasel, J. Spörri, P. Schütz, S. Lorenzetti, and K. Aminian, “An inertial sensor-based method for estimating the athlete’s relative joint center positions and center of mass kinematics in alpine ski racing,” *Front. Physiol.*, vol. 8, no. NOV, pp. 3–4, 2017, doi: 10.3389/fphys.2017.00850.

[33] J. Chardonnens, J. Favre, B. Le Callennec, F. Cuendet, G. Gremion, and K. Aminian, “Automatic measurement of key ski jumping phases and temporal events with a wearable system,” *J. Sports Sci.*, vol. 30, no. 1, pp. 53–61, 2012, doi: 10.1080/02640414.2011.624538.

[34] N. Breslow, “Lessons in biostatistics,” *Past, Present. Futur. Stat. Sci.*, vol. 25, no. 2, pp. 335–347, 2014, doi: 10.1201/b16720-35.

[35] L. S. Nawarathna and P. K. Choudhary, “Measuring agreement in method comparison studies with heteroscedastic measurements,” *Stat. Med.*, vol. 32, no. 29, pp. 5156–5171, 2013, doi: 10.1002/sim.5955.

[36] J. C. Maas *et al.*, “Measuring wearing time of knee-ankle-foot orthoses in children with cerebral palsy: comparison of parent-report and objective measurement,” *Disabil. Rehabil.*, vol. 40, no. 4, pp. 398–403, 2018, doi: 10.1080/09638288.2016.1258434.

[37] B. Desharnais, F. Camirand-Lemyre, P. Mireault, and C. D. Skinner, “Determination of confidence intervals in non-normal data: Application of the bootstrap to cocaine concentration in femoral blood,” *J. Anal. Toxicol.*, vol. 39, no. 2, pp. 113–117, 2015, doi: 10.1093/jat/bku127.

[38] E. Bergamini, G. Ligorio, A. Summa, G. Vannozzi, A. Cappozzo, and A. M. Sabatini, “Estimating orientation using magnetic and inertial sensors and different sensor fusion approaches: Accuracy assessment in manual and locomotion tasks,” *Sensors (Switzerland)*, vol. 14, no. 10, pp. 18625–18649, 2014, doi: 10.3390/s141018625.

Appendix A

In the results chapter the errors in detecting the pole hits and the pole lifts and in calculating the cycle time and the push time were reported only for the wrist sensor because it was showed that the wrist sensor was the one with the best performances and that the other sensors on the upper limb were adequate to calculate the cycle time but not the intra cycle parameters such as the push time. Here, the errors in detecting the cycle events and in calculating the cycle parameters are reported also for the other sensors on the upper limb.

Sensor placed on the middle of the forearm

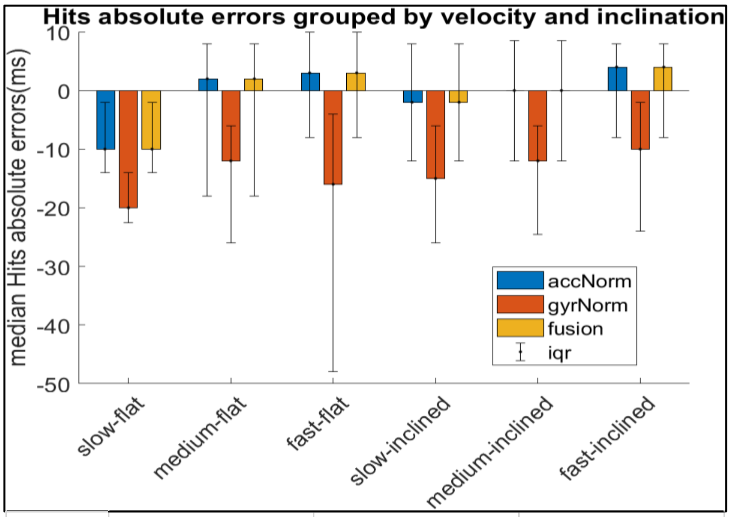

	Acc method		Gyr method		Fusion method	
	median	iqr	median	iqr	median	iqr
slow-flat	-10	12	-20	9	-10	12
medium-fl	2	26	-12	20	2	26
fast-flat	3	18	-16	44	3	18
slow-inclin	-2	20	-15	20	-2	20
medium-in	0	21	-12	19	0	21
fast-incline	4	16	-10	22	4	16

Figure 69 - Pole hits errors in different skiing conditions. Cycle events identification methods comparison. Sensor on the middle of the forearm.

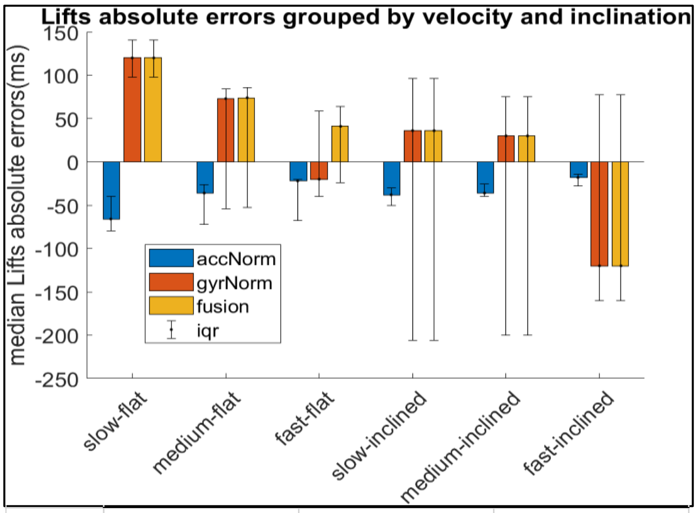

	Acc method		Gyr method		Fusion method	
	median	iqr	median	iqr	median	iqr
slow-flat	-66	40	120	43	120	43
medium-fl	-36	47	73	138	74	139
fast-flat	-22	48	-20	99	41	88
slow-inclin	-38	20	36	302	36	302
medium-in	-36	15	30	276	30	276
fast-incline	-18	14	-120	238	-120	238

Figure 70 - Pole lifts errors in different skiing conditions. Cycle events identification methods comparison. Sensor on the middle of the forearm.

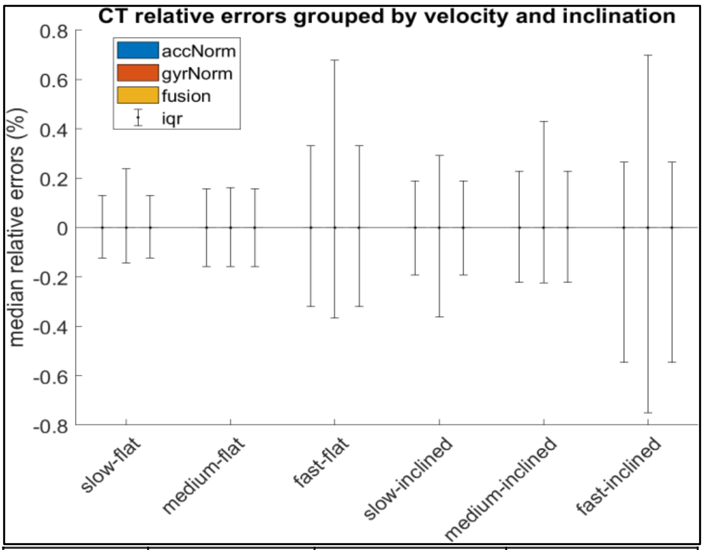

	Acc method		Gyr method		Fusion method	
	median	iqr	median	iqr	median	iqr
slow-flat	0.0	0.3	0.0	0.4	0.0	0.3
medium-flat	0.0	0.3	0.0	0.3	0.0	0.3
fast-flat	0.0	0.7	0.0	1.0	0.0	0.7
slow-inclined	0.0	0.4	0.0	0.7	0.0	0.4
medium-inclined	0.0	0.4	0.0	0.7	0.0	0.4
fast-inclined	0.0	0.8	0.0	1.4	0.0	0.8

Figure 71 – Cycle time errors in different skiing conditions. Cycle events identification methods comparison. Sensor on the middle of the forearm.

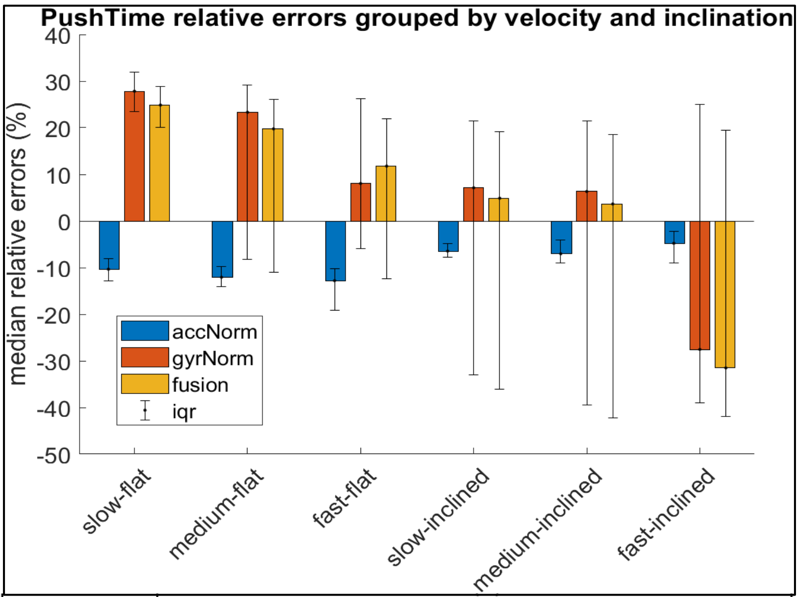

	Acc method		Gyr method		Fusion method	
	median	iqr	median	iqr	median	iqr
slow-flat	-10.3	4.8	27.8	8.4	24.9	8.7
medium-flat	-12.1	4.3	23.3	37.3	19.8	37.1
fast-flat	-12.8	9.0	8.0	32.1	11.8	34.2
slow-inclined	-6.5	2.8	7.1	54.6	4.9	55.3
medium-inclined	-7.0	4.9	6.3	60.8	3.6	60.6
fast-inclined	-4.8	6.6	-27.5	64.0	-31.5	61.3

Figure 72 – Push time errors in different skiing conditions. Cycle events identification methods comparison. Sensor on the middle of the forearm.

Sensor placed distally on the arm

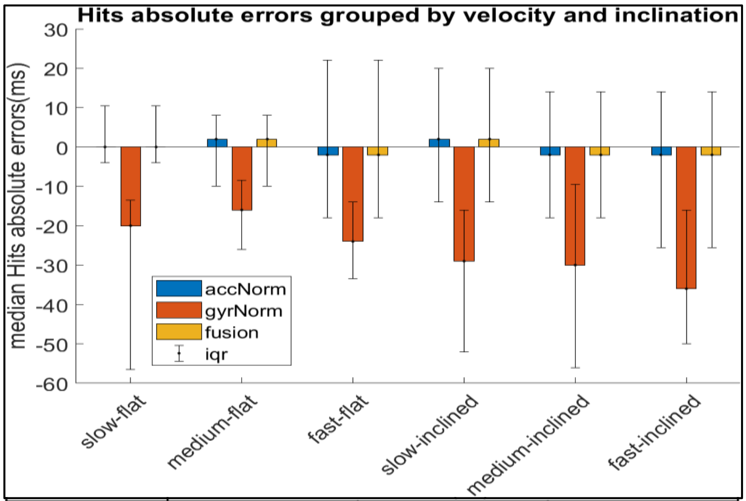

	Acc method		Gyr method		Fusion method	
	median	iqr	median	iqr	median	iqr
slow-flat	0	15	-20	43	0	15
medium-flat	2	18	-16	18	2	18
fast-flat	-2	40	-24	20	-2	40
slow-inclined	2	34	-29	36	2	34
medium-inclined	-2	32	-30	47	-2	32
fast-inclined	-2	40	-36	34	-2	40

Figure 73 - Pole hits errors in different skiing conditions. Cycle events identification methods comparison. Sensor distally on the arm.

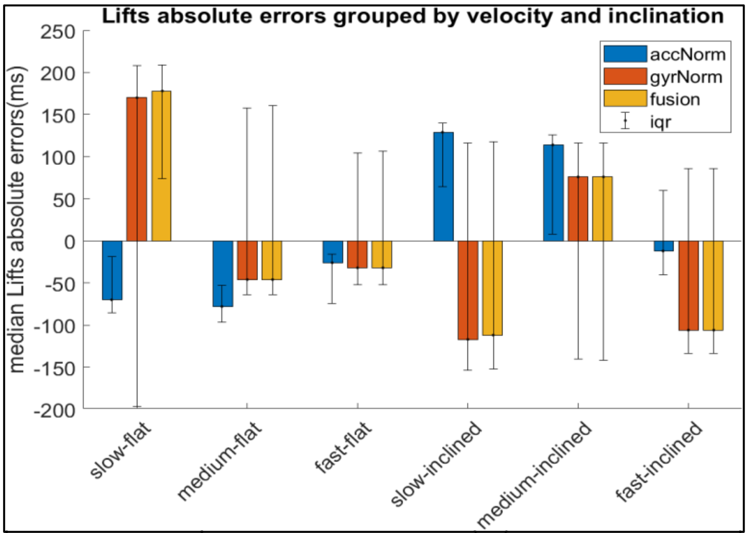

	Acc method		Gyr method		Fusion method	
	median	iqr	median	iqr	median	iqr
slow-flat	-70	67	170	405	178	135
medium-flat	-78	44	-46	222	-46	225
fast-flat	-26	58	-32	156	-32	159
slow-inclined	129	76	-117	270	-112	270
medium-inclined	114	118	76	257	76	258
fast-inclined	-12	100	-106	220	-106	220

Figure 74 - Pole lifts errors in different skiing conditions. Cycle events identification methods comparison. Sensor distally on the arm.

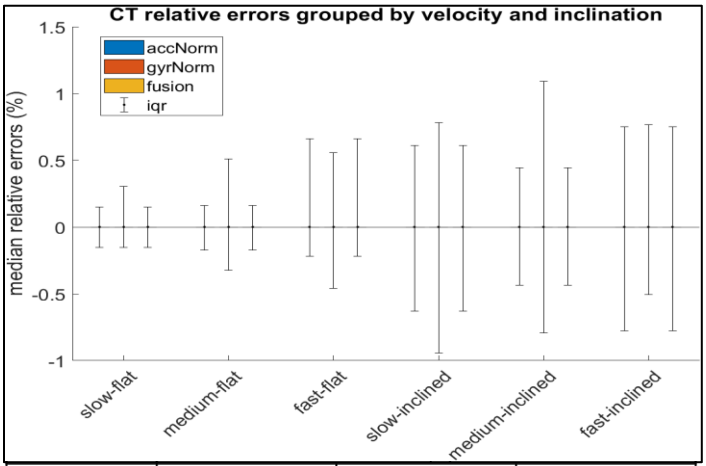

	Acc method		Gyr method		Fusion method	
	median	iqr	median	iqr	median	iqr
slow-flat	0.0	0.3	0.0	0.5	0.0	0.3
medium-flat	0.0	0.3	0.0	0.8	0.0	0.3
fast-flat	0.0	0.9	0.0	1.0	0.0	0.9
slow-inclined	0.0	1.2	0.0	1.7	0.0	1.2
medium-inclined	0.0	0.9	0.0	1.9	0.0	0.9
fast-inclined	0.0	1.5	0.0	1.3	0.0	1.5

Figure 75 – Cycle time errors in different skiing conditions. Cycle events identification methods comparison. Sensor distally on the arm.

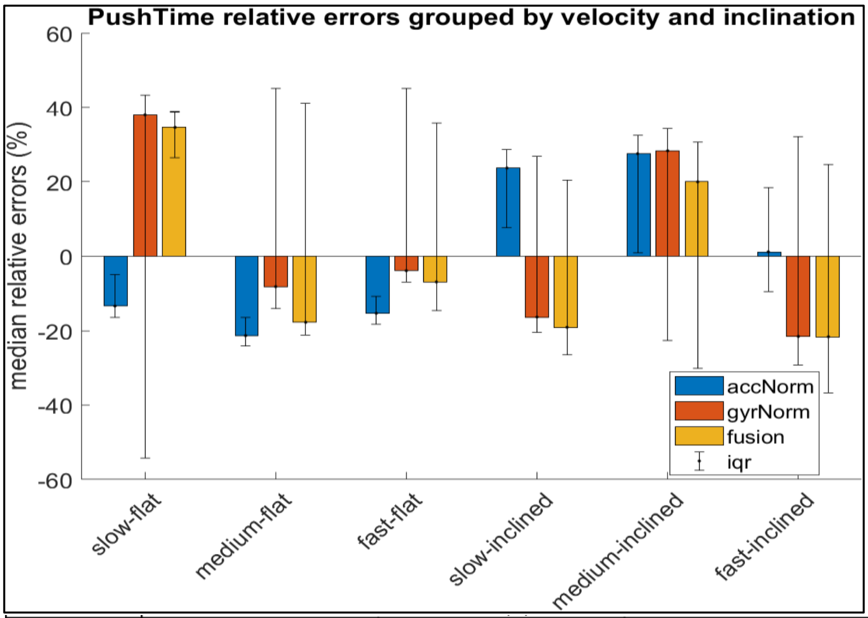

	Acc method		Gyr method		Fusion method	
	median	iqr	median	iqr	median	iqr
slow-flat	-13.4	11.6	38.0	97.5	34.6	12.4
medium-flat	-21.3	7.7	-8.2	59.1	-17.7	62.2
fast-flat	-15.3	7.4	-3.9	52.1	-6.9	50.5
slow-inclined	23.7	21.1	-16.4	47.3	-19.1	47.0
medium-inclined	27.6	31.7	28.3	56.9	20.0	60.8
fast-inclined	1.2	27.9	-21.6	61.3	-21.6	61.4

Figure 76 – Push time errors in different skiing conditions. Cycle events identification methods comparison. Sensor distally on the arm.

Sensor placed on the middle of the arm

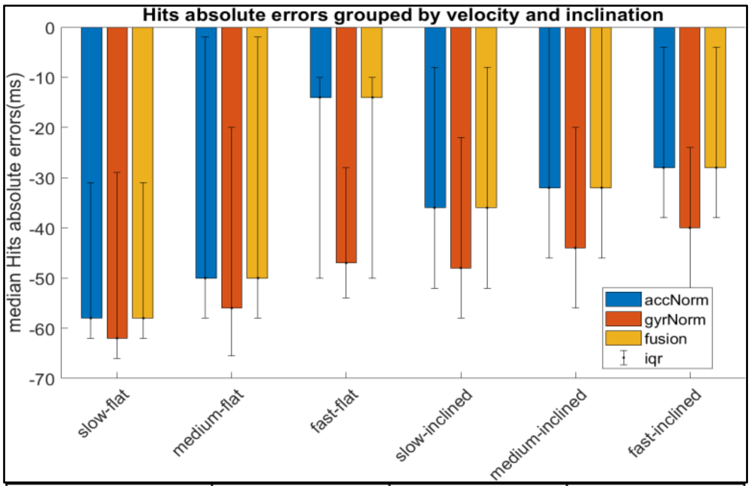

	Acc method		Gyr method		Fusion method	
	median	iqr	median	iqr	median	iqr
slow-flat	-58	31	-62	37	-58	31
medium-flat	-50	56	-56	46	-50	56
fast-flat	-14	40	-47	26	-14	40
slow-inclined	-36	44	-48	36	-36	44
medium-inclined	-32	46	-44	36	-32	46
fast-inclined	-28	34	-40	28	-28	34

Figure 77 - Pole hits errors in different skiing conditions. Cycle events identification methods comparison. Sensor on the middle of the arm.

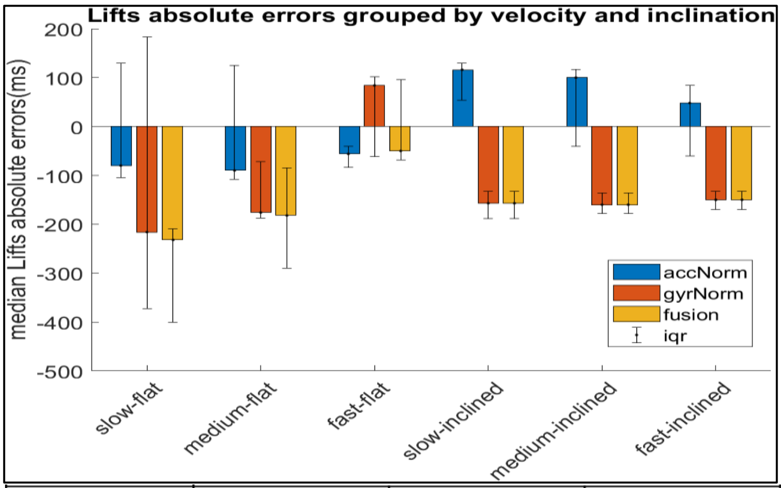

	Acc method		Gyr method		Fusion method	
	median	iqr	median	iqr	median	iqr
slow-flat	-80	235	-216	556	-232	191
medium-flat	-90	232	-176	115	-182	205
fast-flat	-56	44	84	163	-50	164
slow-inclined	116	76	-157	56	-157	56
medium-inclined	100	157	-160	43	-160	43
fast-inclined	48	144	-150	38	-150	38

Figure 78 - Pole lifts errors in different skiing conditions. Cycle events identification methods comparison. Sensor on the middle of the arm.

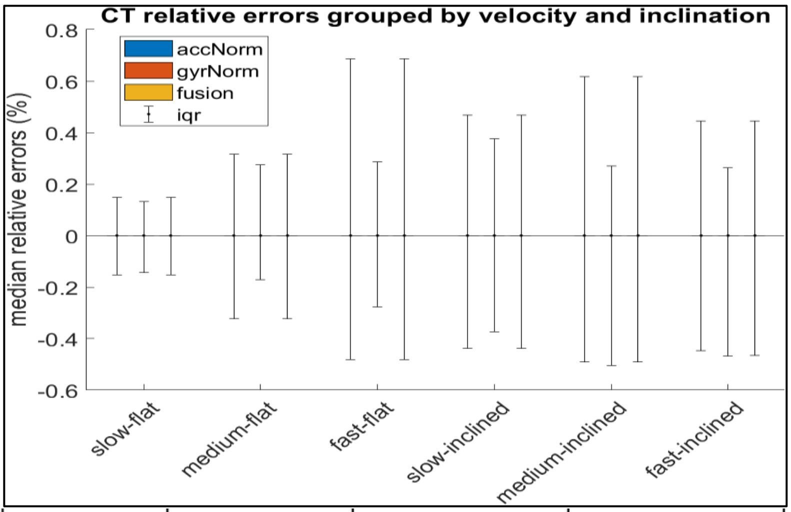

	Acc method		Gyr method		Fusion method	
	median	iqr	median	iqr	median	iqr
slow-flat	0.0	0.3	0.0	0.3	0.0	0.3
medium-flat	0.0	0.6	0.0	0.4	0.0	0.6
fast-flat	0.0	1.2	0.0	0.6	0.0	1.2
slow-inclined	0.0	0.9	0.0	0.8	0.0	0.9
medium-inclined	0.0	1.1	0.0	0.8	0.0	1.1
fast-inclined	0.0	0.9	0.0	0.7	0.0	0.9

Figure 79 – Cycle time errors in different skiing conditions. Cycle events identification methods comparison. Sensor on the middle of the arm.

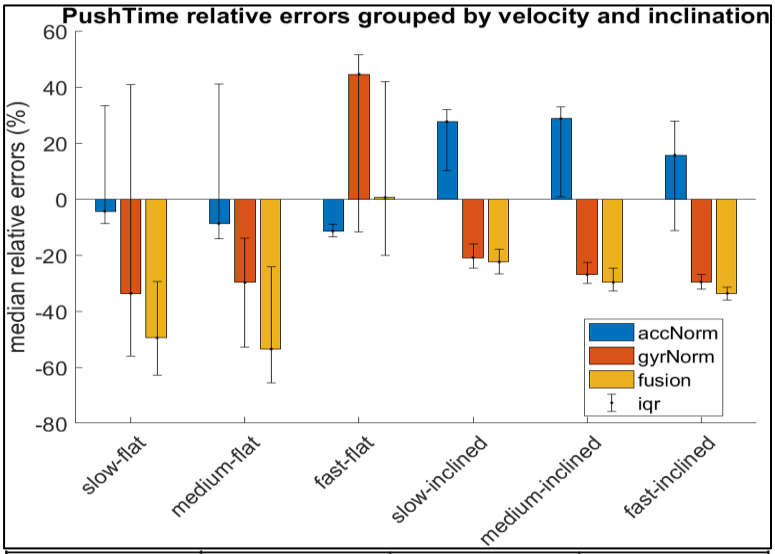

	Acc method		Gyr method		Fusion method	
	median	iqr	median	iqr	median	iqr
slow-flat	-4.4	42.0	-33.7	96.8	-49.5	33.4
medium-flat	-8.7	55.4	-29.8	38.9	-53.5	41.3
fast-flat	-11.5	4.4	44.5	63.1	0.5	62.2
slow-inclined	27.6	21.9	-20.9	8.8	-22.5	8.7
medium-inclined	28.7	32.0	-27.0	7.5	-29.7	8.2
fast-inclined	15.6	39.0	-29.6	5.1	-33.7	4.7

Figure 80 – Push time errors in different skiing conditions. Cycle events identification methods comparison. Sensor on the middle of the arm.

Appendix B

In the paragraph about the IMUs-based cycle events identification methods, two versions of the "fusion" cycle events identification method were introduced. However, after a first evaluation of the results, the results about the 2nd version of this method (the one which identifies a lift as the mean of the corresponding lifts identified by the acceleration norm-based and angular velocity norm-based methods) were considered not particularly relevant with respect to the other "fusion" method version and therefore they were not reported in the results chapter. For completeness, the performance of the 2nd "fusion" method is now reported near the performance of the 1st "fusion" method to allow the comparison.

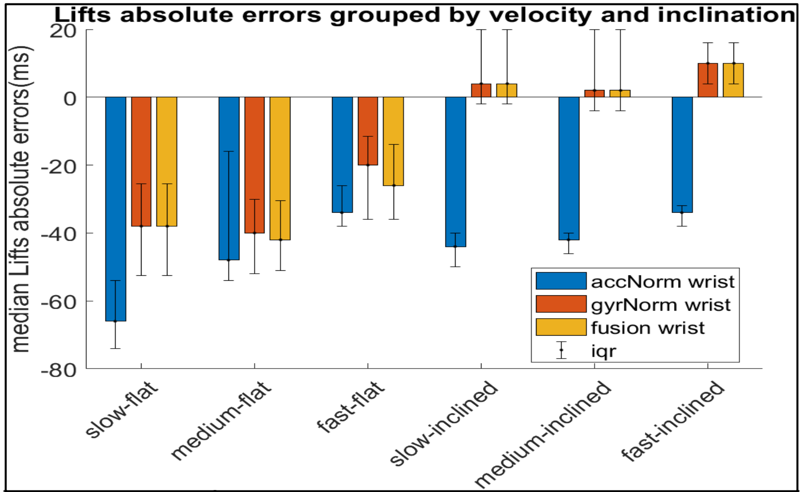

	Acc method		Gyr method		Fusion method	
	median	iqr	median	iqr	median	iqr
slow-flat	-66	20	-38	27	-38	27
medium-flat	-48	38	-40	22	-42	21
fast-flat	-34	12	-20	25	-26	22
slow-inclined	-44	10	4	22	4	22
medium-inclined	-42	6	2	24	2	24
fast-inclined	-34	6	10	12	10	12

Figure 82 – Pole lifts errors in different skiing conditions. Cycle events identification methods comparison. Sensor on the wrist. Fusion method version 1.

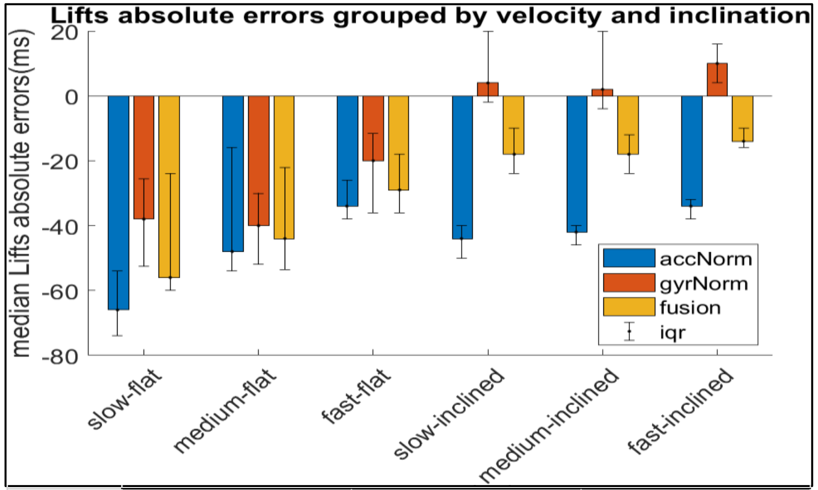

	Acc method		Gyr method		Fusion method	
	median	iqr	median	iqr	median	iqr
slow-flat	-66	20	-38	27	-56	36
medium-fl	-48	38	-40	22	-44	32
fast-flat	-34	12	-20	25	-29	18
slow-inclin	-44	10	4	22	-18	14
medium-in	-42	6	2	24	-18	12
fast-incline	-34	6	10	12	-14	6

Figure 81 – Pole lifts errors in different skiing conditions. Cycle events identification methods comparison. Sensor on the wrist. Fusion method version 2.

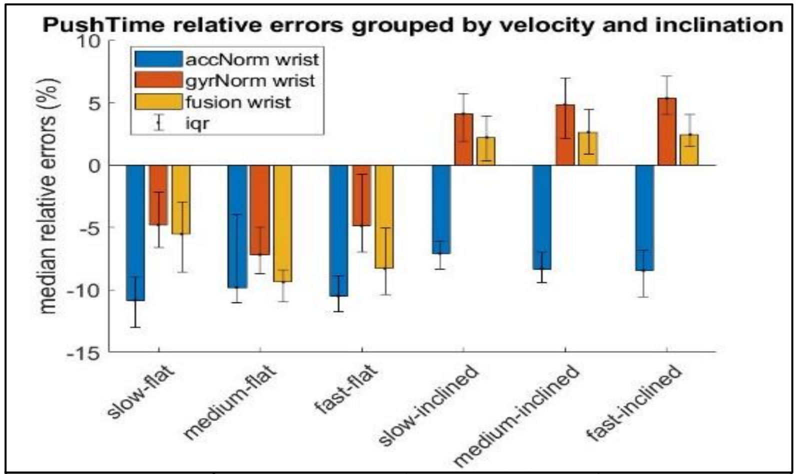

	Acc method		Gyr method		Fusion method	
	median	iqr	median	iqr	median	iqr
slow-flat	-10.8	4.0	-4.8	4.4	-5.5	5.6
medium-flat	-9.8	7.0	-7.2	3.7	-9.4	2.6
fast-flat	-10.5	2.9	-4.9	6.2	-8.3	5.3
slow-inclined	-7.1	2.2	4.1	3.8	2.2	3.6
medium-inclined	-8.3	2.5	4.8	4.9	2.6	3.6
fast-inclined	-8.5	3.7	5.3	3.1	2.4	2.6

Figure 84 –Push time errors in different skiing conditions. Cycle events identification methods comparison. Sensor on the wrist. Fusion method version 1.

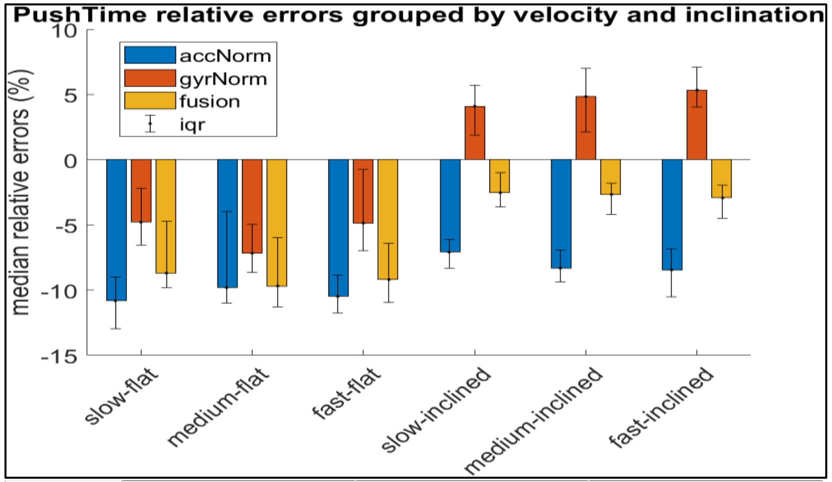

	Acc method		Gyr method		Fusion method	
	median	iqr	median	iqr	median	iqr
slow-flat	-10.8	4.0	-4.8	4.4	-8.7	5.1
medium-fl	-9.8	7.0	-7.2	3.7	-9.7	5.3
fast-flat	-10.5	2.9	-4.9	6.2	-9.2	4.6
slow-inclin	-7.1	2.2	4.1	3.8	-2.5	2.6
medium-in	-8.3	2.5	4.8	4.9	-2.7	2.4
fast-incline	-8.5	3.7	5.3	3.1	-2.9	2.5

Figure 83 – Push time errors in different skiing conditions. Cycle events identification methods comparison. Sensor on the wrist. Fusion method version 2.

Appendix C

In the results chapter two trials about the ski inclination calculated integrating the ski senor angular velocity around the ski mediolateral axis were reported to demonstrate that the gyroscope calibration sorted an effect on the drift error, but that it did not completely solved the drift problem, probably because the gyroscope bias was corrected with only two static measurements very distant from each other over time and also because of the sensor heating. For completeness, all the trials recorded are reported below.

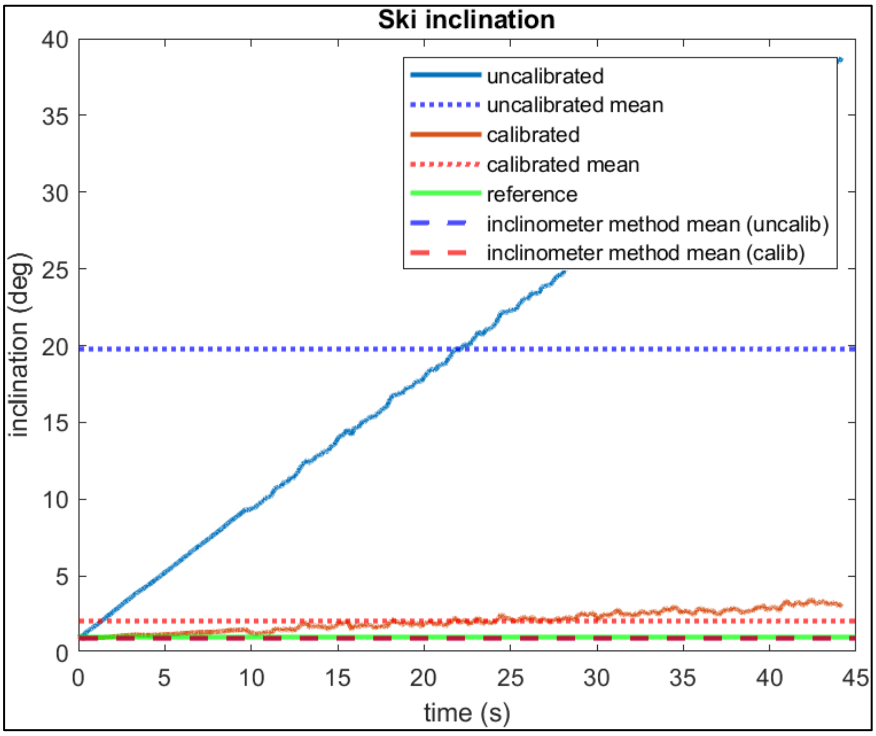

Figure 85 - Ski inclination calculated integrating the linear acceleration. 1st trial recorded from the 1st subject.

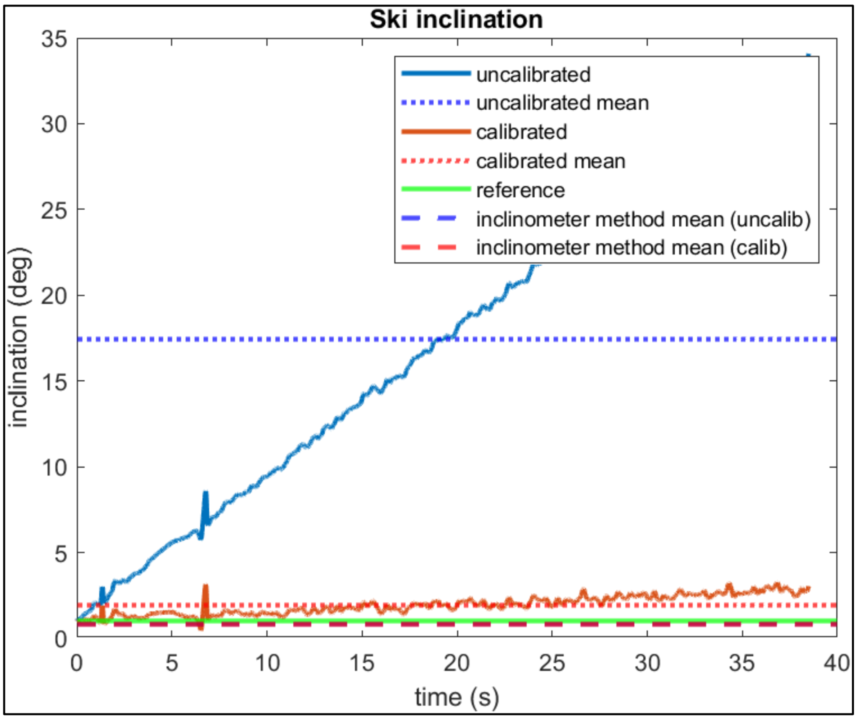

Figure 86 - Ski inclination calculated integrating the linear acceleration. 2nd trial recorded from the 1st subject.

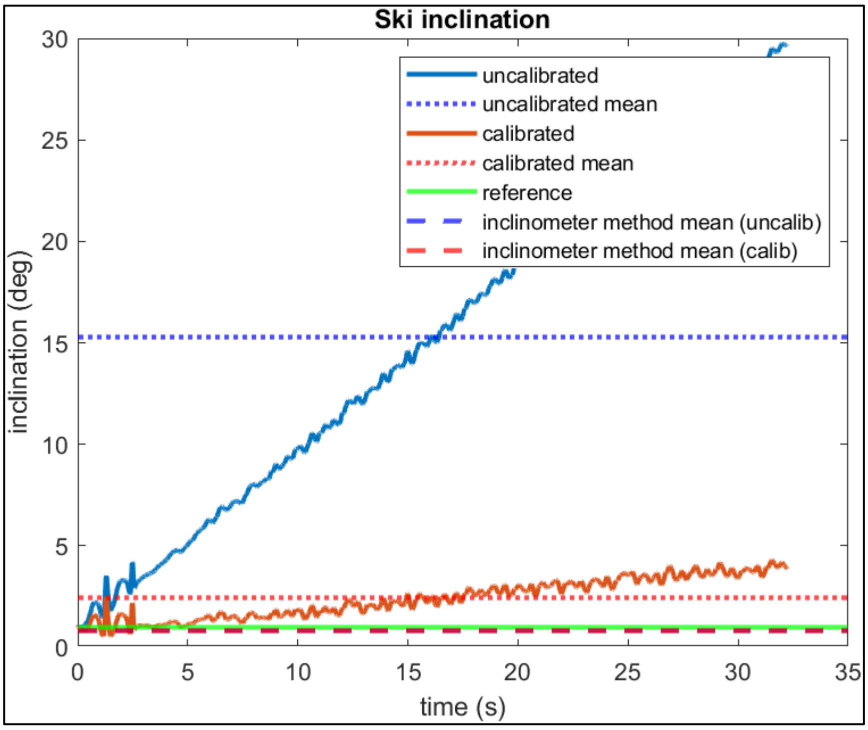

Figure 87 - Ski inclination calculated integrating the linear acceleration. 3rd trial recorded from the 1st subject.

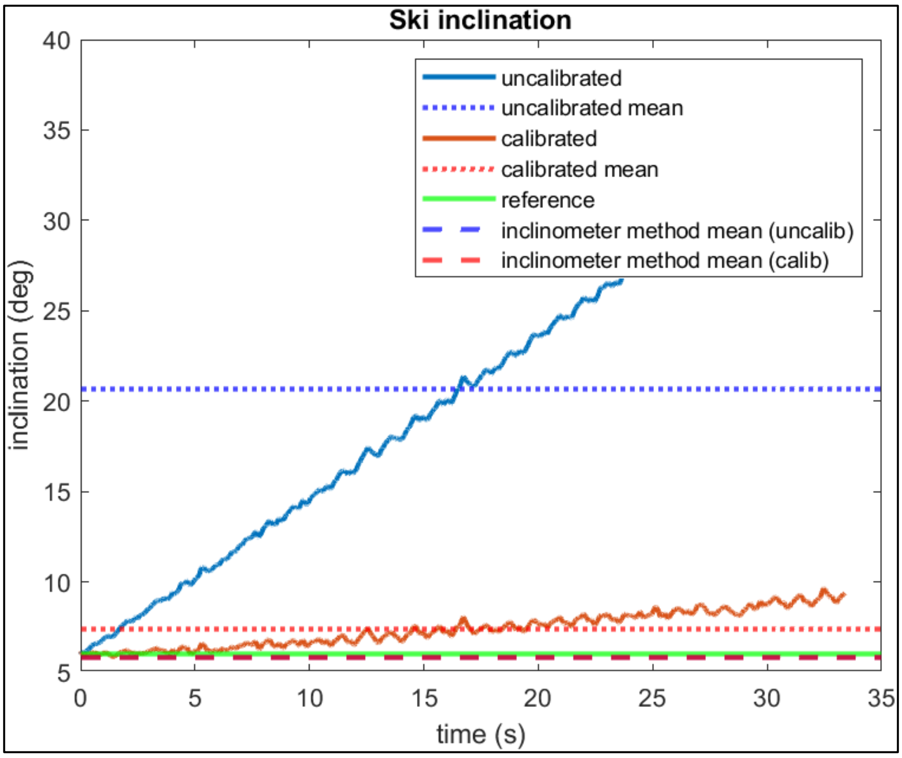

Figure 88 - Ski inclination calculated integrating the linear acceleration. 4th trial recorded from the 1st subject.

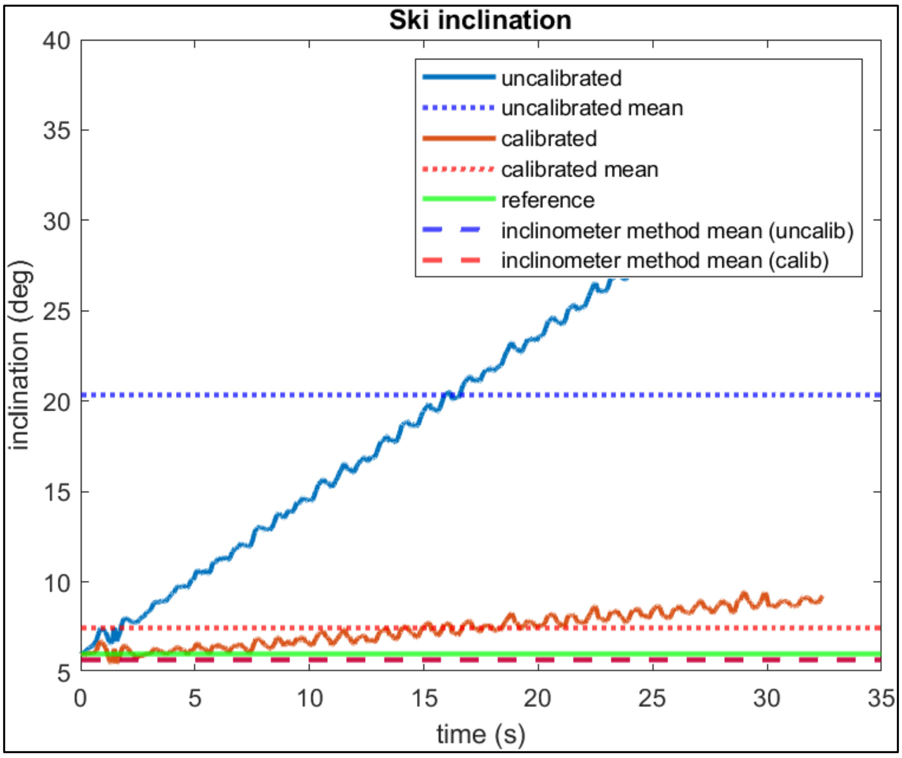

Figure 89 - Ski inclination calculated integrating the linear acceleration. 5th trial recorded from the 1st subject.

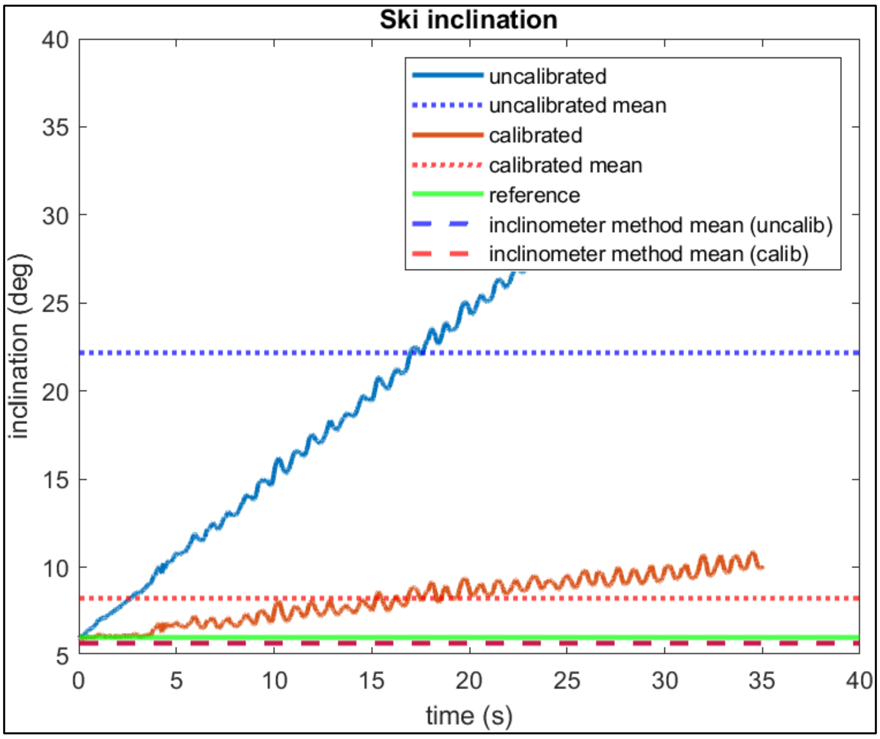

Figure 90 - Ski inclination calculated integrating the linear acceleration. 6th trial recorded from the 1st subject.

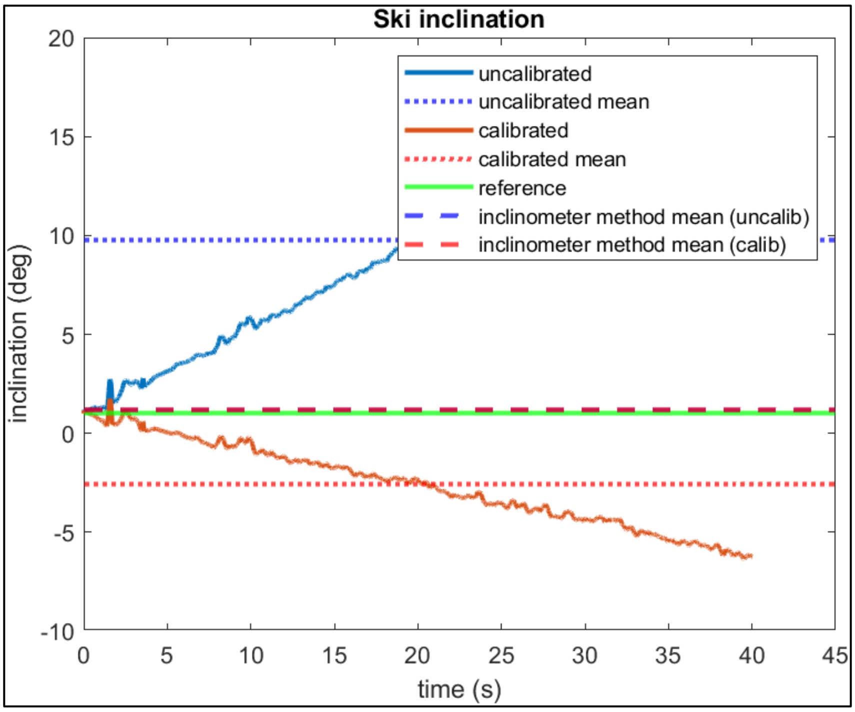

Figure 91 - Ski inclination calculated integrating the linear acceleration. 7th trial recorded from the 1st subject.

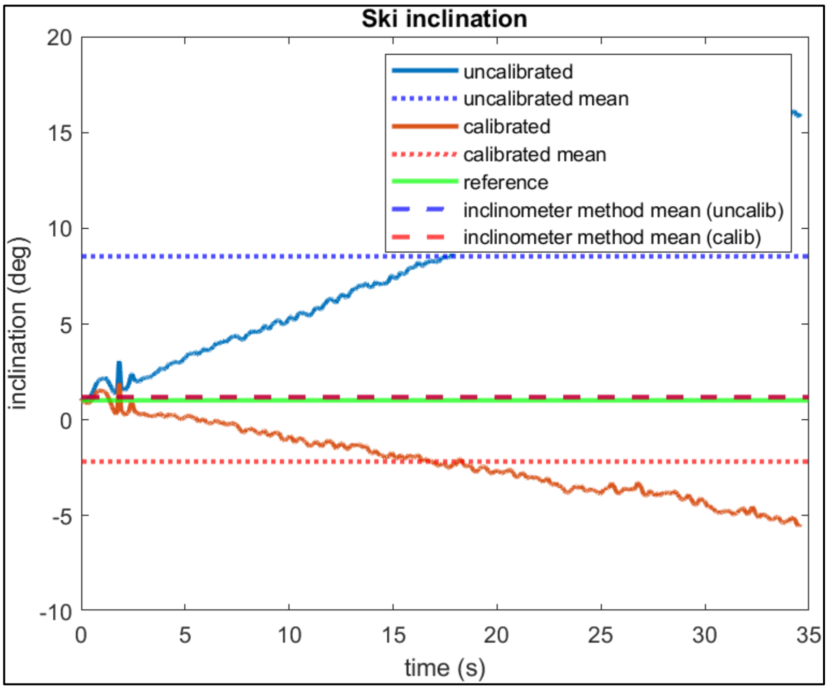

Figure 92 - Ski inclination calculated integrating the linear acceleration. 8th trial recorded from the 1st subject.

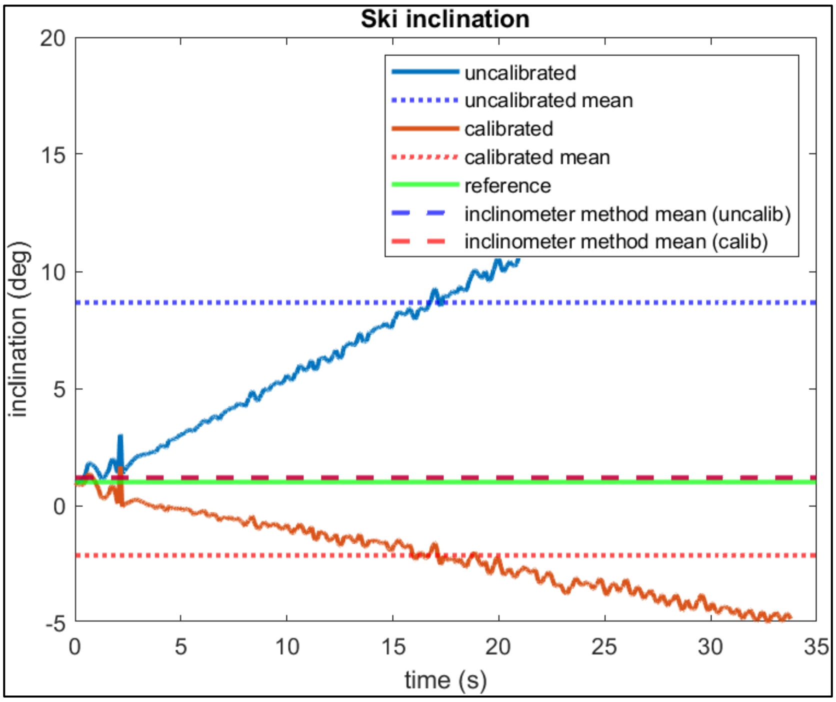

Figure 93 - Ski inclination calculated integrating the linear acceleration. 9th trial recorded from the 1st subject.

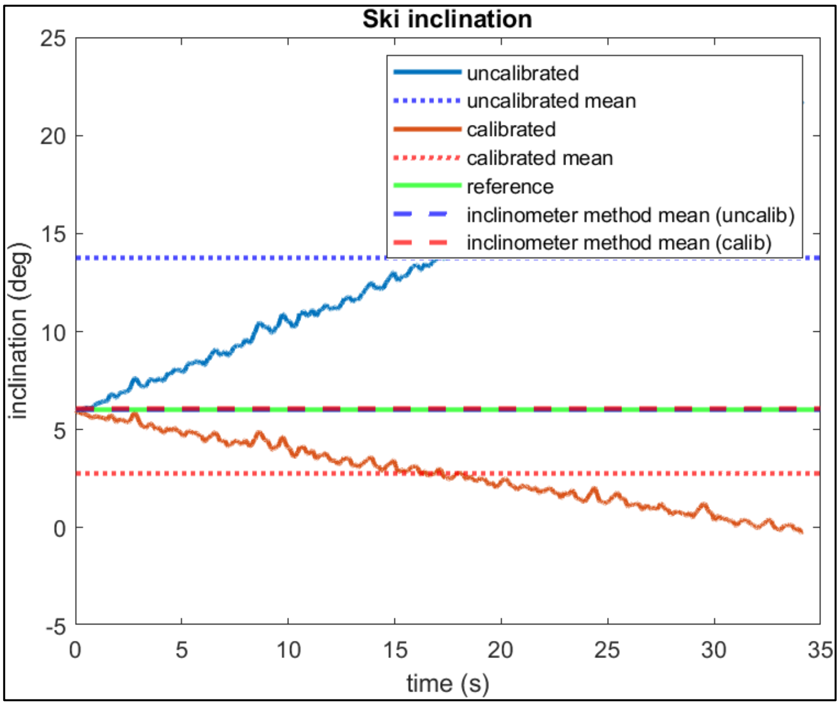

Figure 94 - Ski inclination calculated integrating the linear acceleration. 10th trial recorded from the 1st subject.

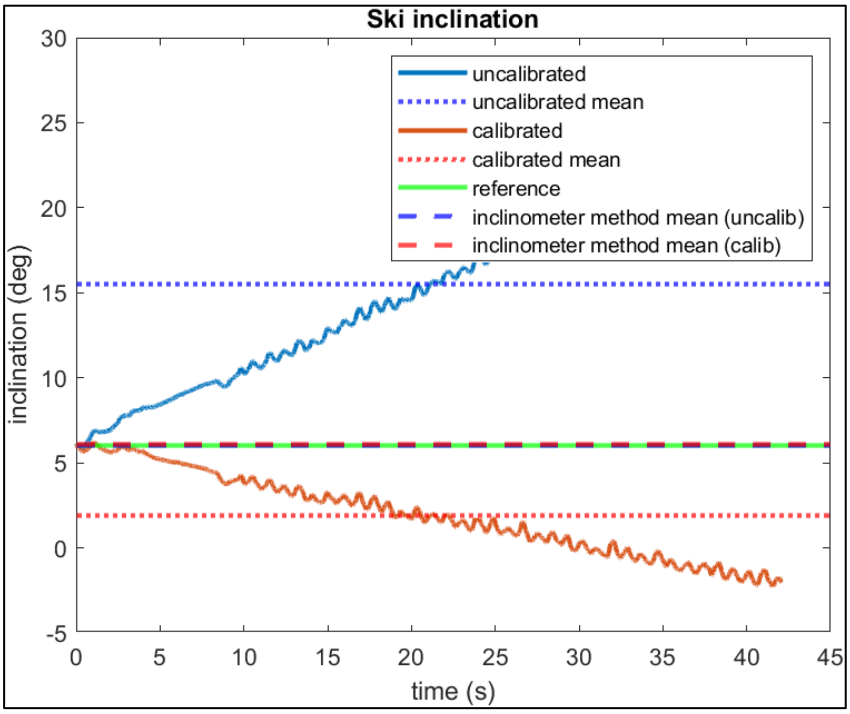

Figure 95 - Ski inclination calculated integrating the linear acceleration. 11th trial recorded from the 1st subject.

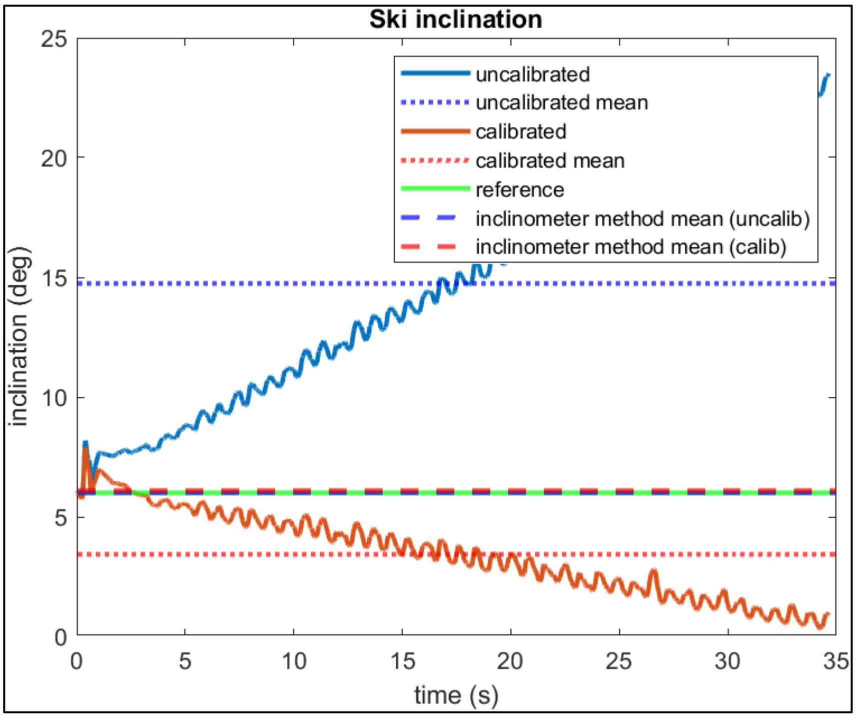

Figure 96 - Ski inclination calculated integrating the linear acceleration. 12th trial recorded from the 1st subject.

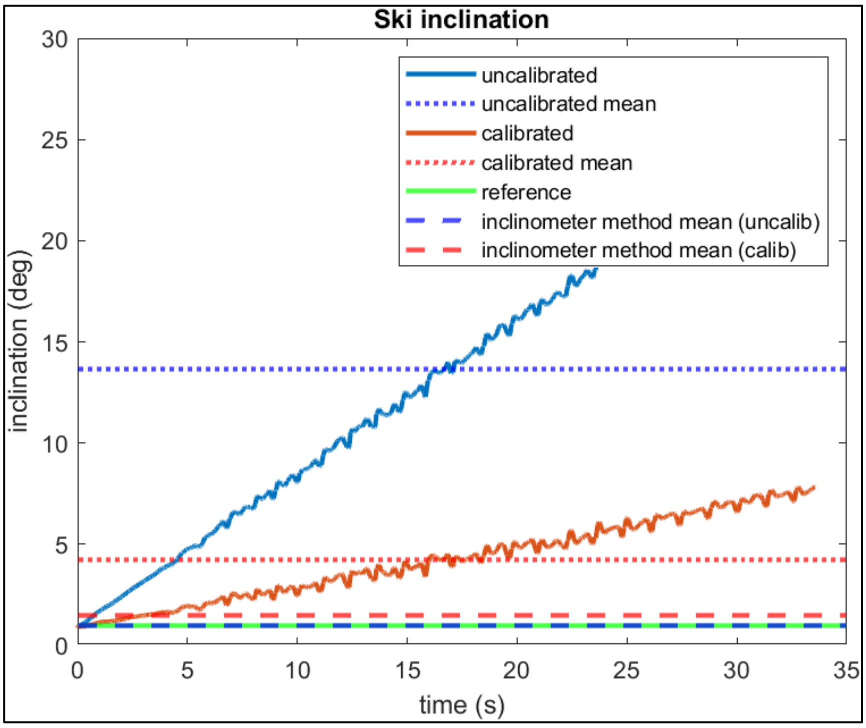

Figure 97 - Ski inclination calculated integrating the linear acceleration. 2nd trial recorded from the 2nd subject.

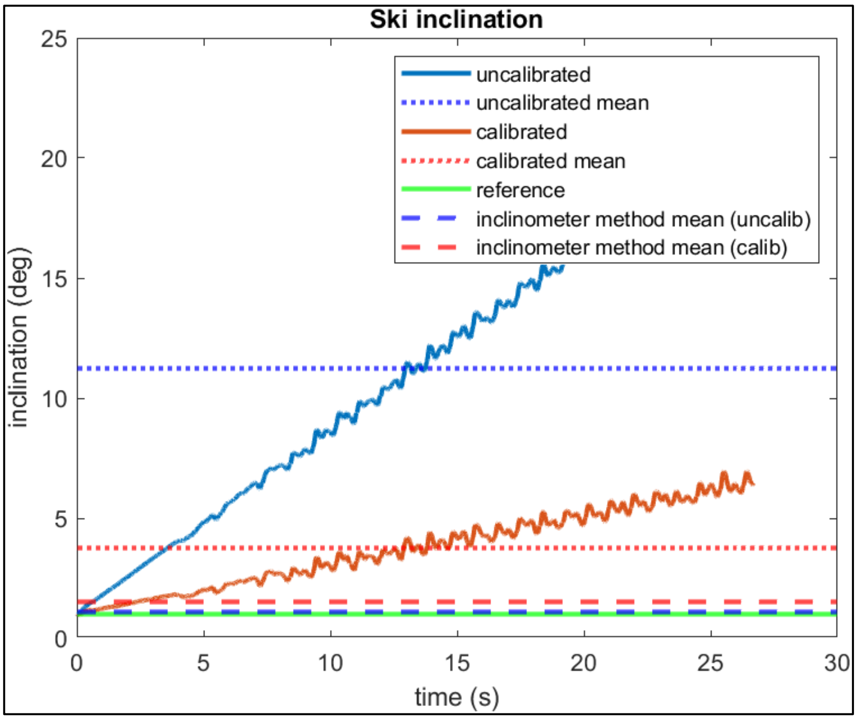

Figure 98 - Ski inclination calculated integrating the linear acceleration. 3rd trial recorded from the 2nd subject.

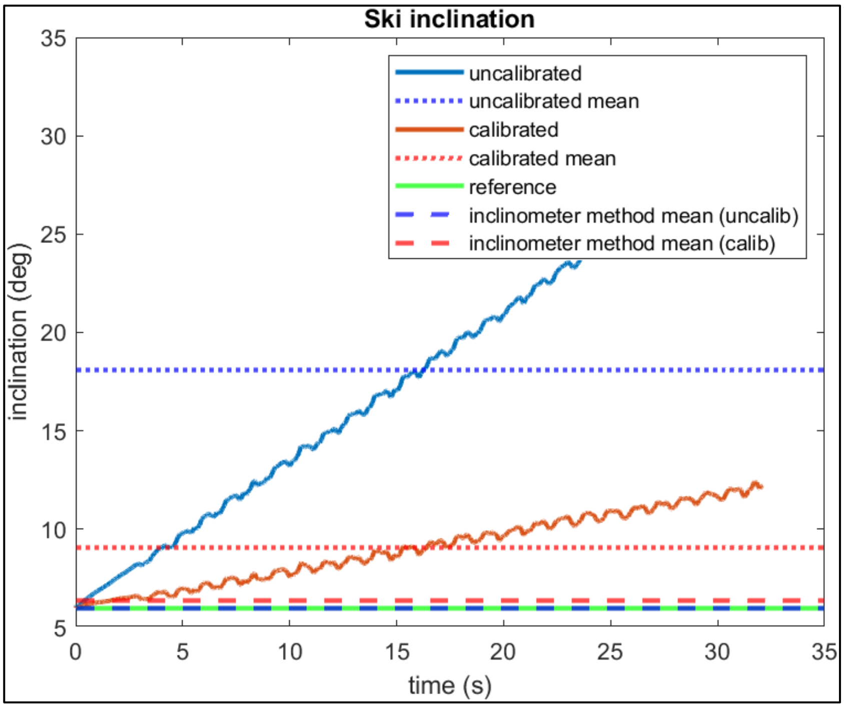

Figure 99 - Ski inclination calculated integrating the linear acceleration. 4th trial recorded from the 2nd subject.

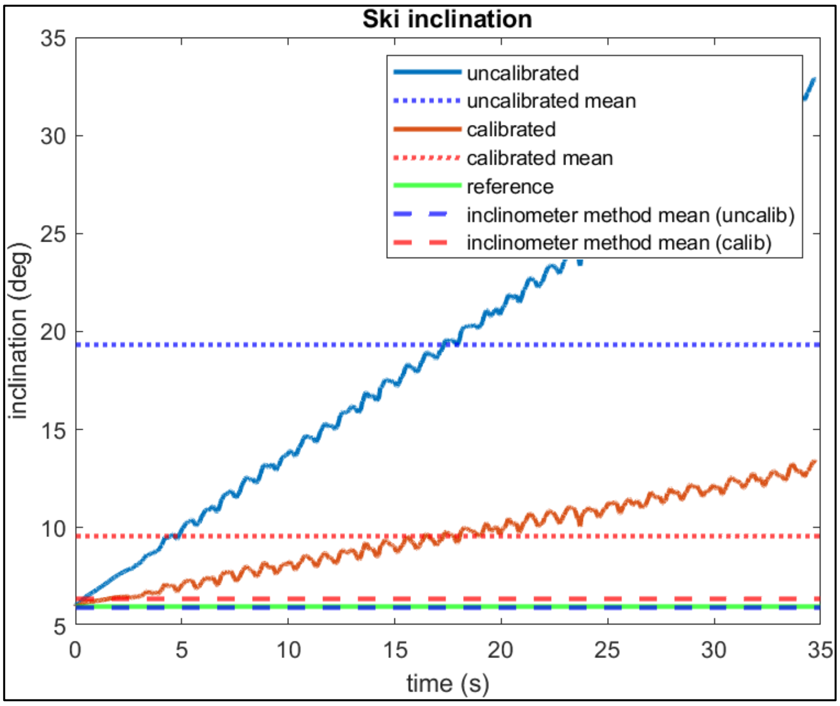

Figure 100 - Ski inclination calculated integrating the linear acceleration. 5th trial recorded from the 2nd subject.

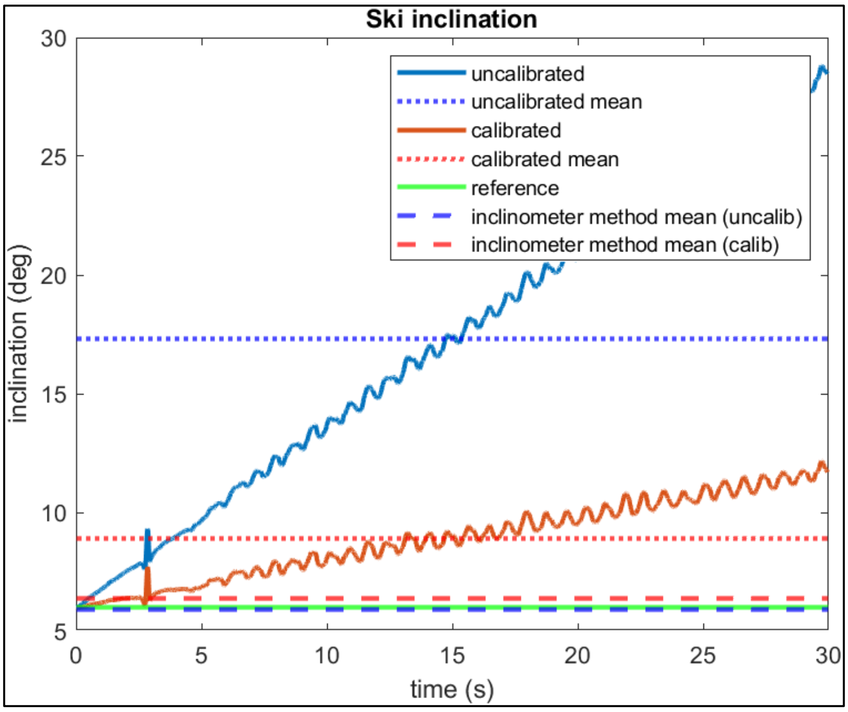

Figure 101 - Ski inclination calculated integrating the linear acceleration. 6th trial recorded from the 2nd subject.

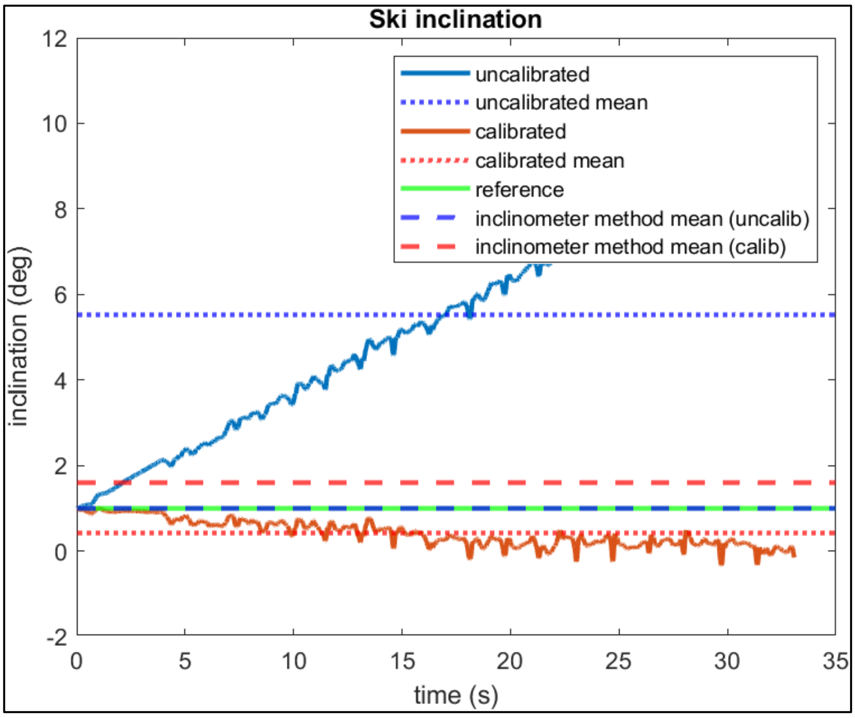

Figure 102 - Ski inclination calculated integrating the linear acceleration. 7th trial recorded from the 2nd subject.

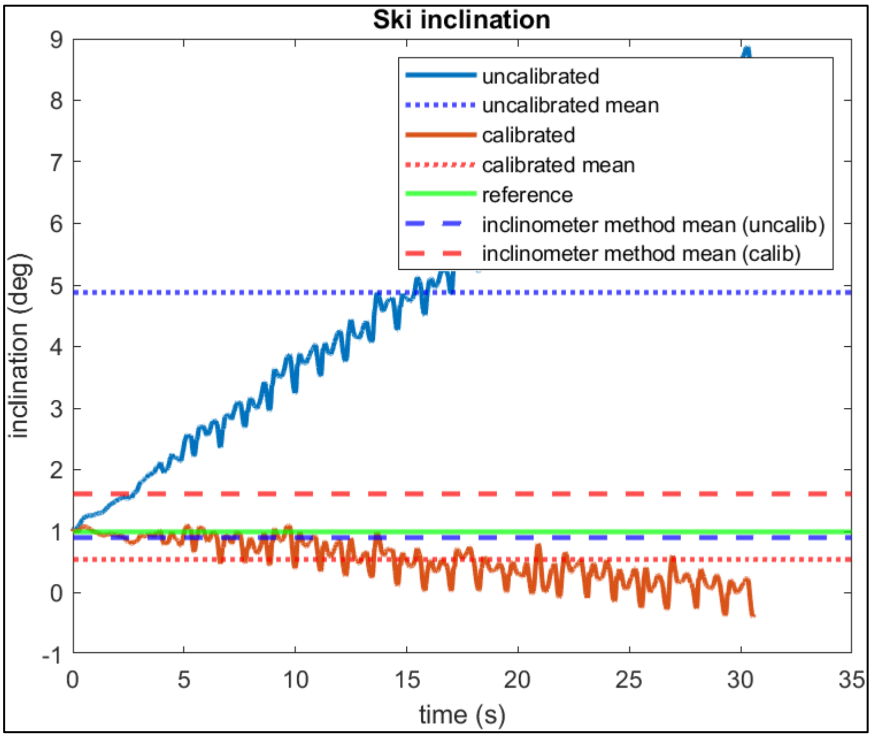

Figure 103 - Ski inclination calculated integrating the linear acceleration. 8th trial recorded from the 2nd subject.

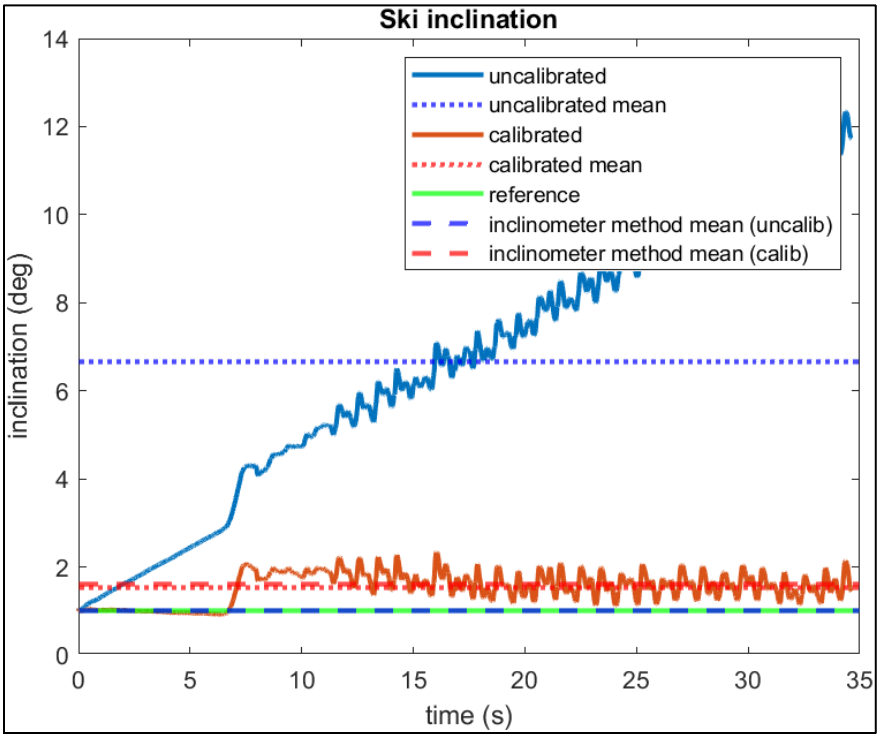

Figure 104 - Ski inclination calculated integrating the linear acceleration. 9th trial recorded from the 2nd subject.

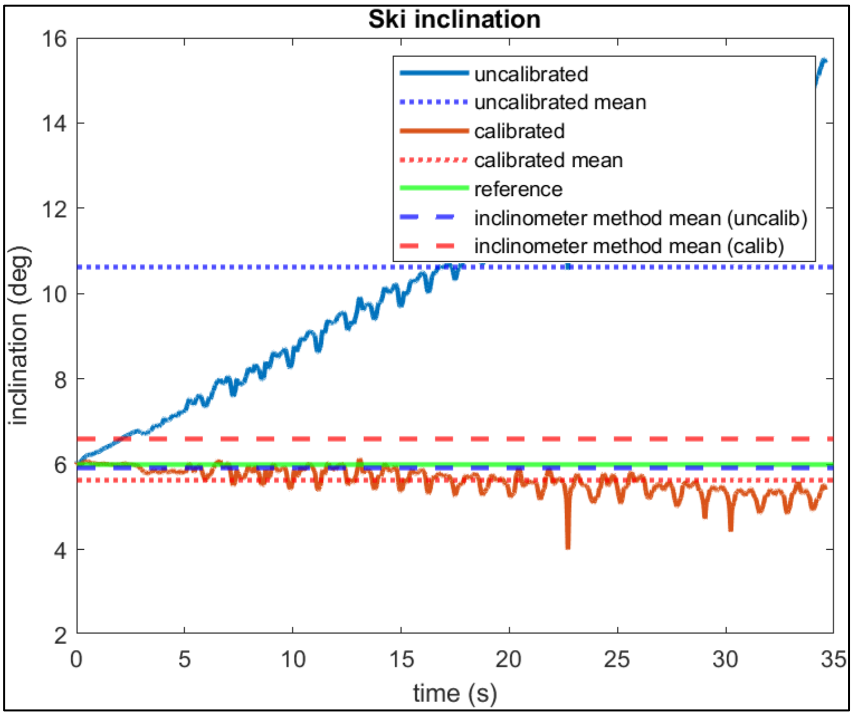

Figure 105 - Ski inclination calculated integrating the linear acceleration. 10th trial recorded from the 2nd subject.

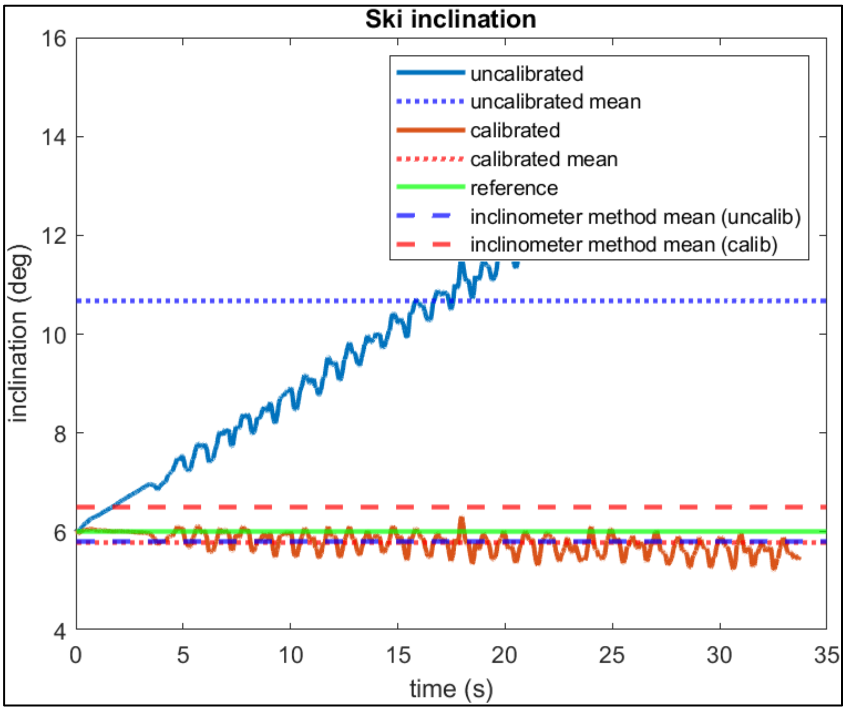

Figure 106 - Ski inclination calculated integrating the linear acceleration. 11th trial recorded from the 2nd subject.

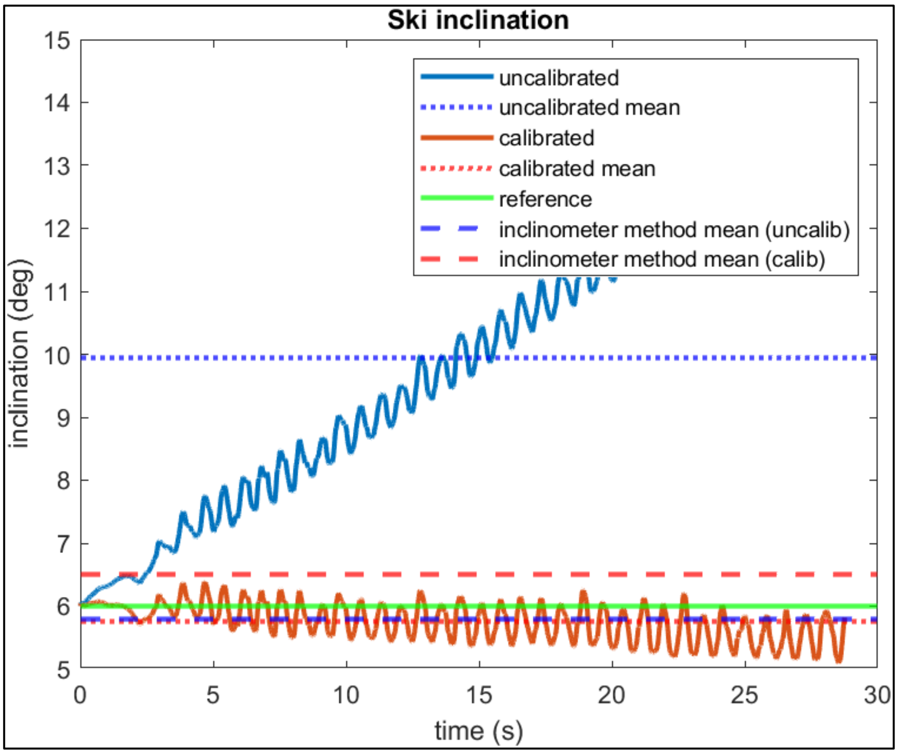

Figure 107 - Ski inclination calculated integrating the linear acceleration. 12th trial recorded from the 2nd subject.

Appendix D

In the results chapter two trials about the ski velocity and displacement calculated integrating the ski senor acceleration along the ski longitudinal axis were reported to show how, depending on the trial, the method sorted good or bad results. For completeness, all the trials recorded are reported below.

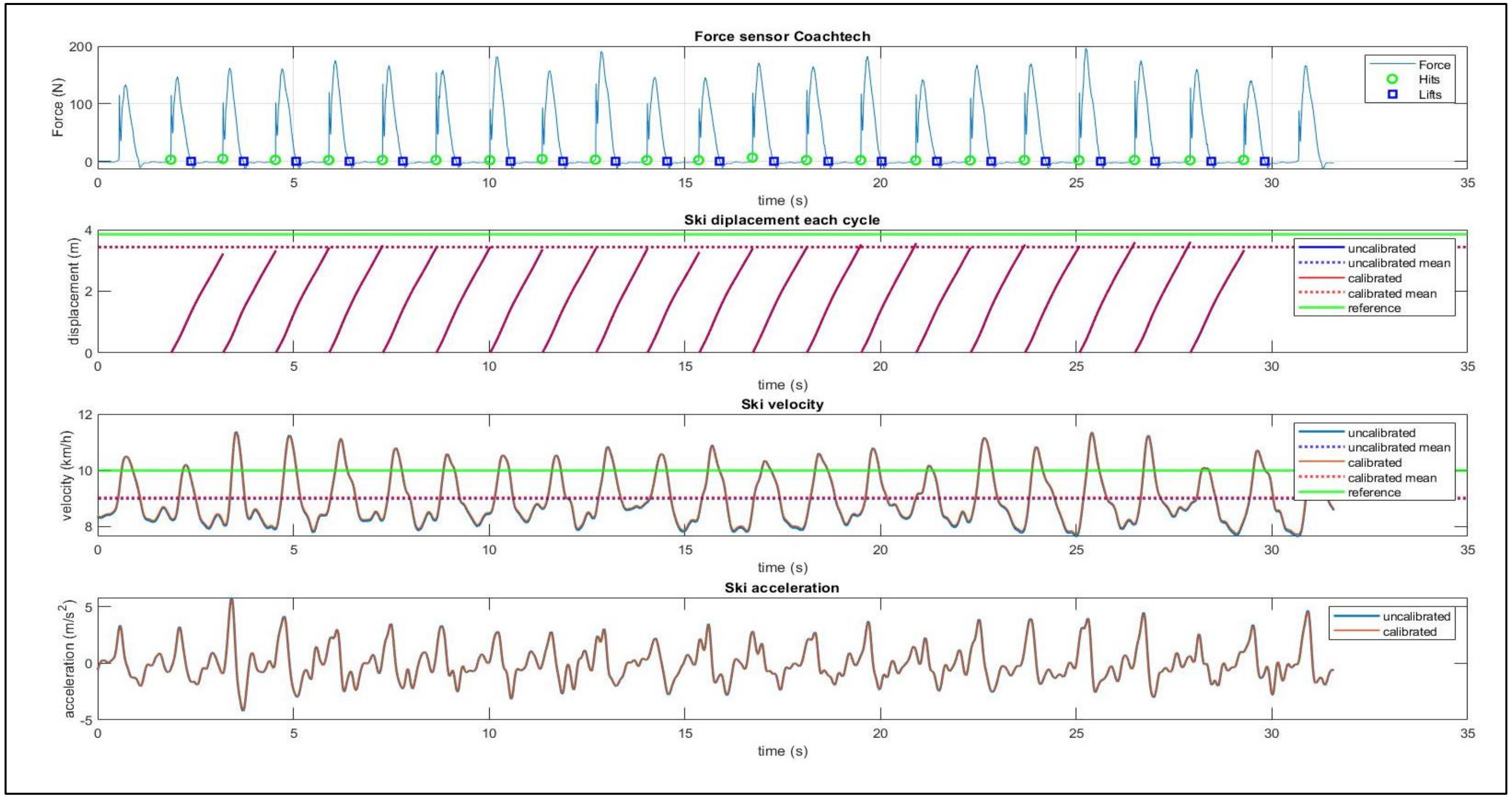

Figure 108 - Ski velocity and displacement. 1st trial acquired from the 1st subject.

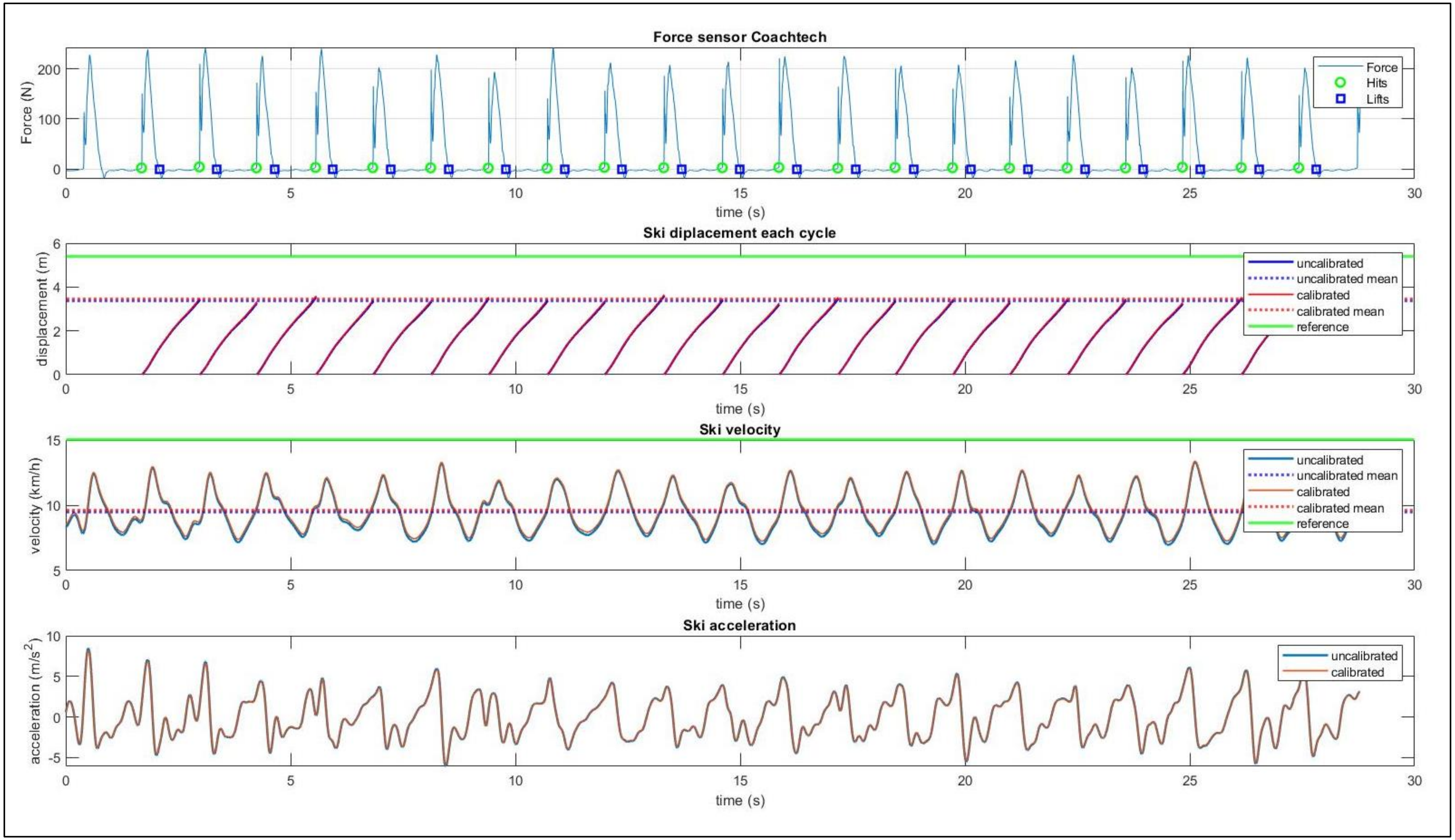

Figure 109 - Ski velocity and displacement. 2nd trial acquired from the 1st subject.

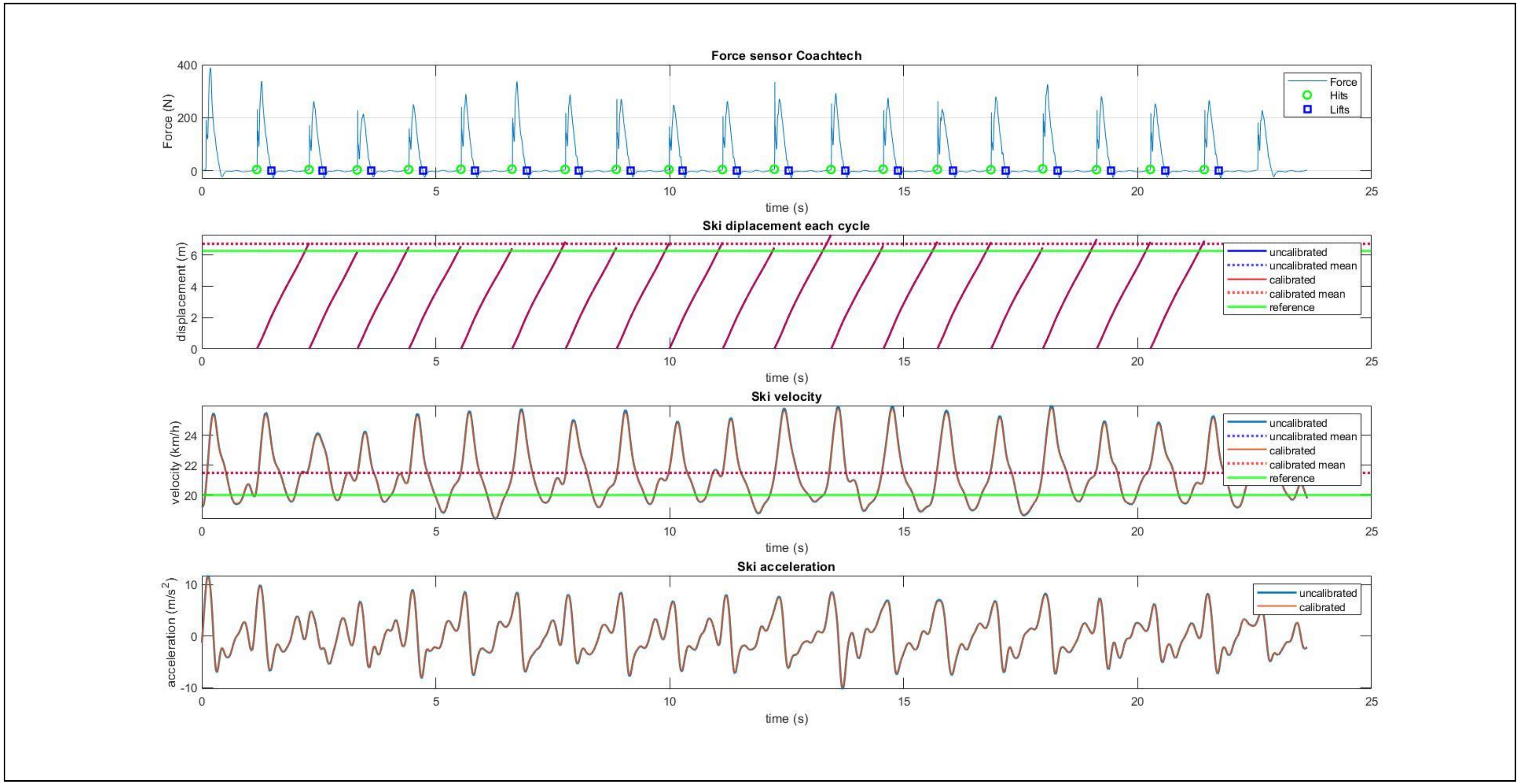

Figure 110 - Ski velocity and displacement. 3rd trial acquired from the 1st subject.

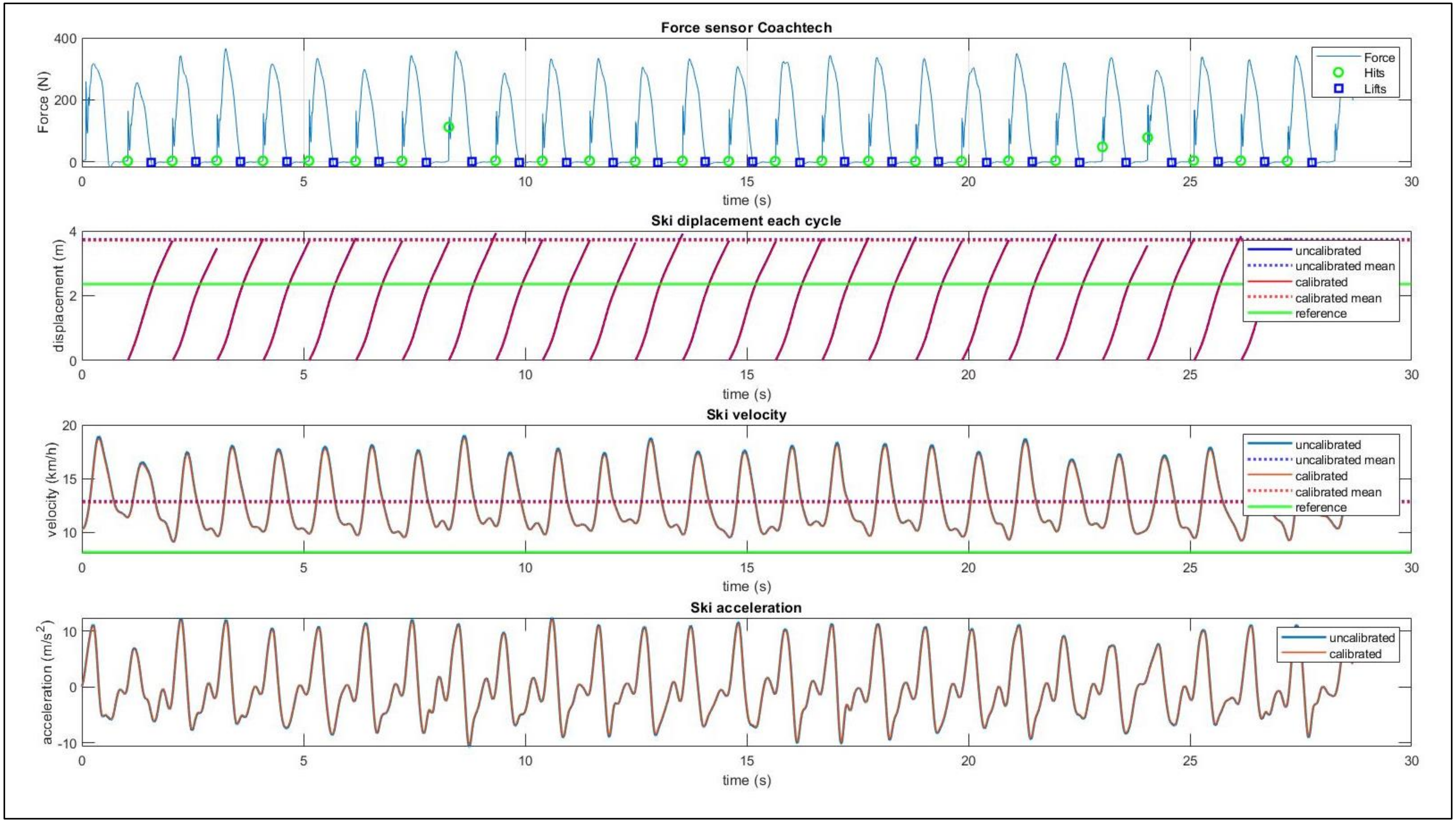

Figure 111 - Ski velocity and displacement. 4th trial acquired from the 1st subject.

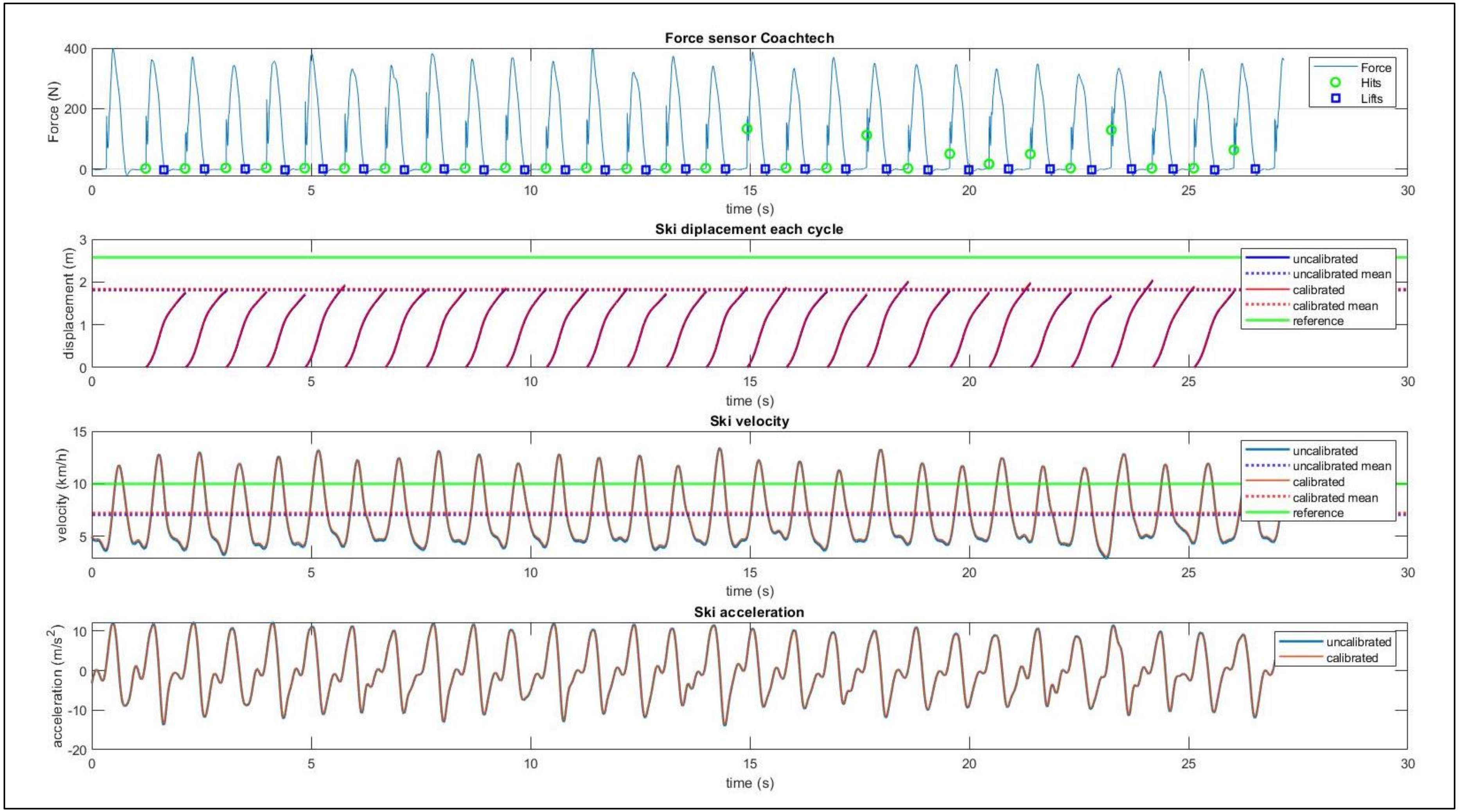

Figure 112 - Ski velocity and displacement. 5th trial acquired from the 1st subject.

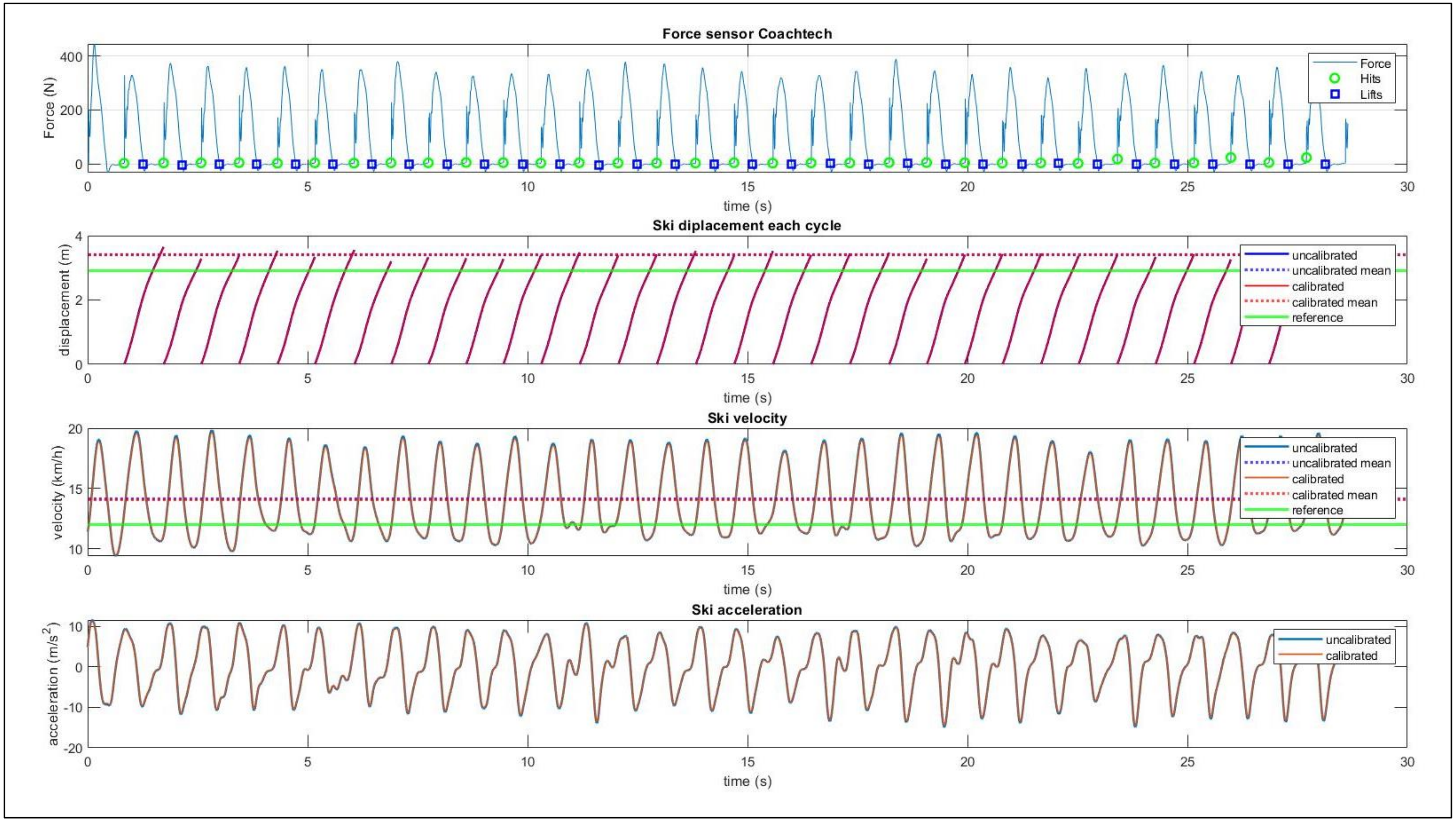

Figure 113 - Ski velocity and displacement. 6th trial acquired from the 1st subject.

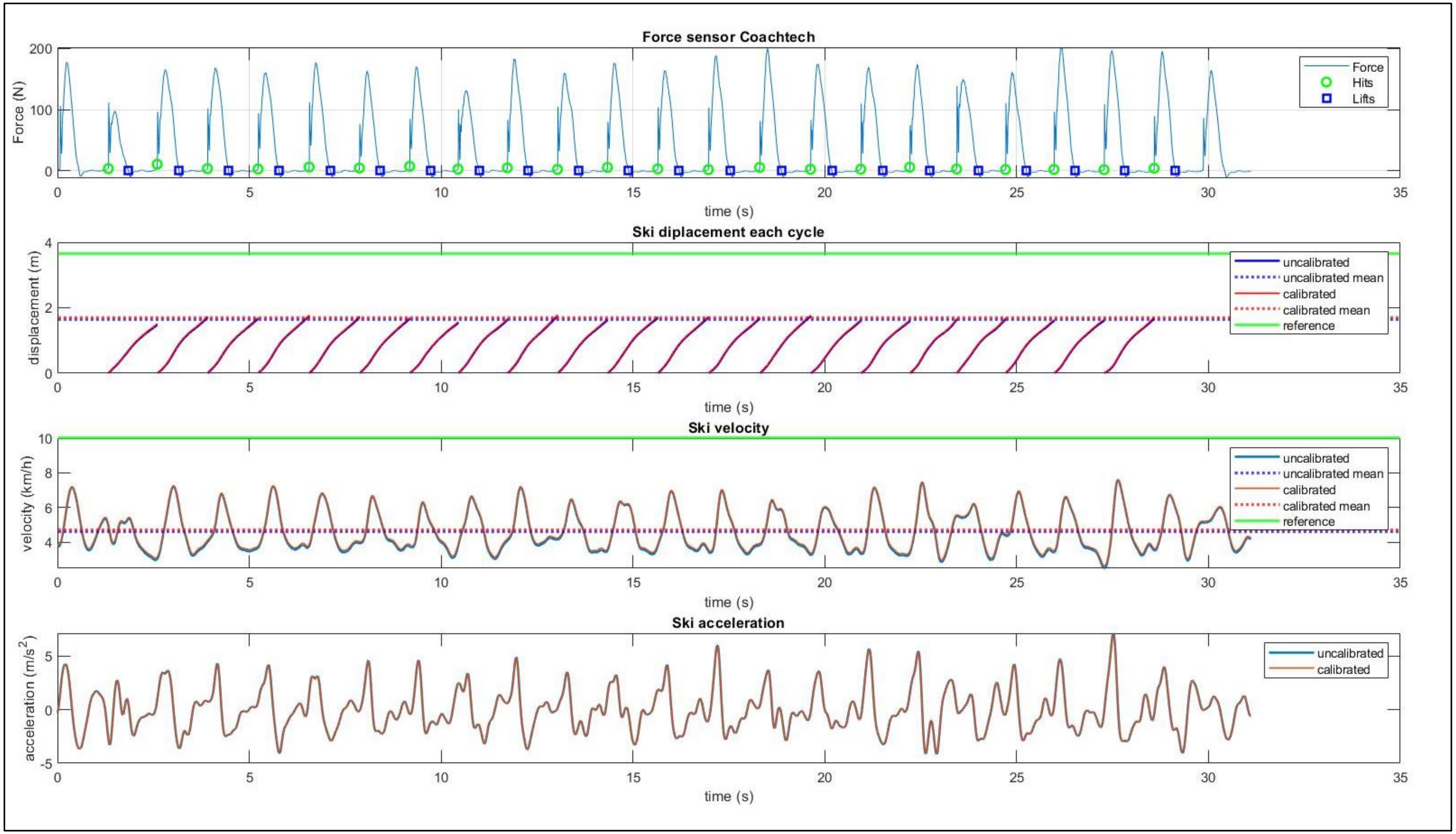

Figure 114 - Ski velocity and displacement. 7th trial acquired from the 1st subject.

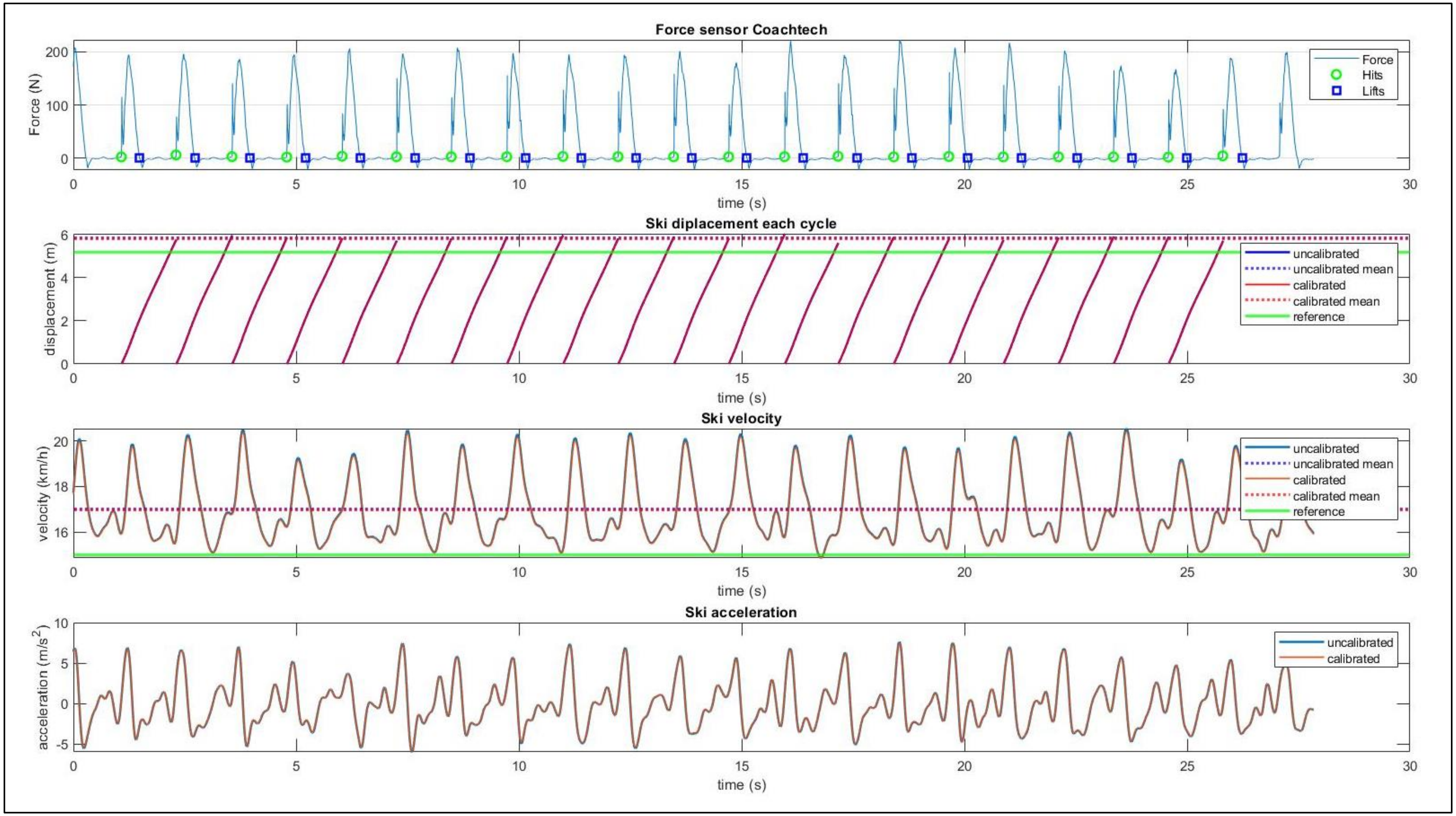

Figure 115 - Ski velocity and displacement. 8th trial acquired from the 1st subject.

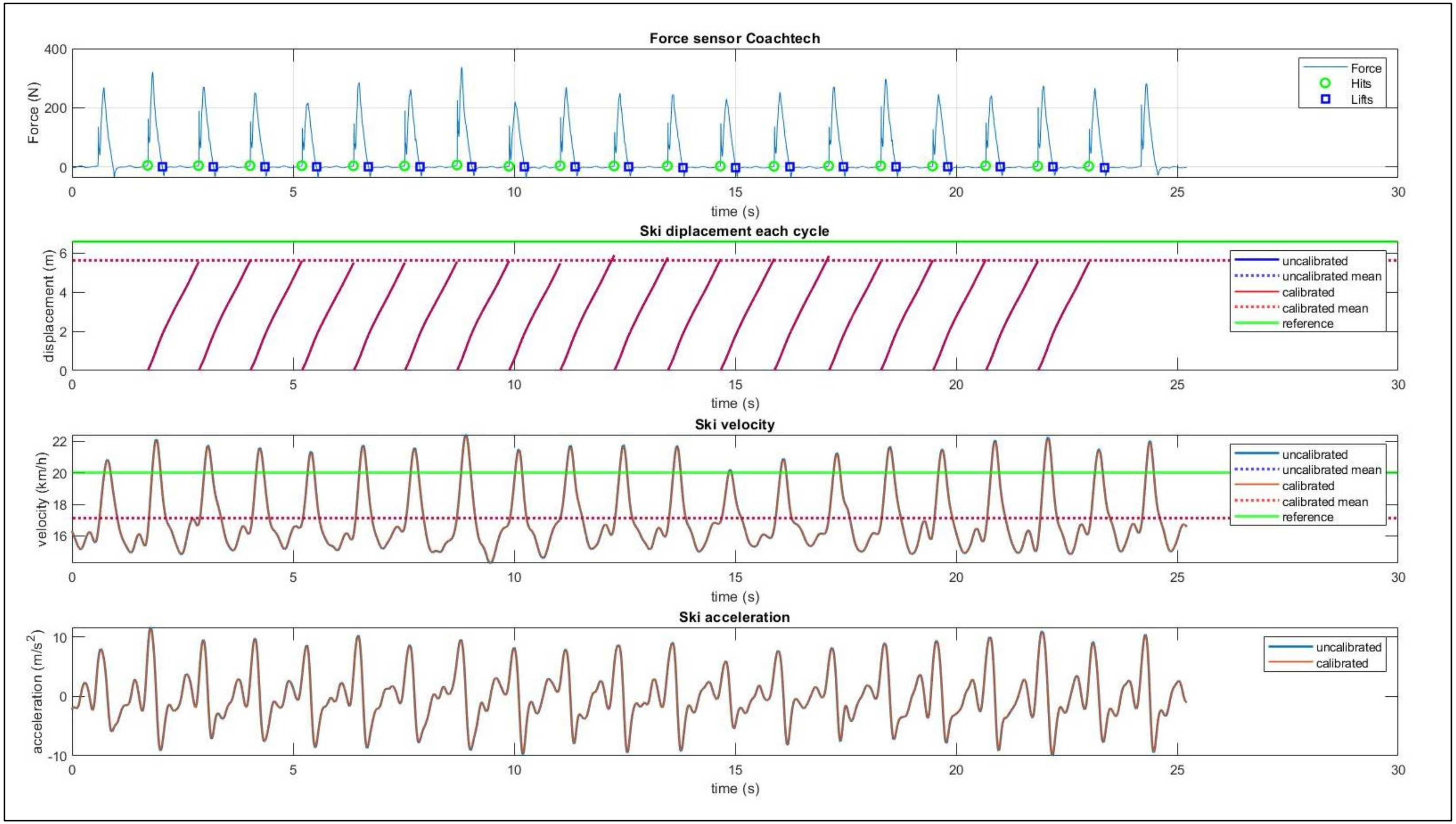

Figure 116 - Ski velocity and displacement. 9th trial acquired from the 1st subject.

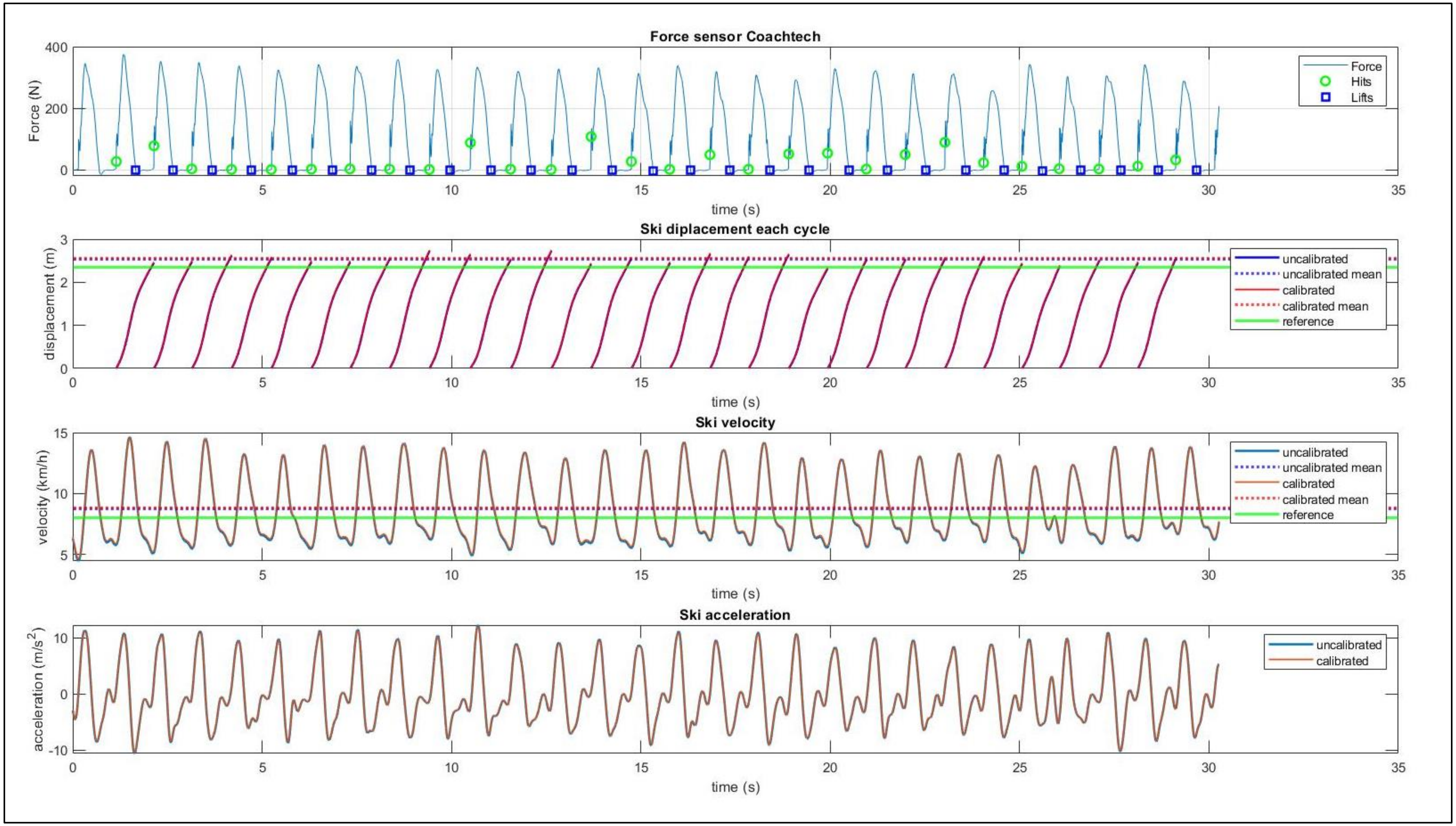

Figure 117 - Ski velocity and displacement. 10th trial acquired from the 1st subject.

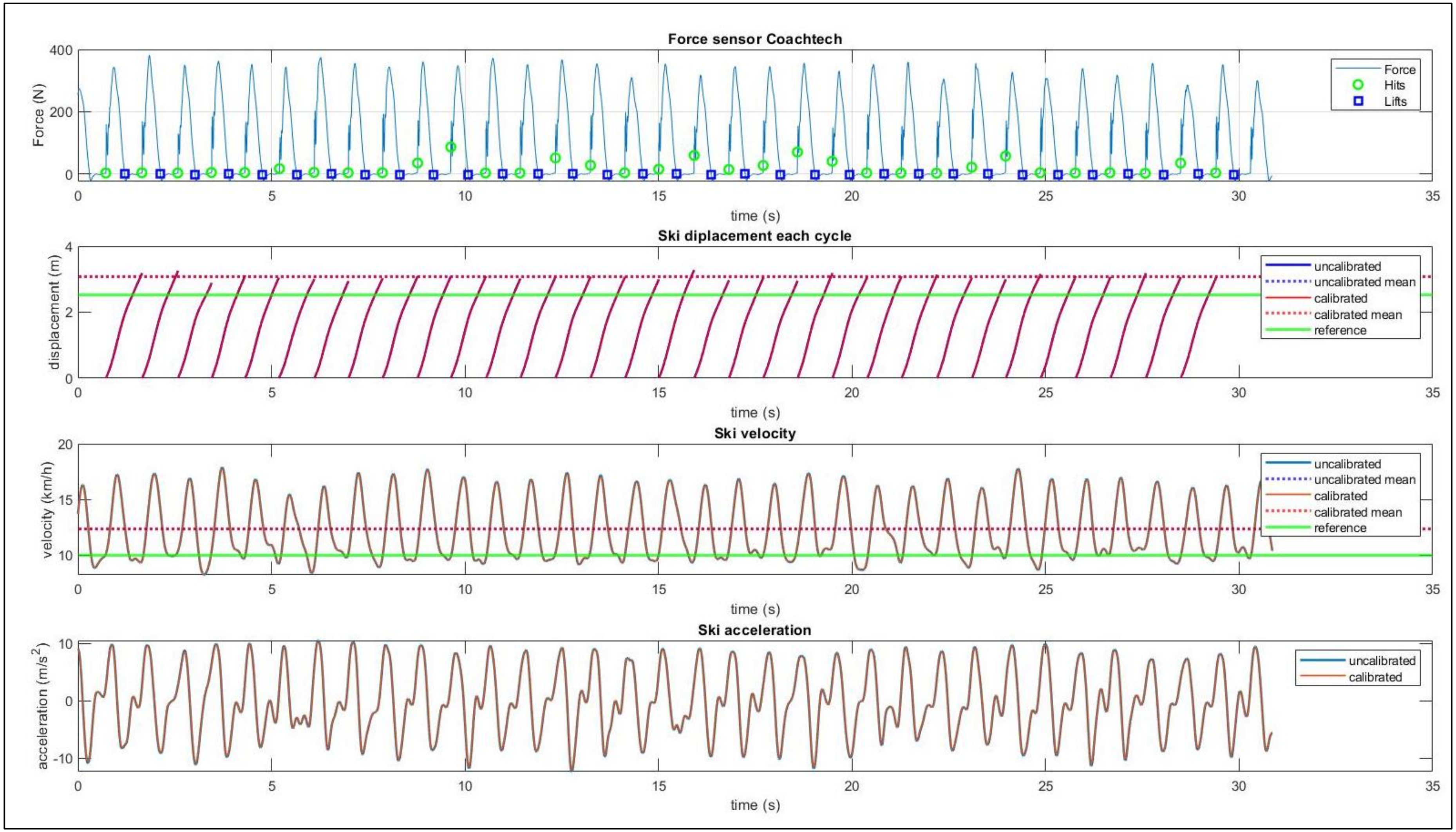

Figure 118 - Ski velocity and displacement. 11th trial acquired from the 1st subject.

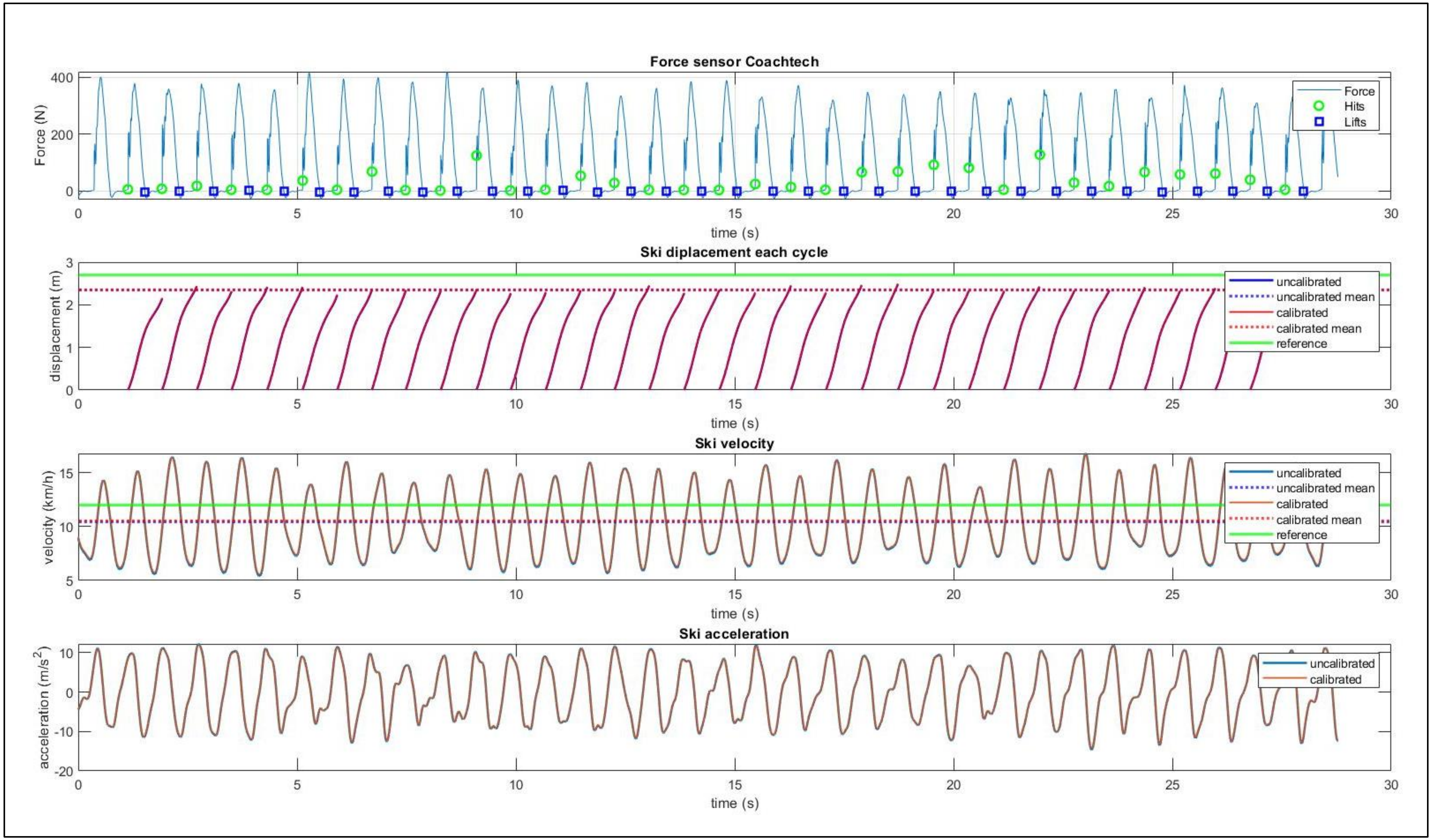

Figure 119 - Ski velocity and displacement. 12th trial acquired from the 1st subject.

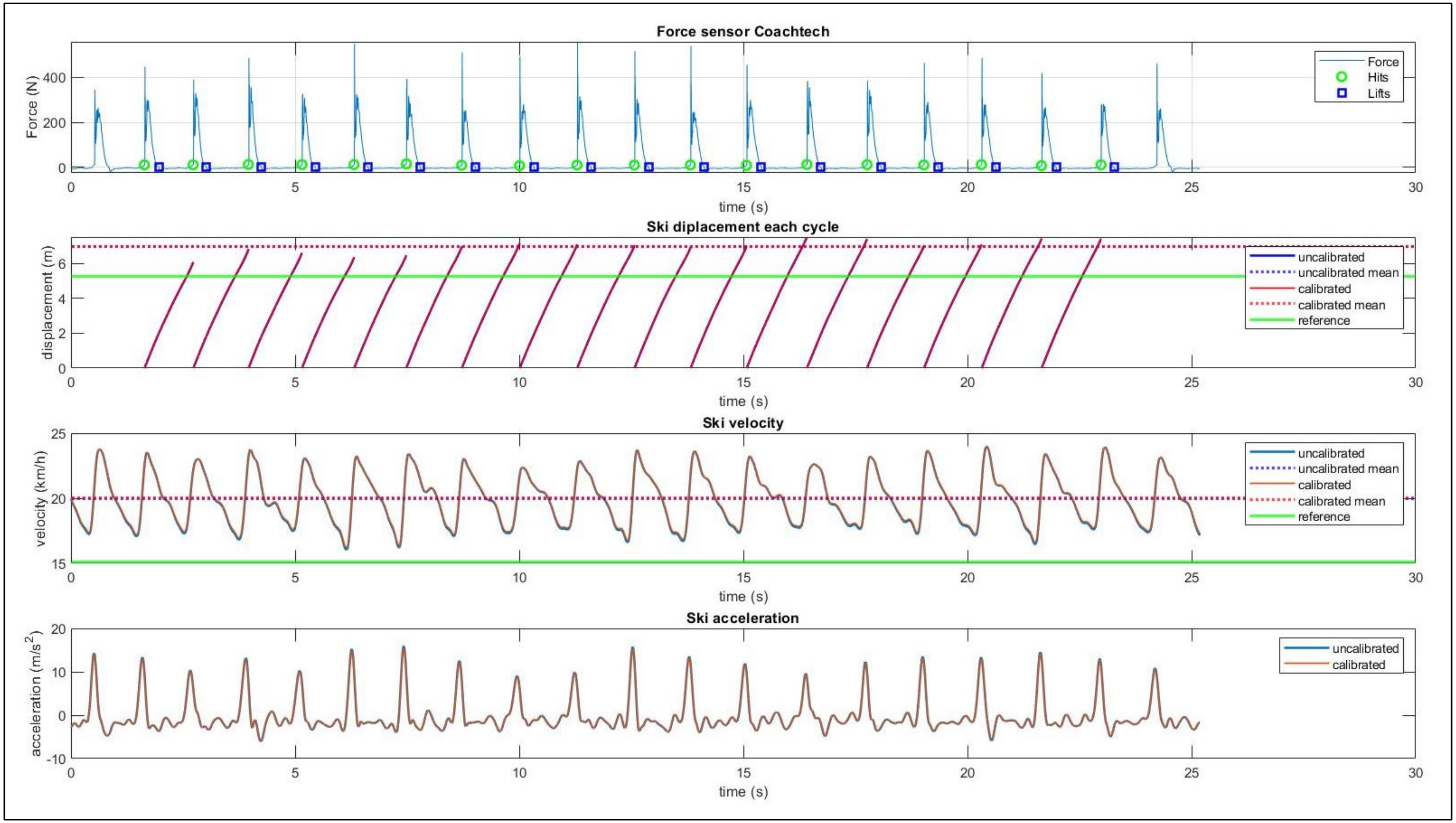

Figure 120 - Ski velocity and displacement. 2nd trial acquired from the 2nd subject.

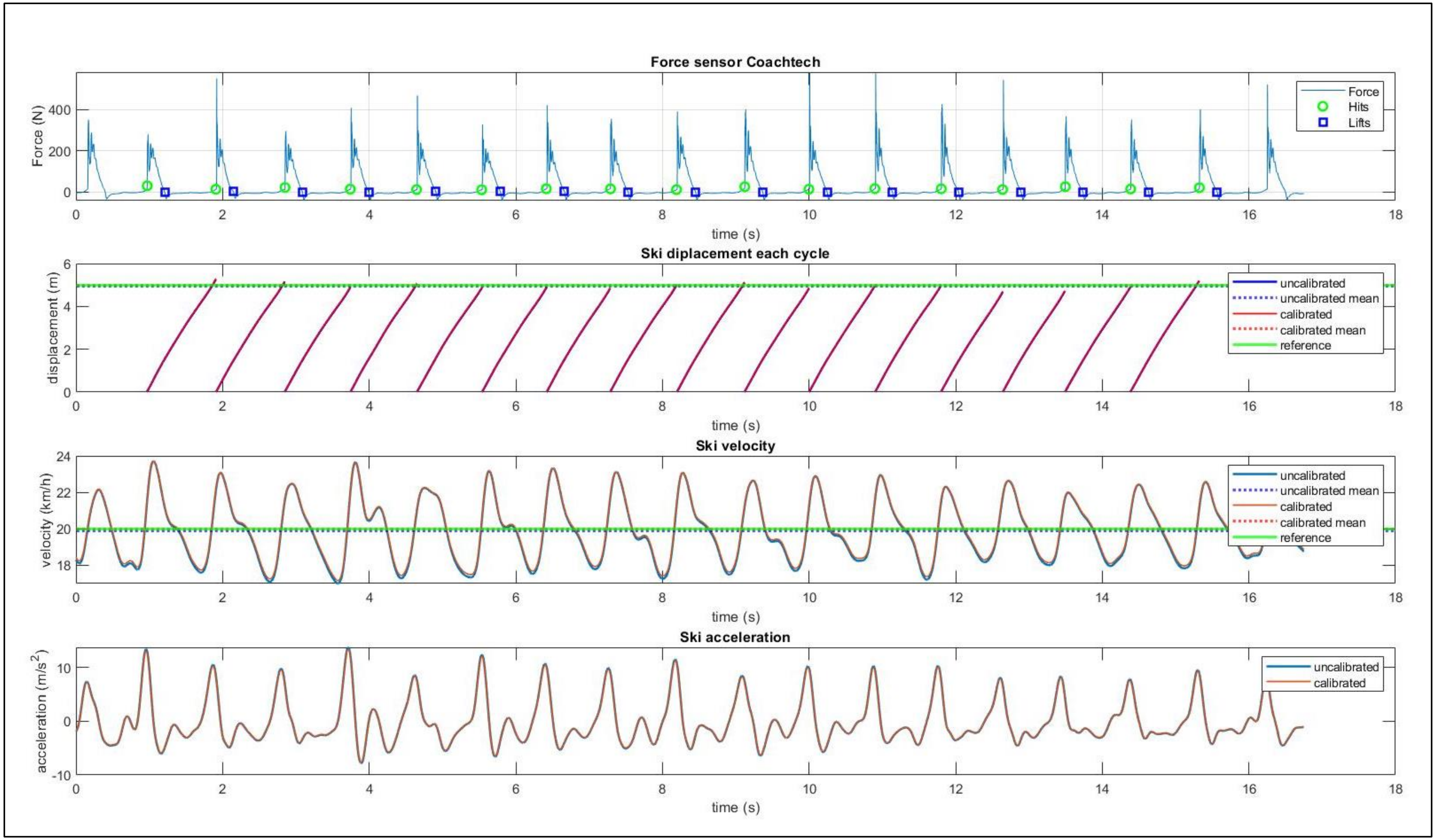

Figure 121 - Ski velocity and displacement. 3rd trial acquired from the 2nd subject.

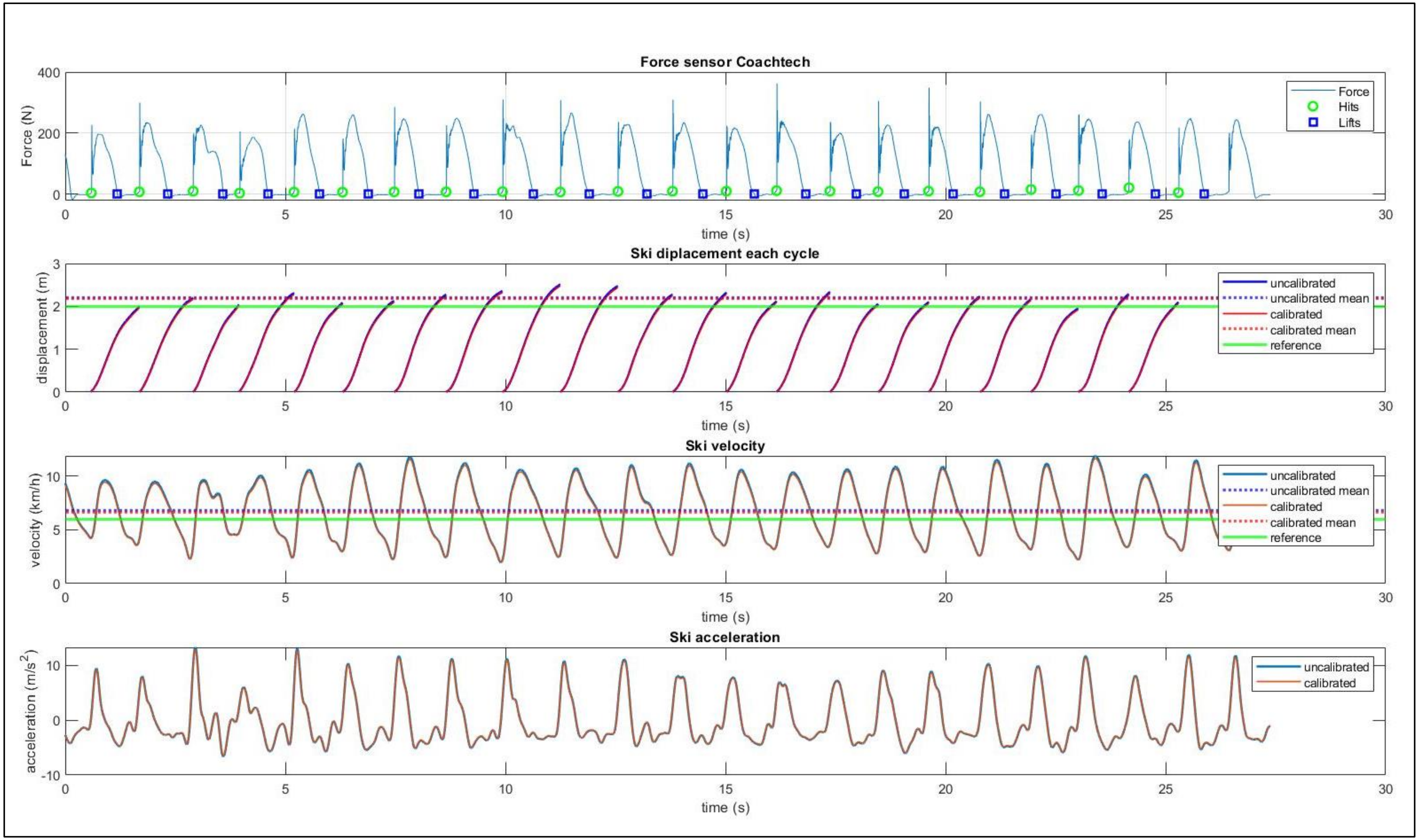

Figure 122 - Ski velocity and displacement. 4th trial acquired from the 2nd subject.

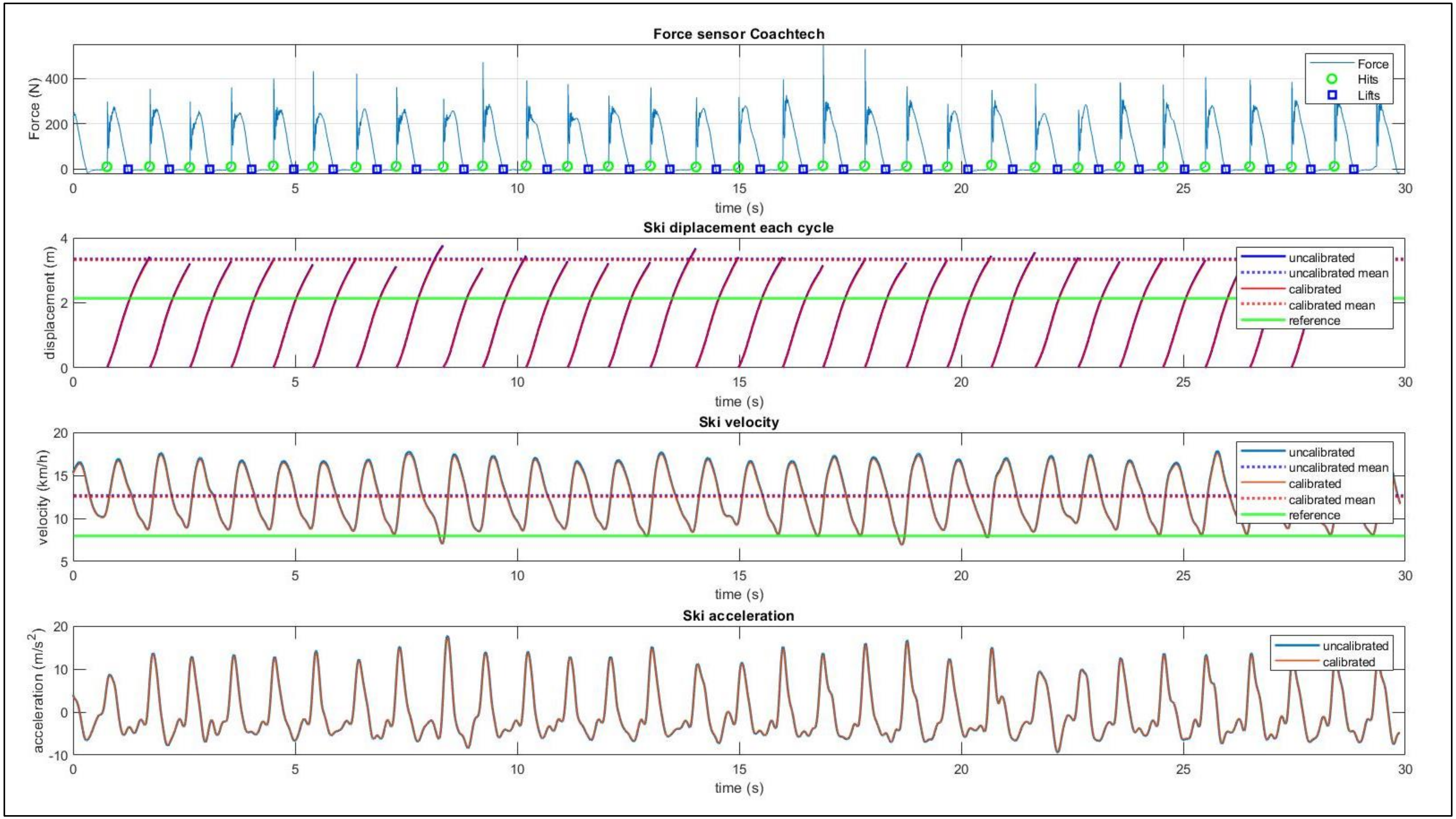

Figure 123 - Ski velocity and displacement. 5th trial acquired from the 2nd subject.

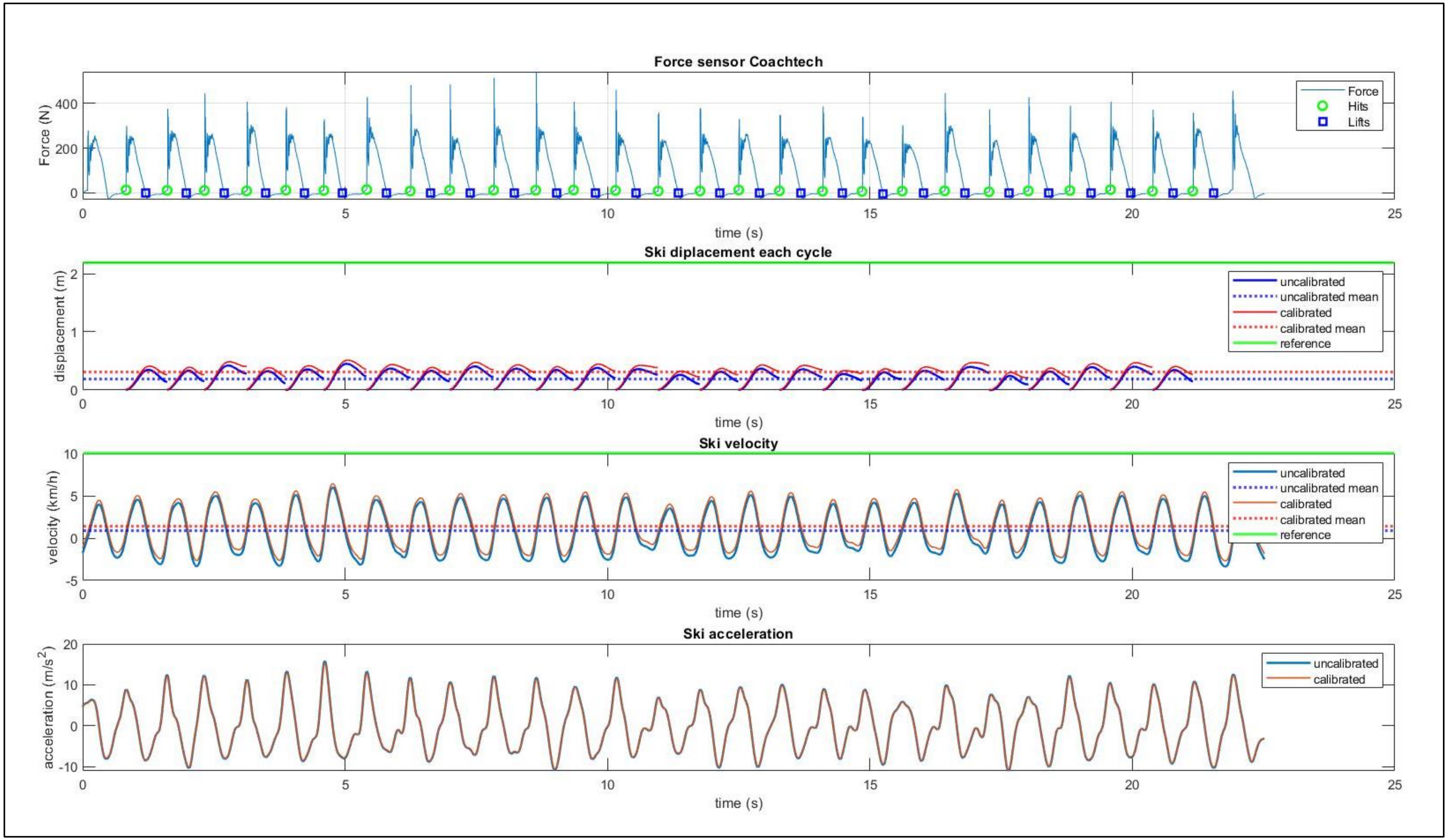

Figure 124 - Ski velocity and displacement. 6^th trial acquired from the 2^nd subject.

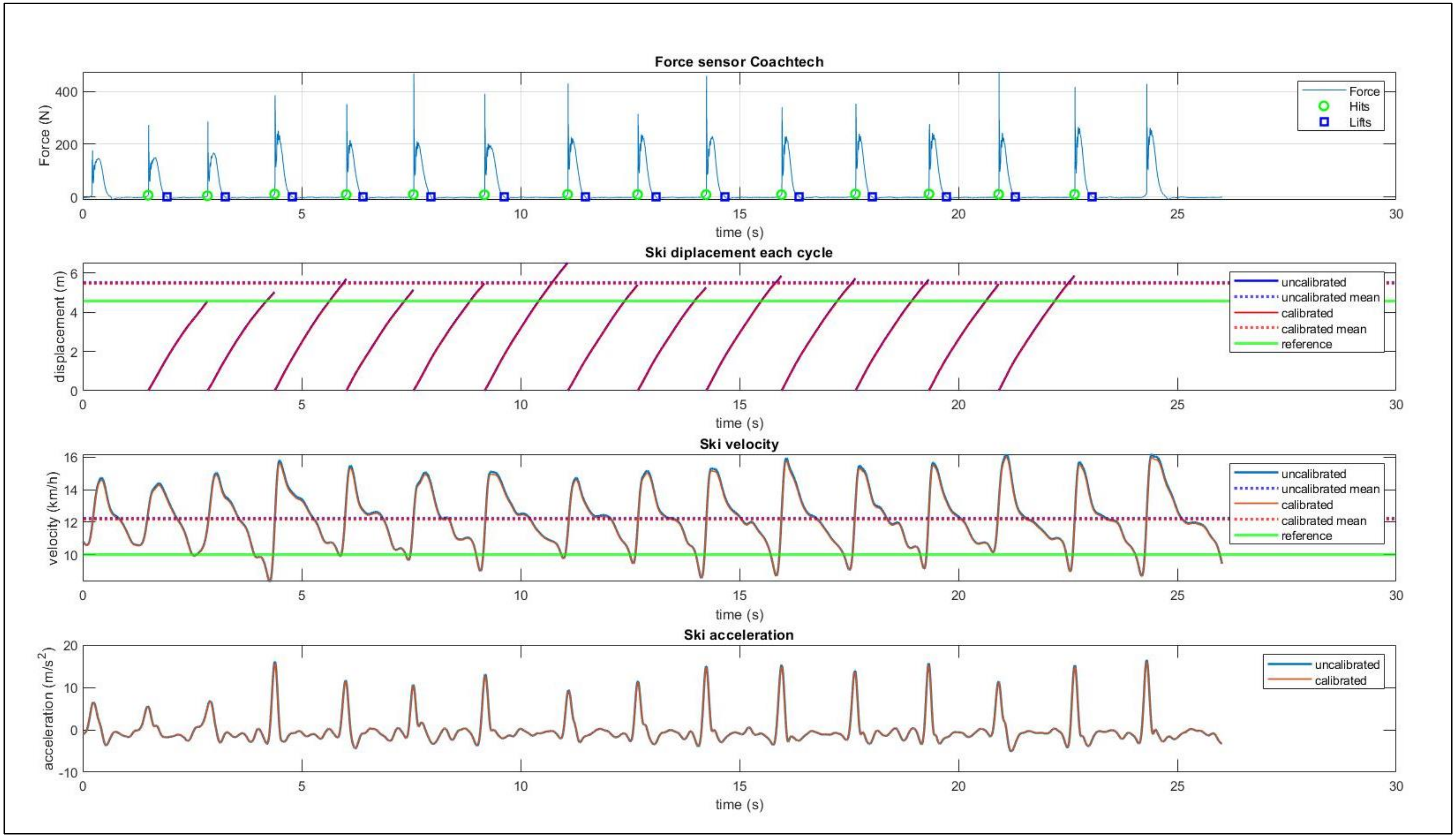

Figure 125 - Ski velocity and displacement. 7th trial acquired from the 2nd subject.

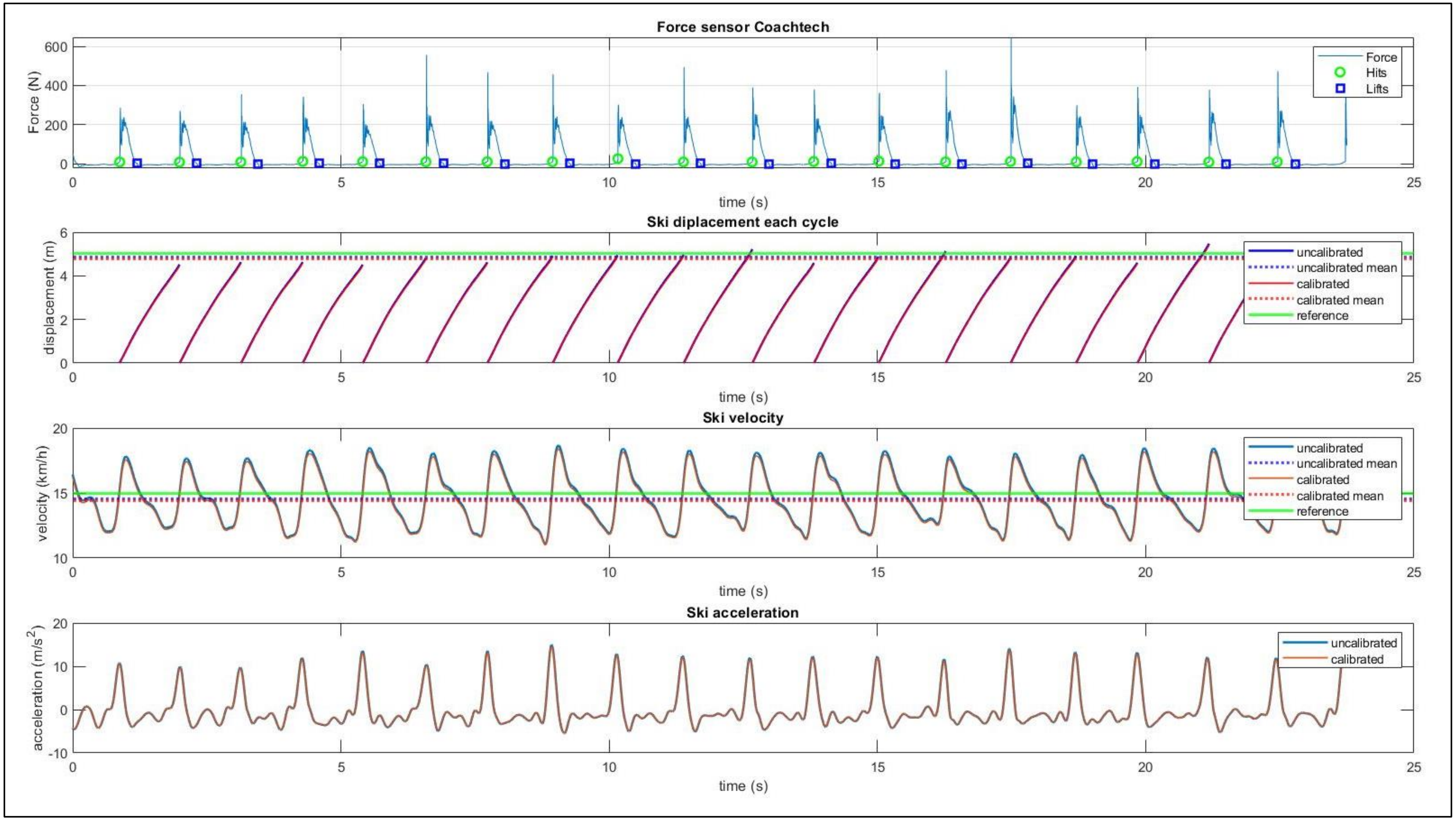

Figure 126 - Ski velocity and displacement. 8th trial acquired from the 2nd subject.

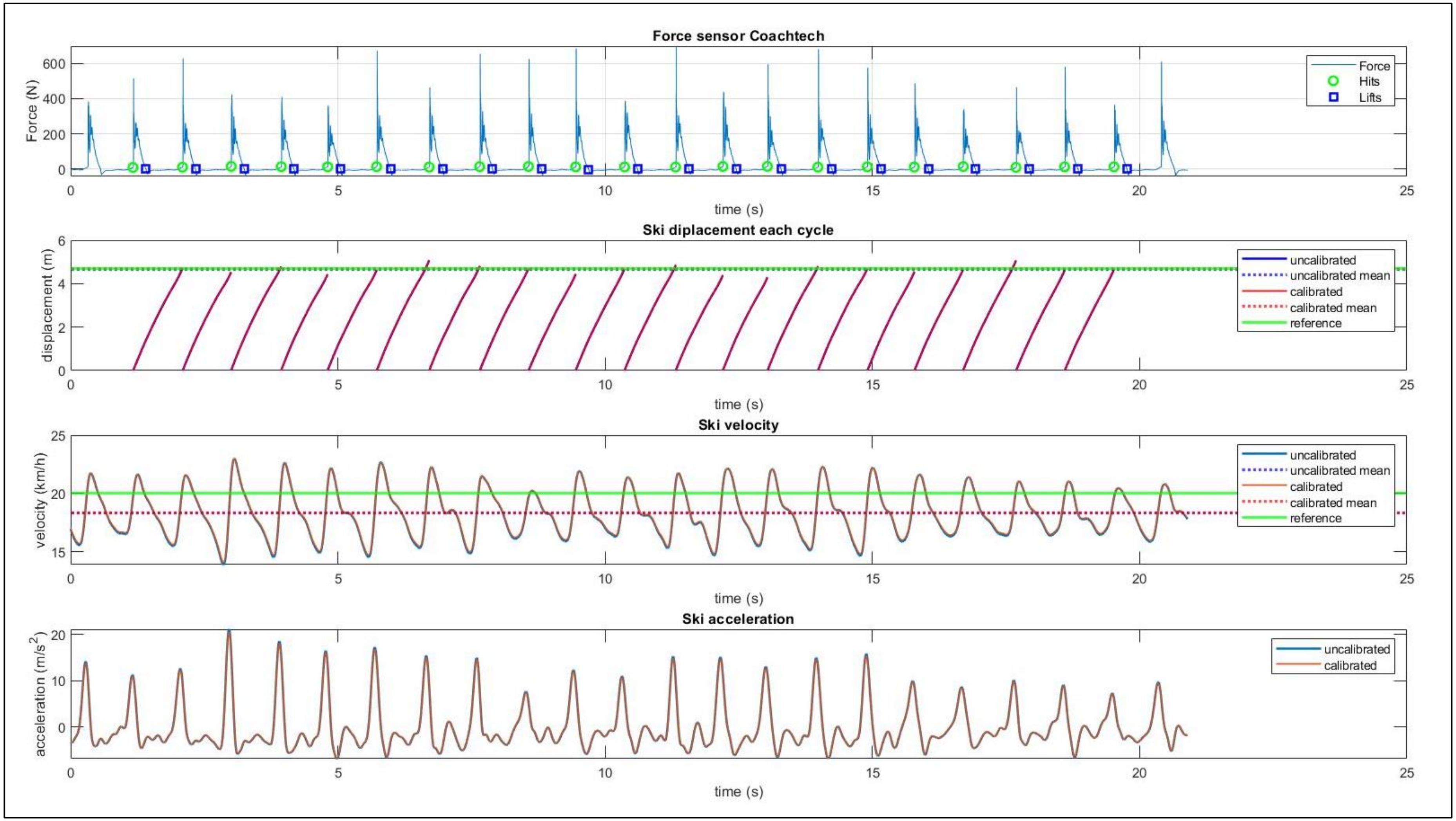

Figure 127 - Ski velocity and displacement. 9th trial acquired from the 2nd subject.

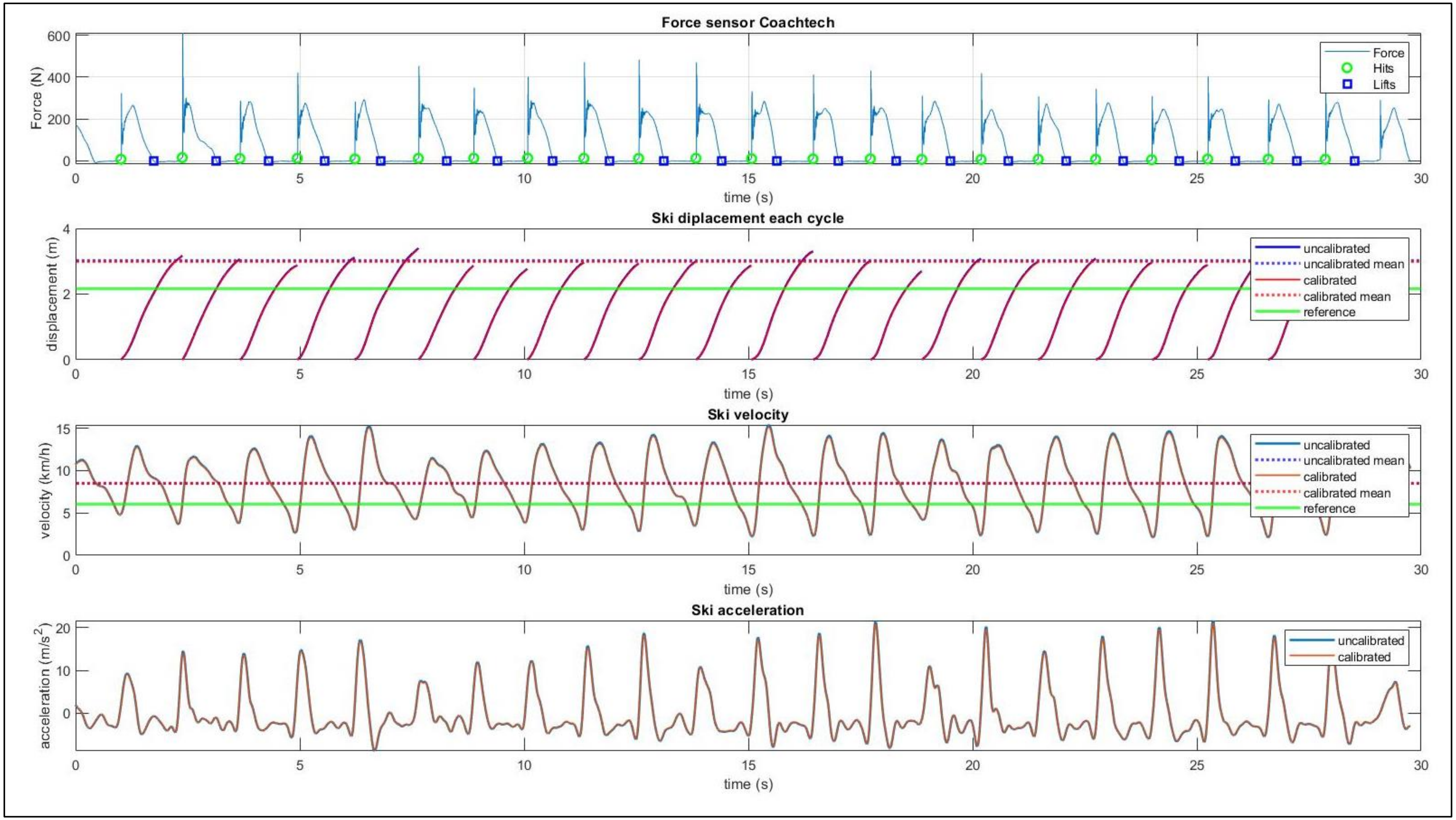

Figure 128 - Ski velocity and displacement. 10th trial acquired from the 2nd subject.

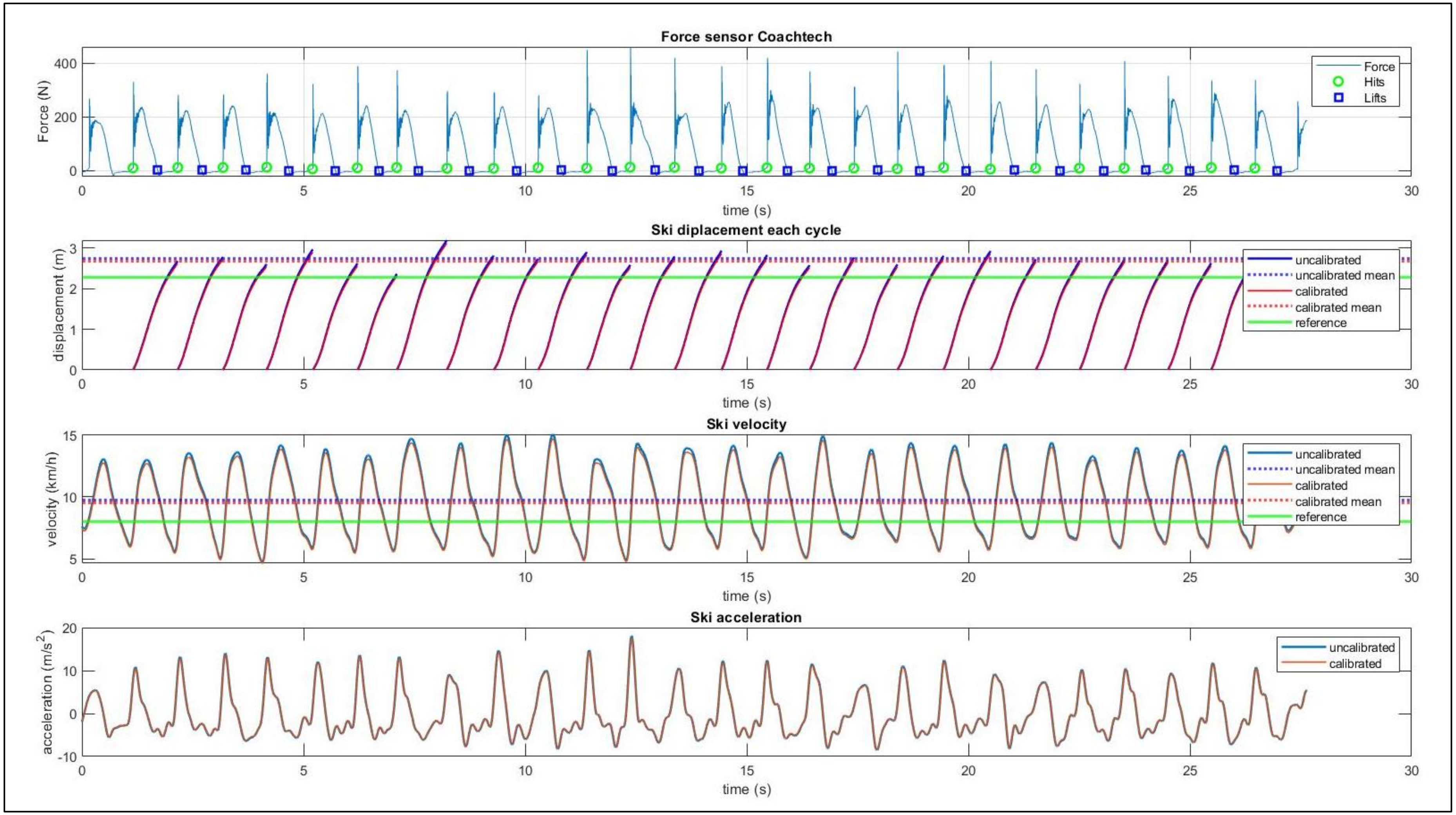

Figure 129 - Ski velocity and displacement. 11th trial acquired from the 2nd subject.

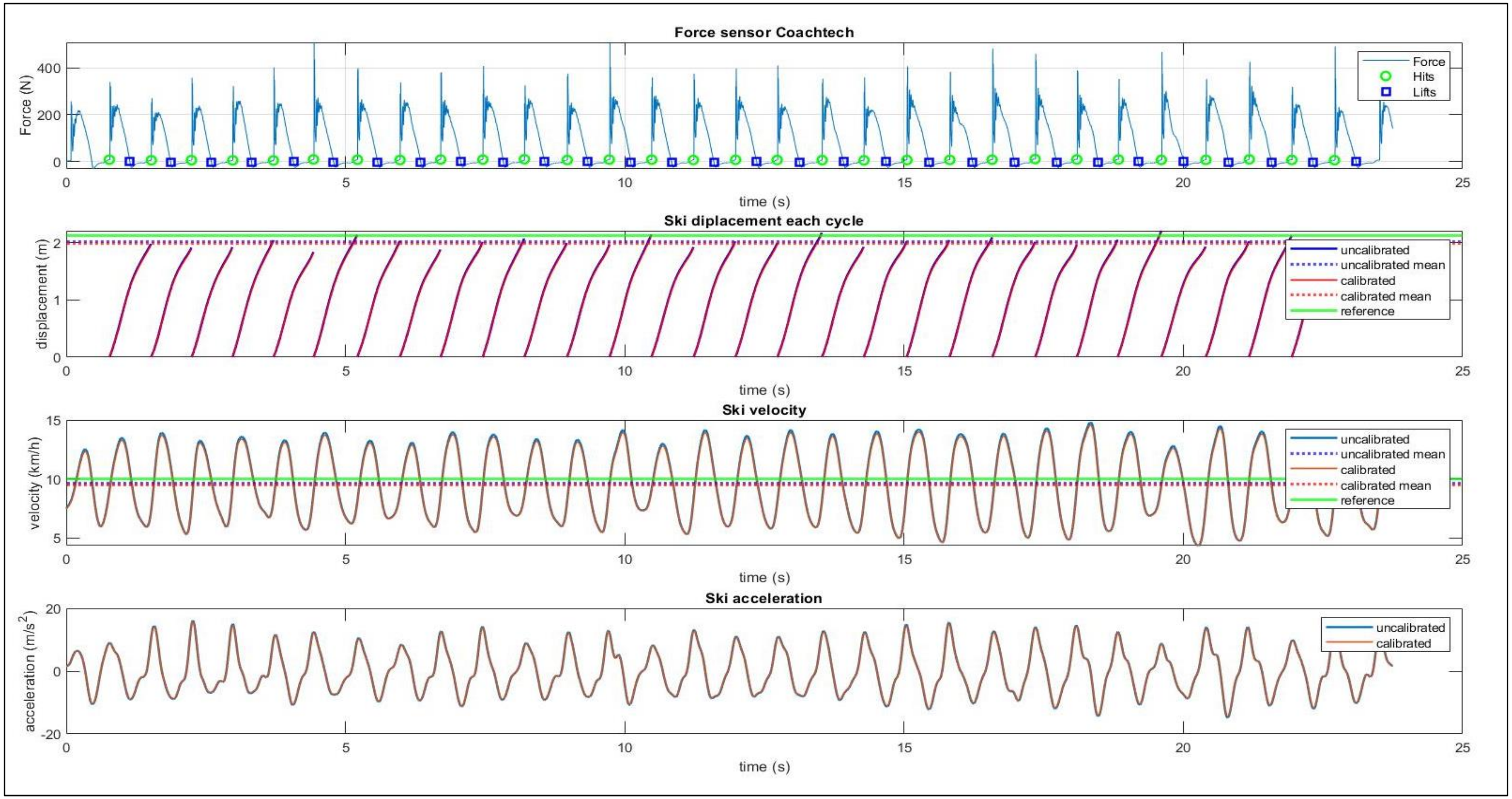

Figure 130 - Ski velocity and displacement. 12th trial acquired from the 2nd subject.